STRUCTURE AND BIOACTIVITY OF A RATIONALLY DESIGNED NICOTINIC ACETYLCHOLINE RECEPTOR ANTAGONIST TARGETING THE ALPHA-3 BETA-2 SUBTYPE

by

Leanna Marquart

A thesis

submitted in partial fulfillment

of the requirements for the degree of

Master of Science in Chemistry

Boise State University

December 2019

BOISE STATE UNIVERSITY GRADUATE COLLEGE

DEFENSE COMMITTEE AND FINAL READING APPROVALS

of the thesis submitted by

Leanna Marquart

Thesis Title: Structure and Bioactivity of a Rationally Designed Nicotinic Acetylcholine Receptor Antagonist Targeting the Alpha-3 Beta-2 Subtype

Date of Final Oral Examination: 18 October 2019

The following individuals read and discussed the thesis submitted by student Leanna Marquart, and they evaluated the student's presentation and response to questions during the final oral examination. They found that the student passed the final oral examination.

Owen McDougal, Ph.D.	Chair, Supervisory Committee
Lisa Warner, Ph.D.	Member, Supervisory Committee
Matthew King, Ph.D.	Member, Supervisory Committee

The final reading approval of the thesis was granted by Owen McDougal, Ph.D., Chair of the Supervisory Committee. The thesis was approved by the Graduate College.

ACKNOWLEDGEMENTS

The work described in this thesis was made possible by the individuals who came before me, trained me, and worked alongside me. I would like to acknowledge Matthew Turner for his preliminary foundational work with PC12 cells at BSU, in developing a decontamination method for conotoxins, and his thorough literature reviews. Dr. Tim Andersen gave years of collaboration in the development of the DockoMatic software, and Dr. Thomas Long gave us his creativity to produce the GAMPMS application that led to the sequence for KTM. All of this led to the computational chemistry by Dr. Matthew King that the work in this thesis is based on. I would like to thank Paul Phillips for his foundational literature review, James Groome for providing his time and resources for electrophysiology work, Joe Dumais for his consultation with NMR, and Shin Pu for his consultation with MS-MS.

I would also like to thank the members of my graduate committee, Drs. Owen McDougal, Lisa Warner, and Matthew King, for their guidance, input, correction, and insight. Dr. Owen McDougal was a valuable resource of thorough knowledge in the field of conotoxins and wisely guided my placement onto this project. Dr. Lisa Warner offered her NMR expertise including extensive troubleshooting with computer programs including CCPNMR, CYANA, and others. Dr. Matthew King provided proficiency and training in Dockomatic and other computational chemistry programs to help pave the way for the future of this work.

I would like to acknowledge the financial support provided by Institutional Development Awards (IDeA) from the National Institute of General Medical Sciences of the National Institutes of Health under Grants #P20GM103408 (INBRE) and P20GM109095 (COBRE in Matrix Biology); from the Biomolecular Research Center at Boise State University with funding from the National Science Foundation, Grants # 0619793 and #0923535; from the MJ Murdock Charitable Trust, Idaho State Board of Education, and Research Corporation; and from the Department of Chemistry and Biochemistry, Graduate College, and Research Office at Boise State University for access to graduate student stimulus funds that made this work possible.

Lastly, I would like to describe my personal thanks for a few key individuals. Owen McDougal taught me to be confident in myself as a scientist. Thank you for being transparent, gently but realistically teaching me the intricacies of the system, and never standing to see me sad. You were exactly what I needed in this journey. Lisa Warner reminded me of the impact of being good-humored no matter how stressful things are. You gave me the peace of making everything relatable. When my surroundings were turbulent, you helped keep my eyes at an inspired perspective. Matt King was my quiet and steady support. You gave me precisely the tools I needed without distraction and deserve a gold medal in being there for us. James Groome has seen my best and worst times and was only ever compassionate and merciful. You showed me that it really is possible to overcome obstructions, no matter how big or numerous. Sometimes you just need someone to show you how it's done. Matthew Turner advocated for me at all stages. I only hope someday I will have the scientific wit and critical thinking that you do.

ABSTRACT

The work presented in this thesis contributes to ongoing development of an efficient workflow for identification of lead compounds, based on the molecular scaffold of α-conotoxin MII, for drug therapies targeting nicotinic acetylcholine receptors. Nicotinic acetylcholine receptors (nAChRs) are pentameric, ligand-gated ion channels with distribution throughout the central nervous system and are implicated in a variety of neurological diseases including schizophrenia, nicotine addiction, Alzheimer's disease, and Parkinson's disease. However, ligand effect on nAChR function is not well understood. Consequently, drug therapies for neurological diseases either do not exist, or have short-lasting efficacy and/or severe side effects. Barriers to the comprehension of nAChR function, pharmacology, and detailed knowledge of their ligand binding domains are limited due to difficulties expressing functional receptors in heterologous systems, inability to crystallize their structures, and difficulty efficiently assessing predicted binding paradigms using current wet-lab experimental methods. To better understand the effect α-CTx binding to nAChRs has on cell signaling, we utilized a combination of computational tools to predict binding affinity and a PC12 cell-based assay the ability to qualitatively assess real-time bioactivity of predicted ligands. The computational tools permitted screening of α-CTx MII analogs for optimal characteristics for binding to the α3β2 nAChR isoform, producing the KTM peptide. The PC12 cell assay was developed to quickly and economically pre-screen ligands for nAChR bioactivity qualitatively prior to resource-intensive electrophysiology or animal studies, increasing efficiency of

investigations into nAChR binding and function. The work in this thesis demonstrates the merit of computational prediction in nAChR ligand binding, provided an accessible qualitative bioassay to efficiently validate predicted ligand bioactivity on nAChRs, and presents a case study of the rationally designed KTM peptide including structure activity relationship results in cell-based assay and electrophysiology experiments. Future studies will involve using computational programs to identify pharmacophore features required as ligand binding determinants to discover small molecule scaffolds based on peptide model compounds, and characterizing these small molecules for desired activity in cell lines heterologously expressing disease-relevant nAChR subtypes.

TABLE OF CONTENTS

ACKNOWLEDGEMENTS iv

ABSTRACT vi

LIST OF TABLES xi

LIST OF FIGURES xii

LIST OF ABBREVIATIONS xvi

CHAPTER ONE: A REVIEW OF MUTAGENESIS OF ALPHA-CONOTOXINS FOR ENHANCING ACTIVITY AND SELECTIVITY FOR NICOTINIC ACETYLCHOLINE RECEPTORS 1

Introduction 2

Mutagenesis Strategies for Alpha-Conotoxins 6

nAChR Structural Data to Rationalize Alpha-Conotoxin Mutagenesis 8

Alpha-Conotoxin Mutational Analysis 11

α-CTx Vc1.1 11

α-CTx PeIA 15

α-CTx ArIB 21

α-CTx ImI 22

α-CTx BuIA 26

α-CTx Lt1.3 29

α-CTx TxIB 30

α-CTx GIC 31

α-CTx TxID 32

α-CTx GID 34

α-CTx PnIA 39

α-CTx MII 42

Conclusions 49

CHAPTER TWO: QUALITATIVE ASSAY TO DETECT DOPAMINE RELEASE BY LIGAND ACTION ON NICOTINIC ACETYLCHOLINE RECEPTORS 51

Introduction 52

Results 60

Discussion 63

Conclusions 69

Materials and Methods 69

Cell Culture 70

Cell Assay 70

CHAPTER THREE: STRUCTURE AND BIOACTIVITY OF KTM, A COMPUTATIONALLY DESIGNED NICOTINIC ACETYLCHOLINE RECEPTOR ANTAGONIST INSPIRED BY A-CONOTOXIN MII 72

Introduction 73

Results 78

Bioactivity 78

Structure Determination 80

Structure Determination 86

Discussion 87

Materials and Methods 92

Synthesis 92

Disulfide Bond Analysis 93
Circular Dichroism Spectropolarimetry 94
2D Nuclear Magnetic Resonance Spectroscopy 95
PC12 Assay 96
Electrophysiology 97
Molecular Dynamics Simulations 99
Conclusions 100
CHAPTER FOUR: CONCLUSION AND FUTURE DIRECTIONS 101
REFERENCES 103
APPENDIX A 134
APPENDIX B 140
NMR Assignments 141
Partial Reduction MS-MS 142
Molprobity Scores 143

LIST OF TABLES

Table 1.1 CTxs and analogs discussed in the text, with primary sequence and nAChR isoform target shown. Mutations in analog CTxs are shown in red. Non-natural amino acids are indicated as follows: B: 2-aminobutyric acid; Z: norvaline; O: hydroxyproline; γ: γ-carboxyglutamic acid; P/5(R)-Ph: proline-5-(R)-phenyl; Aph: 4-aminophenylalanine; Nle: norleucine. IC_{50} values were determined by electrophysiology, unless otherwise noted. ...12

Table 2.1. EC_{50} and E_{max} values for agonist-stimulated $^{86}Rb^{+}$ efflux in NGF-treated PC12 cells for acetylcholine, nicotine, and cytisine. EC_{50} and E_{max} values are in units of μM.[166] 56

Table 3.1. Proton chemical shift assignments for amino acids in KTM. 83

Table 3.2. NMR restraints used in CYANA and the resulting structure statistics for KTM. 85

Table B.1 Parameter set details for NMR experiments. 142

Table B.2 Molprobity scores for the 20 NMR ensemble structures. The lowest percentile was 76th for model 10. 144

LIST OF FIGURES

Figure 1.1. The general structure of the nAChR, from the crystal structure of Torpedo marmorata (PDB: 2BG9). A) View from the side of the nAChR, parallel with the cell membrane, showing the extracellular, transmembrane, and intracellular domains. B) Dimer of two subunits showing the ligand binding site and select loops and helical regions. C) Top view of the pentametic nAChR looking through the conducting pore. D) A homology model of the ligand-binding domain (LBD) of an α3 (shown in green) and β2 (shown in yellow) dimer with α-CTx MII bound, illustrating the orientation of CTx binding in context of the structural features of the nAChR subunits. Figures were prepared using UCSF Chimera.[65] 10

Figure 1.2. Structural comparison of select α-CTxs A) LvIA B) MII C) PeIA and D) TxIB. These bind α3β2- and/or α6α3β2β2-nAChR. LvIA selectively binds α3β2-nAChR, MII and PeIA bind α3β2- and/or α6α3β2β2-nAChRs with approximately equal affinity, and TxIB is selective for only α6α3β2β2-nAChR. 20

Figure 1.3. Differences in electrostatic topography for two conotoxins A) α-CTx BuIA and B) α-CTx MII [S4A, E11A, L15A] that exhibit different selectivity for nAChR subtypes. The increased positive charge, contributed by Asn14, His12 and His9, on α-CTx MII [S4A, E11A, L15A] as compared to α-CTx BuIA is thought to contribute to the different selectivity profile of these peptides (see Table 1.1). The negatively charged surface surrounding Tyr12, Thr5 and Ser4 of α-CTx BuIA is thought to contribute to binding affinity for α6α3β4-nAChR. 27

Figure 1.4. α-Subunit sequence alignment for human nAChRs; α4 and α6 have 60.00% sequence homology, α4 and α3 have 61.43% sequence homology, and the α6 and α3 have 66.67% sequence homology. Homologous residues are highlighted in green. Stars are placed above residues that were mutated to assess the influence of residues of the α4 versus α6 responsible for the selectivity of α-CTx BuIA. 45

Figure 1.5. Structural comparison between A) α-CTx MII and B) the computationally predicted structure of KTM. Select amino acids are labeled. The backbone scaffold is predicted to be maintained by conserving the structurally important cysteine and proline residues. The cysteine pattern in both peptides is C1-C3 and C2-C4.....48

Figure 2.1. Chemical changes proposed to occur in the PC12 assay, from nAChR-induced dopamine release to luminescence detection. More dopamine release leads to a greater signal. Antagonists of nAChRs block dopamine release, diminishing signal. 55

Figure 2.2. α-CTx peptide sequence and disulfide connectivity for rα3β2 nAChR antagonists evaluated in the PC12 assay. 58

Figure 2.3. Integrated luminescence response versus ACh for (A) NGF(-), (B) NGF(+), and (C) NGF/nicotine. ACh response at 0 µM is not shown; the first point in each plot corresponds to the 10 µM ACh treatment to maximize visualization of data points and error bars. 60

Figure 2.4. Luminescence response in the PC12 assay for normal cells incubated at 37°C (A), and cells incubated at 30°C for 1 hr (B) and room temperature (21°C) for 2 hrs (C) before detection. Incubating cells at a lower temperature before detection significantly increases response in a temperature-dependent manner, but decreases sensitivity to α-CTx MII.. 62

Figure 2.5. PC12 assay screen using (A) 50 µM nAChR agonists (acetylcholine, nicotine, cytisine), and (B) 10 µM nAChR antagonists (α-CTxs MII, ImI, LvIA, PeIA) upon stimulation with ACh, under the optimal growth conditions identified in Figures 2.3 and 2.4 (treatment with NGF and nicotine, and incubation at 37°C). The PC12 assay provided qualified bioactivity assessment for each agonist and antagonist..... 63

Figure 3.1. A) Sequence of KTM with disulfide bond connectivity consistent with the expected native folding (dashed line), and predominant cysteine pattern resulting from oxidative folding following solid phase peptide synthesis (solid line). B) Sequence comparison of KTM to α-CTx MII. Of the 10 residues in α-CTx MII that were allowed to vary in the GAMPMS algorithm (orange), all but one amino acid (S13, boxed) changed to give the sequence of KTM. 77

Figure 3.2. Qualitative PC12 assay luminescence responses upon stimulation of nAChRs with acetylcholine (ACh), with and without 10 µM toxin. Assays performed with the addition of α-CTx MII and KTM resulted in a diminished luminescence recording compared to an ACh control. 79

Figure 3.3. Responses to local application of ACh for 30 ms are shown for control and after 3 nM toxin application; calibration horizontal 3 sec, vertical 2.5 µA (A). Concentration-dependent response curves for blocking rα3β2 nAChR by α-CTx MII (red) and KTM (blue) (B). Hill coefficients for the concentration response curves of α-CTx MII and KTM are 0.5 and 0.7, respectively. IC_{50} values of KTM and α-CTx MII are 0.19±0.02 nM and

0.35±0.08 nM, respectively. Data are means ± SEM from 8 to 12 oocytes. 80

Figure 3.4. CD spectrum of α-CTx MII (solid black line) and KTM (double lined grey). Measurements for each peptide were taken in water at 50 μM each, and a pathlength of 1 mm. The α-helical content of α-CTx MII and KTM were estimated to be 38.1% and 12.5%, respectively, as calculated from the observed signal at 222 nm. 81

Figure 3.5. Chemical shift difference between α-protons of amino acids in KTM and predicted random coil chemical shifts for the same amino acids.....84

Figure 3.6. NMR solution structure of KTM, where (A) is a ribbon representation of an ensemble of the 20 lowest energy structures, with an average RMSD to the mean structure of 1.7 ± 0.4 Å, and (B) represents an overlay of the mean calculated structure from NMR (cyan) and the computationally predicted structure (magenta) that have an average RMSD of 3.5 Å.....86

Figure 3.7. Root mean square fluctuations for each of the 16 residues of KTM over a 50 ns MD simulation. Residues W1, S4–G7, and K14 were observed to exhibit the greatest root-mean-square fluctuations (RMSFs). 87

Figure 3.8. Fingerprint region of COSY (red) and TOCSY (grey) spectra overlaid for residues 1-5 and 7-16, acquired at 600 MHz for KTM at 298 K in 30% ACN/70% H2O. Residue assignments are indicated by their one-letter amino acid code.....90

Figure 3.9. Ribbon structures of KTM at 0 ns (left), 25 ns (middle), and 50 ns (right) in the molecular dynamics simulation. Loop 2 appears to swing across the peptide over the course of the simulation. 91

Figure 3.10. Electrostatic maps of KTM at 0 ns of the molecular dynamics simulation (A), α-CTx MII (B), and KTM at 50 ns of the molecular dynamics simulation (C). Images on the left and right are rotated by 180 degrees...92

Figure A.1 Light microscopy images of PC12 cell morphology. Non-NGF-treated cells (A) remain round, while NGF-treated cells (B) show long, reaching dendrites at 3 days. No visual difference was observed in cell morphology for treatments including nicotine and/or ethanol in addition to NGF. 135

Figure A.2 Visual state of PC12 cells pre-assay (A) and post-assay after performing assay with both Locke's buffer (B) and HBSS (C). Cells post-assay using HBSS appeared severely lysed and damaged. 138

Figure B.1 Annotated MS-MS spectrum of relevant distinguishing B and Y fragments. Fragments are numbered along the KTM sequence, showing

position of corresponding alkylations with N-ethylmaleimide (NEM) and iodoacetamide (IAA). 143

LIST OF ABBREVIATIONS

BSU	Boise State University
GC	Graduate College
TDC	Thesis and Dissertation Coordinator
nAChR	Nicotinic acetylcholine receptor
ACh	Acetylcholine
CTx	Conotoxin
GAMPMS	Genetic Algorithm Managed Peptide Mutant Screening
SPIDR	Small-molecule Peptide-influenced Drug Repurposing
AChBP	Acetylcholine binding protein
PD	Parkinson's Disease
MAO	Monoamine oxidase
POD	Horseradish peroxidase
DA	Dopamine
NMR	Nuclear magnetic resonance
COSY	Correlation Spectroscopy
TOCSY	Total Correlation Spectroscopy
NOESY	Nuclear Overhauser Effect Spectroscopy
TEV	Two-electrode voltage clamp
PS-SCL	Positional scanning substrate combinatorial library
PST	Protein surface topography

CHAPTER ONE: A REVIEW OF MUTAGENESIS OF ALPHA-CONOTOXINS FOR ENHANCING ACTIVITY AND SELECTIVITY FOR NICOTINIC ACETYLCHOLINE RECEPTORS

Published in *Toxins* (Open access)

Matthew W. Turner,[1] Leanna A. Marquart,[2] Paul D. Phillips,[2] and Owen M. McDougal[2]

[1] Biomolecular Sciences Graduate Programs, Boise State University

[2] Department of Chemistry and Biochemistry, Boise State University

Nicotinic acetylcholine receptors (nAChRs) are found throughout the mammalian body and have been studied extensively because of their implication in a myriad of diseases. α-Conotoxins (α-CTxs) are peptide neurotoxins found in the venom of marine snails of genus *Conus*. α-CTxs are potent and selective antagonists for a variety of nAChR isoforms. Over the past 40 years, α-CTxs have proven to be valuable molecular probes capable of differentiating between closely related nAChR subtypes and have contributed greatly to understanding the physiological role of nAChRs in the mammalian nervous system. Here, we review the amino acid composition and structure of several α-CTxs that selectively target nAChR isoforms and explore strategies and outcomes for introducing mutations in native α-CTxs to direct selectivity and enhance binding affinity for specific nAChRs. This chapter will focus on structure-activity relationship studies involving native

α-CTxs that have been rationally mutated and molecular interactions that underlie binding between ligand and nAChR isoform.[1]

Keywords: conotoxins (α-CTxs); nicotinic acetylcholine receptors (nAChRs); mutational analysis; positional scanning synthetic combinatorial libraries (PS-SCL); acetylcholine binding protein (AChBP); protein surface topography (PST); genetic algorithm managed peptide mutant screening (GAMPMS); molecular dynamics (MD); solid phase peptide synthesis (SPPS)

Introduction

Snails of the genus *Conus* inhabit tropical and subtropical waters, where they hunt prey by injection of a venom rich in pharmacologically active peptides, referred to as conopeptides.[2-4] Cone snails are relatively slow moving aquatic organisms and have evolved venom to serve as an efficient chemical cocktail for prey incapacitation, retrieval and predator protection. The diversity of conopeptides is staggering. With >700 known *Conus* species, the venom of each species is comprised of hundreds to thousands of distinct conopeptides, equating to an estimated hundreds of thousands of unique, pharmacologically active conopeptides.[5-7] As of December 2018, the database for conopeptides, ConoServer, contained 6274 entries for conopeptide proteins with 220 protein structures.[8]

Conotoxins (CTxs) are a subset of conopeptides that are small, disulfide rich peptides that primarily target voltage or ligand gated ion channels.[9, 10] CTxs are classified by their molecular targets, as indicated by the first letter in Greek in the naming convention

based on the International Union of Basic and Clinical Pharmacology Committee on Receptor Nomenclature and Drug Classification system.[11, 12] For example, ω-CTxs target voltage gated calcium channels, δ- and μ-CTxs target voltage gated sodium channels, χ-CTxs target norepinephrine transporter channels, ρ-CTxs target α1A-adrenoreceptor, and α-CTxs target nicotinic acetylcholine receptors (nAChRs).[12, 13] Conopeptides are also classified into 16 genetically distinct superfamilies, to which α-CTxs primarily belong to the A and O superfamilies.[12] This diversity in molecular targets make CTxs particularly useful research tools for understanding the physiological role of indigenous mammalian receptors and ion channels, thereby making CTxs appealing as prospective selective therapeutics for human diseases. The therapeutic potential of CTxs is illustrated in the example of ω-CTx MVIIA. ω-CTxs have been investigated as therapeutic drugs due to their ability to selectively bind voltage-gated calcium channels (VGCCs), which are directly associated with pain pathways.[14] ω-CTx MVIIA, marketed by Elan Corporation under the trade name Prialt®, is a nonaddictive pain analgesic, 1000 times more potent than morphine.[15] Following twenty years of research, the United States Food and Drug Administration accepted the use of Prialt®to treat chronic pain in 2004.[16]

The focus of this chapter is to review α-CTxs, which target and act as competitive antagonists of nAChRs. α-CTxs generally contain between 12–20 amino acid residues, including four cysteines that form two highly conserved disulfide bonds. In native α-CTxs, the disulfide bonds are formed between Cys1 to Cys3, and Cys2 to Cys4. The first and second cysteine residues are always adjacent, but the number of amino acid residues between Cys2 and Cys3, and between Cys3 and Cys4 can vary, resulting in two loops of intervening amino acids denoted m and n, respectively. The cysteine framework refers to

the number of residues in the m and n loops. For example, α-CTxs with a 4/7 cysteine framework contain four and seven residues in their respective m and n loops.

nAChRs are a class of ligand-gated ion channels in the Cys-loop superfamily, to which γ-aminobutyric acid (GABA), glycine and 5-HT3 receptors also belong.[17, 18] nAChRs are pentameric ligand-gated ion channels found in both the central and peripheral nervous systems in mammals.[19] To date, 16 human nAChR subunit genes coding for subunits α1-α7, α9, α10, β1-β4, γ, δ, and ε have been identified.[20] nAChR subunit expression varies by tissue, with α1, β1, γ, δ, and ϵ subtypes being expressed in muscle. α2–α7, α9, α10, and β2–β4 subunits are referred to as "neuronal," despite their presence in non-neuronal tissues.[19, 21] nAChRs can be composed of heterogeneous or homogenous combinations nAChR subunits, forming different nAChR isoforms, with distinct physiological properties. Heteromeric combinations of α2–α6 and β2–β4, complexes of α9α10, and homomeric combinations of α7 or α9 subunits are known to exist.[22] nAChR subunits are composed of an N-terminal extracellular domain that contains the acetylcholine (ACh) binding site, four hydrophobic transmembrane domains that form the ion-pore and an intracellular loop.[23-25]

nAChRs are pharmaceutically important because they modulate the release of neurotransmitters (e.g., glutamate, norepinephrine, dopamine, acetylcholine), and because particular nAChR isoforms are expressed within specific neuronal pathways.[26] Different nAChR subunits may be expressed in defined regions in the mammalian body.[26] For example, dopaminergic neurons of the midbrain express α3-α7 and β2-β3 subunits, resulting in expression of nAChR isoforms such as α4α6β2β3, α4α6β2 and α6β2β3 that are highly and specifically expressed in select neuronal pathways.[27, 28] Dopaminergic pathways

are involved in numerous processes, including reward/reinforcement, attention, cognition, and voluntary movement. The well-defined and specific expression of α6-containing nAChRs in these neuronal types suggests they may be candidate drug targets for more selective approaches to treating disorders involving dopamine transmission.[29-31]

The significance of ligands that selectively bind to nAChRs lies in the variety and severity of neurological disorders in which degradation or altered activity of nAChRs is associated. Examples of neurological disorders associated with nAChRs are schizophrenia, nicotine addiction, Alzheimer's disease and Parkinson's disease.[29, 32-34] Therefore, differentiating between nAChR isoforms is an important step in better understanding neurological disorders.[35, 36] The high degree of sequence homology between different nAChR subunits makes discovery of selective antagonists for particular nAChR isoforms challenging. The lack of selectivity for the intended channel subtype may cause serious side effects and represents a major hurdle in the application of α-CTxs in pharmacological context. Frequently, a particular α-CTx is capable of inhibiting multiple nAChR isoforms.[37] For example, α-CTx MII blocks both α3β2 nAChR and α6-containing nAChRs isoforms, α-CTx ImI blocks α3β2, α7, and α9 nAChR subtypes, and α-CTx OmIA block α7, α3β2, and α6/α3β2β3 nAChRs. Although it may be evolutionarily advantageous for CTxs to be promiscuous amongst related receptors, this is undesirable in pharmaceutical and biotechnological applications.

For this reason, much effort has gone into the mutation of native CTxs to enhance their selectivity and potency to specifically target individual nAChR subtypes. Mutagenesis can also provide information regarding the significance of a given amino acid in the potency and selectivity of a CTx, as well as provide information regarding the

molecular determinants that govern ligand/receptor interactions. Researchers have explored many strategies to mutate CTxs for improved selectivity and potency with the aim of understanding the structure-function relationships that govern ligand-receptor interaction. Mutations introduced to synthetic α-CTxs to improve their pharmacological properties have been reviewed previously.[38] However, recent insights into the molecular structure of nAChRs and the development of contemporary computational tools capable of rational mutagenesis of α-CTxs merit an additional review of this topic. Table 1.1 includes the primary sequence and the activity of the CTxs discussed in this chapter. Recent excellent reviews have summarized the activity of native CTxs in a more comprehensive manner.[12, 14, 37-41] We start with a general discussion of different strategies used to rationalize and inform α-CTx analogue development and then provide a brief review of structural data available for nAChRs, followed by specific structure-activity relationship examples of the mutational analysis of individual α-CTxs designed to target specific nAChR isoforms.

Mutagenesis Strategies for Alpha-Conotoxins

Various approaches have been employed to alter the primary sequence of α-CTxs to enhance their affinity and selectivity for particular nAChR subtypes. Alanine scanning mutagenesis has been used extensively to determine the importance of a given amino acid in binding of a particular α-CTx to a particular receptor. Changes in activity for a mutated amino acid provide information on the significance of a given residue in the binding event and provide insight to the interaction between the α-CTx and the corresponding structural features in the nAChR binding pocket. Systematic replacement of residues with non-Ala amino acids also provides more subtle detail regarding the ligand/receptor interactions of

CTxs with nAChRs. Most mutagenesis studies of α-CTxs have focused on single amino acid substitutions, with a more limited number of reports describing synthesis and analysis of α-CTx analogs. Recent approaches have applied mixture-based combinatorial methods as a high throughput strategy to synthesize α-CTx analogs. The use of positional scan synthetic combinatorial libraries (PS-SCLs) has provided a way of acquiring functional information regarding all possible variable positions within the α-CTx framework.[42] This approach relies upon medium to high throughput screening assays for particular nAChR subtypes, and screening of pooled mixtures of α-CTx analogs to determine which amino acid positions confer higher activity. PS-SCL allows for the determination of a consensus sequence, which is an α-CTx peptide with multiple site mutations, intended to exhibit greater affinity for the desired nAChR subtype. The consensus sequence peptide can then be synthesized for focused pharmacological analysis using electrophysiology recordings.

Computational modeling of α-CTx/nAChR interactions have emerged as a useful tool for rationalizing mutagenesis design. In particular, the use of computational docking methods coupled with molecular dynamics (MD) simulations has proven useful for accelerating the discovery α-CTx analogues with enhanced binding affinity and selectivity for target nAChRs. In this methodology, the most energetically favorable binding poses predicted by computational docking are used as a starting point for MD simulations. The affinity of the α-CTx/nAChR interactions can be increased by inspecting the ligand/receptor binding paradigm and mutating those residues on the peptide that could lead to more, or stronger, contacts with the residues in the receptor's binding site. Because such structure-based virtual screening protocols depend upon structural data for nAChRs on the atomic scale, we will briefly review the advances in the structural data available for

nAChRs and the application of these data to generated models for particular nAChR subtypes.

nAChR Structural Data to Rationalize Alpha-Conotoxin Mutagenesis

Electron microscopic analysis of nAChRs isolated from the electric ray organ of *Torpedo marmorata* provided the first structural insights into human nAChRs.[43] This study revealed the overall organization of the pentameric assembly and the architecture of the extracellular domain and the pore region of nAChRs. However, in-depth information about the fine molecular details of the ligand binding domain was limited by the low resolution of the nAChR structure at 4 Å.[44] Figure 1.1A-D shows the general structure of the heteropentameric nAChR, including the side view of the receptor, in parallel with the cell membrane in a two-subunit interface showing the ligand binding domain, a view through the ion pore perpendicular to the cell membrane, and the α3β2 nAChR dimer bound to α-CTx MII. Another breakthrough in the understanding of the atomic structure of nAChRs was the discovery of acetylcholine binding protein (AChBP), a non-channel homolog of the extracellular domain of nAChRs, first isolated and crystalized from the fresh water snail *Lymnea stagnalis* (Ls).[45] Other AChBPs were subsequently identified in *Bulinus truncatus* (Bt) and *Aplysia californica* (Ac).[46, 47] Many crystal structures of AChBPs have been solved in different ligand-bound states, providing atomic-resolution details of the interactions between the extracellular domain and a variety of agonists and antagonists,[48] including α-CTx PnIA[47] and cobratoxin.[49] Combined, these studies provided a wealth of structural information upon which homology models for human nAChRs have been constructed. However, AChBPs do not function as ion channels and may lack the necessary structural features required for ligand-binding signals across the protein body.

Additionally, AChBP shares only 20–38.1% sequence homology with the nAChRs, further limiting their utility as structural templates for homology models of nAChRs. More recently, the x-ray structure of the extracellular domain of the mouse α1 nAChR was solved, revealing two hydrophilic residues conserved in nAChRs (and not AChBP) that are buried in the internal portion of the protein.[50] These observations strongly suggest that the hydrophilic interior of nAChRs is important for channel function, probably by conferring the receptor-specific structural flexibility required for the allosteric channel gating. Additionally, the crystal structures of homopentamers of human α7[51] and α9[52] nAChRs were solved. The X-ray crystallographic structure of the human α4β2 nAChR with nicotine bound was recently solved.[53] Several studies have used the 3D structure of AChBP as a template for homology model creation of nAChRs,[54, 55] and a few examples exist where the mouse α1 subunit was used as a template.[56, 57] Recently, studies have used the crystal structure of the homomeric human α9 nAChR subtype,[58, 59] as well as the crystal structure of the heteromeric human α4β2 nAChR subtype[60] to inform the homology models of heteromeric nAChR subtypes. However, because effective virtual screening requires that the conformation of the ligand bound complex be known to high accuracy, AChBPs still represent the most commonly used template for the characterization of α-CTx binding to the extracellular ligand-binding domain of nAChRs.[61-64]

The following section provides specific structure-activity relationship examples chosen to most clearly illustrate mutational analysis of individual α-CTxs designed to target specific nAChR isoforms.

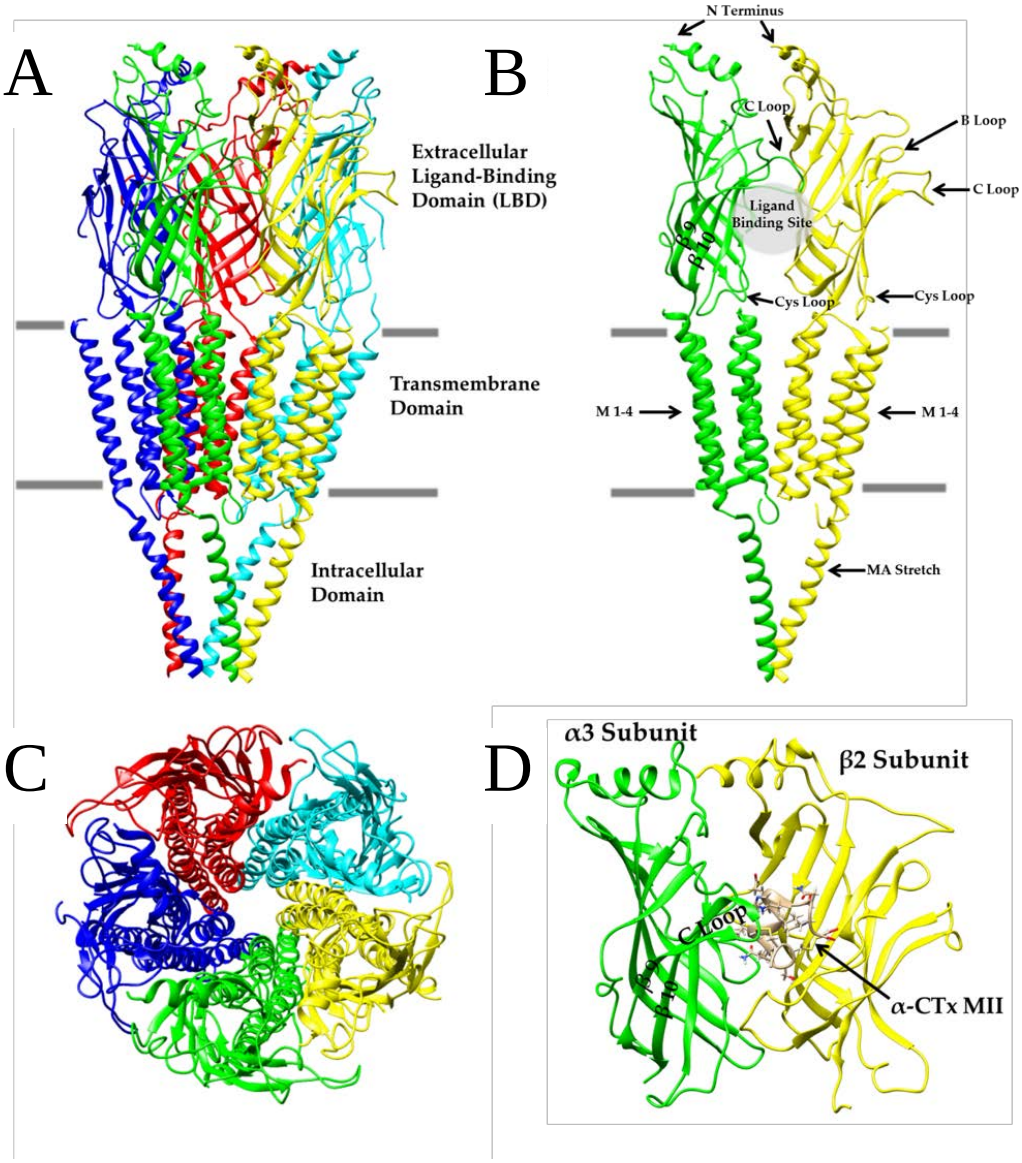

Figure 1.1. The general structure of the nAChR, from the crystal structure of Torpedo marmorata (PDB: 2BG9). A) View from the side of the nAChR, parallel with the cell membrane, showing the extracellular, transmembrane, and intracellular domains. B) Dimer of two subunits showing the ligand binding site and select loops and helical regions. C) Top view of the pentametic nAChR looking through the conducting pore. D) A homology model of the ligand-binding domain (LBD) of an α3 (shown in green) and β2 (shown in yellow) dimer with α-CTx MII bound, illustrating the orientation of CTx binding in context of the structural features of the nAChR subunits. Figures were prepared using UCSF Chimera.[65]

Alpha-Conotoxin Mutational Analysis

α-CTx Vc1.1

α-CTx Vc1.1, with primary sequence GCCSDPRCNYDHPEIC, was first discovered using PCR screening of cDNAs isolated from the venom ducts of *Conus victoriae* in 2003.[66] Later, this α-CTx peptide was identified in the venom of *C. victoriae* using mass spectrometry, and found to contain an amidated C-terminus, as well as post-translationally modified hydroxyproline and γ-carboxyglutamate in positions Pro6 and Glu14, respectively.[67] The native, post-translationally modified peptide was designated vc1a to distinguish it from the synthetic Vc1.1 containing the same primary sequence.

Synthetic Vc1.1 was shown to antagonize neuronal nAChRs in bovine chromaffin cells and was demonstrated to alleviate neuropathic pain in rat models of human neuropathic pain, as well as accelerate the functional recovery of injured neurons.[68] Clark et al. determined the NMR solution structure of α-CTx Vc1.1 and characterized the inhibition of individual nAChRs using electrophysiology with *Xenopus* oocytes expressing various rat nAChR subtypes.[69] α-CTx Vc1.1 demonstrated inhibition of α3α5β2, α3β2, and α3β4 nAChRs, with IC_{50} values of 7.2, 7.3, and 4.2 μM, respectively. No inhibition was demonstrated for α3α5β4, α4β2, α4β4, α7, or αβγδ nAChRs up to >30 μM. Although it was initially thought that α-CTx Vc1.1 targets α3-containing nAChR, subsequent reports demonstrated a much higher affinity for the α9α10 nAChR subtype, suggesting this may be the basis for the reduction in neuropathic pain upon α-CTx Vc1.1 administration.[70, 71]

Table 1.1 CTxs and analogs discussed in the text, with primary sequence and nAChR isoform target shown. Mutations in analog CTxs are shown in red. Non-natural amino acids are indicated as follows: B: 2-aminobutyric acid; Z: norvaline; O: hydroxyproline; γ: γ-carboxyglutamic acid; P/5(R)-Ph: proline-5-(R)-phenyl; Aph: 4-aminophenylalanine; Nle: norleucine. IC_{50} values were determined by electrophysiology, unless otherwise noted.

α-CTx	Primary sequence	nAChR isoform (IC_{50})	Ref.
Vc1.1	GCCSDPRCNYDHPEIC	rα3β4(4.2 μM) > rα3α5β2(7.2 μM) > rα3β2(7.3 μM)	69
		rα9α10(109 nM) > hα9α10(549 nM) > rα3β2(5.5 μM)	72
	GCCSDPRCAYDHPEIC	rα9α10(13 nM) > hα9α10(27 nM) > rα3β2(185 nM)	
	GCCKDPRCAYDHPEIC	hα9α10(19 nM) > rα9α10(93 nM) > rα3β2(>3 μM)	
PeIA	GCCSHPACSVNHPELC*	rα9α10 (6.9 nM) > rα6/α3β2β3 (17.2 nM) > rα3β2 (19.2 nM) > rα3β4 (480 nM)	73
	GCCSHPVCHARHPALC*	rα6/α3β2β3 (2.16 nM) > rα3β2 (30.9 μM)	42
ArIB	DECCSNPACRVNNPHVCRRR*	rα7 (1.81 nM) > rα6/α3β2β3 (6.45 nM) > rα3β2 (60.1 nM)	74
	DECCSNPACRLNNPHACRRR*	rα7 (0.356 nM) > rα3β2 (74.5 nM) > rα6/α3β2β3 (120 nM)	
	DECCSNPACRLNNPHDCRRR*	rα7 (1.09 nM) > rα6/α3β2β3 (828 nM) > rα3β2 (>10 μM)	
ImI	GCCSDPRCAWRC*	rα7 (220 nM) > rα7 (1.8 μM) > mα1β1γδ (51 μM) hα3β2(40.8 nM) > hα7 (595 nM)	75 76
	GCCSDP/5(R)-PhRCAWRC*	hα7 (0.70 μM) ǀ native (2.6 μM) > rα3β4 (3.7 μM) ǀ native (>300 μM)	77δ
BuIA	GCCSTPPCAVLYC*	rα6/α3β2 (0.258 nM) > rα6/α3β4 (1.54 nM) > rα3β2 (5.72 nM) > rα3β4 (27.7 nM)	78
	GCCSAOPCAVLYC*	rα6/α3β4 (58.1 nM) > rα3β4 (1.2 μM) > rα6/α3β2β3 (>10 μM)	79

	GCCSHPBCFBZYC*	α3β4 (2.3 nM) > α3β2 (>10 μM) ≈ α7 (>10 μM)	80
Lt1.3	GCCSHPACSGNNPYFC*	rα3β2 (44.8 nM)	81
	GCCSHPACAGNNPYFC*	rα3β2 (35.4 nM)	
	GCCSHPACSGNNPAFC*	rα3β2 (216 nM)	
TxIB	GCCSDPPCRNKHPDLC*	rα6/α3β2β3 (28 nM)	82
	GCCSDPPCRNAHPDLC*	rα7 (200 nM) > hα7 (>10 μM)	83
GIC	GCCSHPACAGNNQHIC*	hα3β2 (1.1 nM) > hα4β2 (309 nM) > hα3β4 (755 nM)	84
	GCCSHPACAGNNAHIC*	hα3β2 (8.41 nM) > hα3β4 (660 nM)	85
	GCCSPHVCSAMSPIC*	rα3β4 (12.5 nM) > rα6/α3β4 (94 nM) > rα3β4 (4.5μM)	86
TxID	GCCSPHVCSAMSPIC*	rα3β4 (3.6 nM) > rα6/α3β4 (34 nM)	60
	GCCSPHVCAAMSPIC*	rα3β4 (3.9 nM) > rα6/α3β4 (178 nM)	59
	GCCSPHVCRAMSPIC*	rα3β4 (5.4 nM) > rα6/α3β4 (350 nM)	60
	GCCSPHVCDAMSPIC*	rα3β4 (380 nM) > rα6/α3β4 (>10 μM)	60
	GCCSPHVCSAISPIC*	rα6/α3β4 (50 nM) > rα3β4 (75 nM)	59
	GCCSPHVCKAMSPIC*	rα3β4 (6.9 nM) > rα6/α3β4 (>10 μM)	60
GID	IRDγCCSPNACRVNNOHVC	rα3β2 (3.1 nM) > rα7 (4.5 nM) > rα4β2 (152 nM)	87
	----CCSPNACRVNNOHVC	rα3β2 (4.6 nM) > rα7 (5.5 nM) > rα4β2 (670 nM)	55θ

	IRDECCSPNACRVNNOHVC	rα3β2 (36 nM) > rα4β2 (4.8 μM)	
	IRDECCSPNACRVNNOHNC	rα4β2 (1.85 μM) > rα3β2 (>100 μM)	
	IRDECCSPNACRVNNOHVC	hα3β2 (10 nM) > hα7 (100 nM) > hα4β2 (3 μM)	88θ
	IRDECCSPNACRYNNOHVC	hα3β2 (20 nM) > hα4β2 (3 μM) > hα7 (4 μM)	
PnIA	GCCSLPPCAANNPDYC-*	rα3β2 (9.56 nM) > rα7 (252 nM)	89
	GCCSLPPCALNNPDYC-*	rα7 (12.6 nM) > rα3β2 (99.3 nM)	
	GCCSLPPCANleNNPDYC-*	rα3β2 (0.7 nM) > rα7 (4.3 nM)	90
MII	GCCSNPVCHLEHSNLC-*	rα6/α3β2β3 (0.39 nM) > rα3β2 (2.18 nM)	
	GCCSNPVCHLAHSNLC-*	rα6/α3β2β3 (0.16 nM) > rα3β2 (8.72 nM)	36
	GCCSNPVCALAHSNAC-*	rα6/α3β2β3 (0.16 nM) > rα6/α3β4 (269 nM) > rα3β2 (4850 nM)	
	GCCANPVCHLAHSNAC-*	rα6/α3β2β3 (1.2 nM) > rα3β2 (1400 nM)	91

A scanning mutagenesis study in 2009 by Halai et al. aimed to determine the key residues and interactions that govern the binding of α-CTx Vc1.1 to the α9α10 nAChR subtype, because of the α9α10 nAChR was sought after as a therapeutic target for the treatment of neuropathic pain.[72] It was determined the IC_{50} of Vc1.1 for rat (r)α9α10, human (h)α9α10, and rα3β2 nAChR isoforms at 0.109, 0.549, and 5.532 μM, respectively. They performed a two-stage mutation screen on each non-Cys residue to either an “inert” residue (Ala), a negatively charged residue (Asp), or a positively charged residue (Lys) to identify key amino acids in the interaction of Vc1.1 with the r/hα9α10 nAChR isoforms.

All mutations imposed on Vc1.1 showed clear selectivity for r/hα9α10 over rα3β2. They first identified Asp5–Arg7 and Asp11–Ile15 as the key residues essential to maintain functional activity. When Asn9 was replaced with a hydrophobic Ala, Leu, or Ile, the IC_{50} was reduced for rα9α10, hα9α10, and rα3β2 nAChR isoforms from 109, 549, and 5,532 nM to 13, 27, 185 nM, respectively. Mutation of Ser4 with a positive residue, either Lys or Arg, shifted the selectivity of Vc1.1 from rα9α10 to hα9α10 and lowered the IC_{50} for hα9α10 to 19 nM. Ser4 is highly conserved among many α-CTxs (see Table 1.1), and a smaller surface hydrophobic patch in loop 1 of 4/7 α-CTxs is thought to increase specificity for rα3β2.[72]

In an electrostatic map of Vc1.1, when Asn9 was replaced with a hydrophobic residue (Ala), the two smaller hydrophobic patches on opposite ends of the α-helix merged into a larger hydrophobic surface across one side of the α-helix. The result of the N9A mutation to Vc1.1 was a 30-fold increase in potency to inhibit the function of rα3β2 and roughly a 10-fold increase in inhibition of r/hα9α10, suggesting that extending the hydrophobic patch on this side of the peptide is favorable for binding to rα3β2 as well as r/hα9α10.

α-CTx PeIA

α-CTx PeIA was originally cloned from a cDNA library of *Conus pergrandis* and has the primary sequence GCCSHPACSVNHPELC.[92] α-CTx PeIA demonstrated inhibition of rα9α10, α6/α3β2β3, α3β2, and α3β4 with IC_{50} values of 6.9, 17.2, 19.2, and 480 nM, respectively.[73] The sequence of PeIA has a proline residue in position 6, which is consistent with α-CTxs MII and GIC.[84, 93] Pro6 initiates the α-helix in PeIA, consistent with observations for MII and GIC, indicating that the peptide backbone of PeIA may have a

similar molecular scaffold. In addition, PeIA has a His12 residue that is essential for biological activity; the same ligand activity dependency has been reported for the His12 in MII, and similar to Asn12 in GIC. Consequently, these three peptides exhibit comparable activity with α3β2 nAChR isoforms: PeIA and MII inhibit the rα3β2 nAChR isoform with IC_{50} values of 9.7 and 0.5 nM respectively, and GIC inhibits the hα3β2 nAChR isoform with an IC_{50} of 1.13 nM.[84, 93] Unlike MII or GIC, PeIA also inhibits rα9α10 with an IC_{50} of 6.9 nM. Thus, the amino acids unique to PeIA (S8, V9, N10, P13, and E14) are suspected to be the determinants of its high selectivity for the rα9α10 nAChR isoform.

α-CTx LvIA, GCCSHPACNVDHPEIC, has the same composition of amino acids in loop 1 as PeIA, but differs by three amino acids (LvIA:PeIA, N9S, D11N, and I15L) in loop 2.[57] The IC_{50} values of PeIA and LvIA for rα3β2 were determined to be 9.7 and 8.65 nM, respectively. LvIA also has high divergence to other α-CTxs in loop 2 and is the first report of an α-CTx with a strong rα3β2 selectivity over rα6/α3β3β2. Both PeIA and LvIA have similar residues at positions 7 and 10, but PeIA inhibits rα9α10, while LvIA does not. Luo et al. propose that this discrepancy could be explained by PeIA binding at a different site on the rα9α10 nAChR isoform than LvIA.[57] The rα9α10 nAChR isoform has two α-CTx binding sites, one at the α9α10 subunit interface and another at the α10α9 subunit interface. The α10α9 subunit interface displays more charged residues than the α9α10 subunit interface. For example, four charged side chains of Vc1.1 (R7, D11, H12, and E14) would be expected to have electrostatically favorable binding to the α10α9 subunit interface. By contrast, PeIA has only one charged side chain (Glu14) in loop 2 and would be expected to bind to the more hydrophobic binding site at the α9α10 subunit interface. The observation that LvIA does not inhibit rα9α10 containing nAChRs may be explained

by the fact that LvIA has charged side chains at Glu14 and Asp11 that could reduce affinity for the α9α10 interface, and binding to the α10α9 interface is unlikely due to poor shape complementarity to the binding site.

Yu et al provided insight into PeIA binding with rα9α10 using a computational homology model generated to describe the binding paradigms for Vc1.1[58] based on the crystal structure of *Ac*-AChBP in complex with PnIA [A10L, D14K] (PDB: 2BR8)[47] and the crystal structure of hα9 (PDB: 4UY2).[57] Similar to Vc1.1, PeIA residues H12 and E14 interact with residues E197 of α10(+) and R113 of α9(−), respectively. (+) corresponds to the subunit that provides the C-loop of the binding site, and (−) corresponds to the subunit that provides the β-sheet of the binding pocket. However, in contrast to Vc1.1, PeIA does not interact with N154 of α9(+) because the side chain of N154 is not in close proximity to PeIA, and PeIA has an additional hydrogen bond between residue N11 (D11 in Vc1.1) and T152 in both α10(+) and α9(+). This suggests PeIA has a lack of binding site preference between α10(+)-α9(−) and α9(+)-α9(−). Indeed, PeIA showed no stoichiometric-dependent activity with hα9α10, suggesting it has no preferred binding to α9(+)-α9(−) versus α10(+)-α9(−).

α-CTx PeIA was used as a starting point to conduct a positional scanning mutagenesis study by Hone et al. to develop a ligand that selectively bound α6β2β3 vs α3β2.[42] Substitution of His5 and His12 with alanine, and Pro6 with hydroxyproline dramatically reduced potency for both receptor types. Alanine substitution with Glu14 and Leu15 modestly decreased affinity for α3β2, and substitution of Asn11 with alanine, and Pro13 with hydroxyproline had little effect on the potency at either receptor isoform. In

summary, substitution of non-cysteine residues with alanine had no significant impact on the ability of α-CTx PeIA to discriminate between α6β2β3 and α3β2.

This led the authors to use amino acid substitutions based on the primary sequence of other α-CTxs, including α-CTx MII and α-CTx TxIB, to guide the development of a peptide capable of discriminating between these closely related nAChR subtypes. Based on the sequence of α-CTx MII, H5N, A7V, V10L, N11E, and P13S were analyzed. Of these, the A7V mutation increased the potency for α6β2β3 while decreasing potency for α3β2, resulting in a ~12-fold enhanced selectivity for α6β2β3. α-CTx TxIB is exclusively selective for α6β2β3[82] and differs from α-CTx PeIA by only six residues, leading to several interesting single mutations. The α-CTx PeIA [S9R] increased potency for both subtypes, whereas α-CTx PeIA [V10R] significantly reduced potency at both subtypes. The N11R substitution eliminated activity at α3β2, while minimally affecting the potency at α6β2β3. Combining these novel mutations that preferentially bind α6β2β3 over α3β2 with [S9H, V10A] analog previously identified with enhanced potency against both α6β2β3 and α3β2 resulted in the combined substitution mutant α-CTx PeIA [A7V, S9H, V10A, N11R, E14A]. This mutant resulted in a >15,000-fold higher affinity for α6β2β3 over α3β2 and enhanced potency at α6β2β3 (IC_{50} 2.16 nM).

To determine the specific amino acids of the α6-subunit that α-CTx PeIA interacts with, three residues of the α6-subunit were mutated to corresponding non-homologous residues of the α3-subunit. These mutations were E152K, D184E, and T195Q, and resulted in a >2000-fold reduced potency for the α-CTx PeIA [A7V, S9H, V10A, N11R, E14A] analog compared to α6β2β3-nAChR. An interesting feature of these mutagenesis analyses was implication of the importance of the positively charged amino acid in position 11

toward selectivity for the α6-subunit. Computational analysis using a homology model of PeIA bound to rα6 and rα3 subunits (based on the crystal structure of AChBP complexed with PnIA [A10L, D14K] (PDB: 2BR8)) indicates that this positive charge interacts with the negatively charged Glu-152 of the α6-subunit. This residue is Lys152 in the α3-subunit, and the E152K mutation significantly reduced potency for α-CTx PeIA [N11R], presumably due to repulsive like charges. This finding is corroborated by α6β2β3-nAChR specificity observed in α-CTx TxIB, in which the amino acid in position 11 is lysine. It may be concluded that α-CTxs with positively charged amino acids in the 11th position, such as α-CTx TxIB or α-CTx PeIA [N11R], interact favorably with the Glu152 of the α6-subunit while binding is disfavored to α3-containing nAChRs due to a repulsive charge-charge interaction with Lys152. Furthermore, the negative charge of Asp11 of α-CTx LvIA and its corresponding interaction with Lys152 has been speculated to be important for α3β2 selectivity.[57] These studies contribute to evidence supporting residue 11 in α-CTxs as being a key contributor to peptide selectivity and potency for nAChR subtypes. Figure 1.2 shows a structural comparison of select α-CTxs LvIA, MII, PeIA and TxIB that bind α3β2 and/or α6α3β2β2 nAChR isoforms.

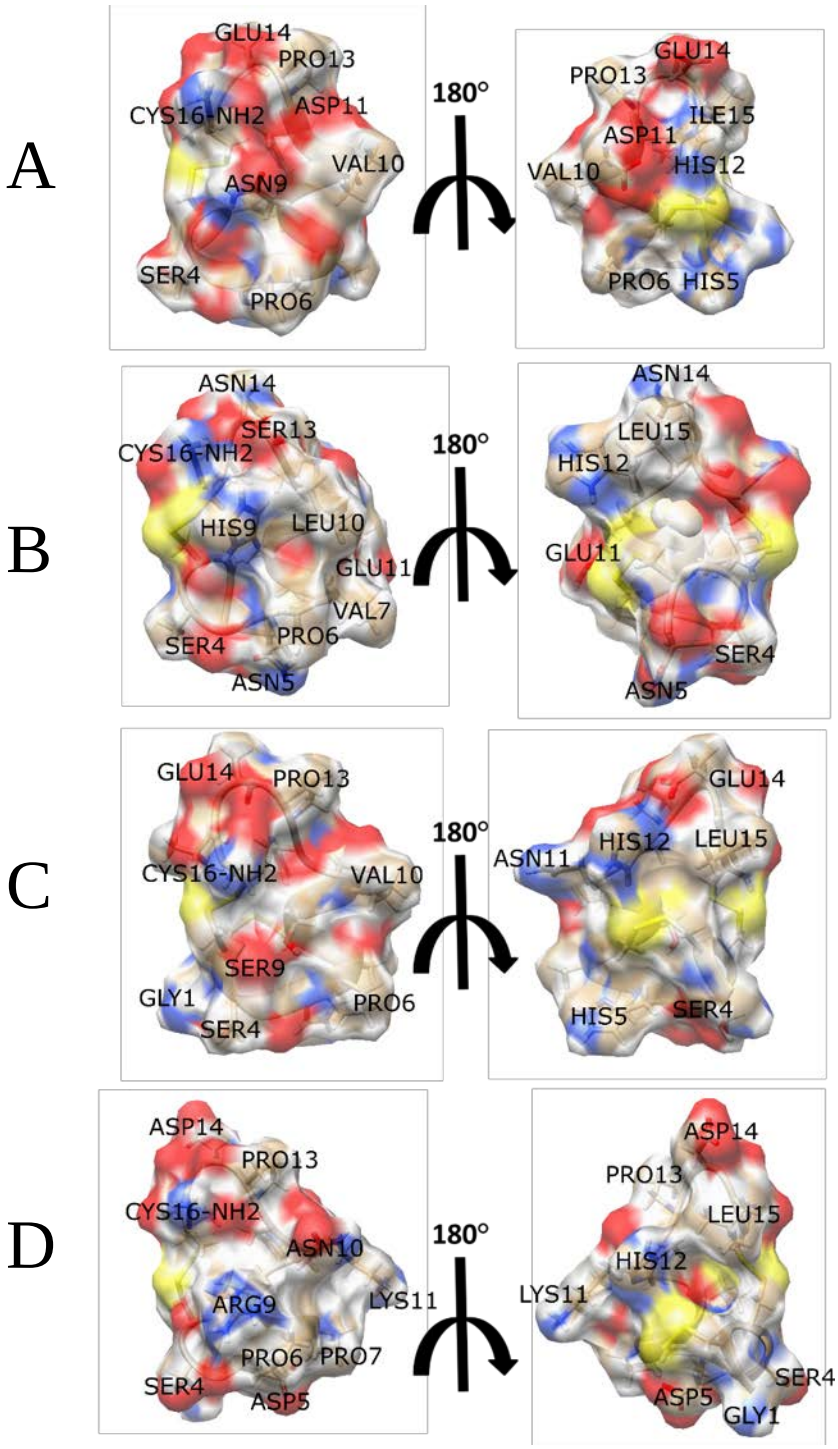

Figure 1.2. Structural comparison of select α-CTxs A) LvIA B) MII C) PeIA and D) TxIB. These bind α3β2- and/or α6α3β2β2-nAChR. LvIA selectively binds α3β2-nAChR, MII and PeIA bind α3β2- and/or α6α3β2β2-nAChRs with approximately equal affinity, and TxIB is selective for only α6α3β2β2-nAChR.

In both the α3 and α6 subunits, receptor residues 184 and 195 are located in the C-loop of strands 9 and 10 (see Figure 1.1B and 1.1D), respectively, but do not appear to interact directly with PeIA because their side chains are oriented away from it. This C-loop is proposed to act like a hinge allowing it to move toward the complementary subunit upon α-CTx binding. Residues 184 and 195 are smaller (Asp184 and Thr195) in α6 and bulkier (Glu184 and Gln195) in α3. This may allow the C-loop of α6 to be more flexible and allow more α-CTxs to be well-accepted in the binding pocket, while causing the C-loop of α3 to be more rigid and hinder α-CTx binding.

Luo et al. proposed computational receptor-toxin binding models for α-CTx LvIA bound to rα3β2 and rα3β4.[57] The docking trials were conducted using a homology model of Vc1.1 in complex with the rα9α10 nAChR (originally created by Yu et al. 2013[94]) as a template. Their model shows that the negatively charged Asp11 is buried in a cluster of the charged receptor residues Asp151, Lys154, and Glu194 in α3, and Lys78 and Arg80 in β2. However, when LvIA binds to the β4 subunit, a salt bridge between Lys58 and Glu35 becomes buried from the solvent. Luo et al. suggest this desolvation energy cost may account for the lower binding of LvIA with rα3β4 compared to rα3β2.

<u>α-CTx ArIB</u>

Native α-CTx ArIB, DECCSNPACRVNNPHVCRRR, was originally identified from the genomic DNA of *Conus arenatus* and exhibited IC_{50} values for rα7 > rα6/α3β2β3 > rα3β2, of 1.81, 6.45, and 60 nM, respectively.[74] Since the peptide has high affinity for all three isoforms, ArIB mutants were designed with the intention of enhanced selectivity for rα7. Because the [A10L] mutation in PnIA shifts selectivity to rα7 over rα3β2,[89] it was reasoned that the [V11L] mutation in the homologous position of ArIB would improve

selectivity for rα7 and reduce activity for rα3β2. Indeed, the α-CTx ArIB [V11L] mutation increased selectivity for rα7 relative to rα3β2, yielding IC_{50} values of 0.539 nM and 38.8 nM, respectively. Secondly, because the [L15A] mutation of MII weakens potency for rα3β2, a [V16D] mutation in the homologous position of ArIB was expected to reduce selectivity for rα3β2.[36, 95] Indeed, potency for rα3β2 (IC_{50} >10 μM) was lowered without significantly lowering the potency for rα7 (IC_{50} 1.09 nM).

α-CTx ImI

α-CTx ImI, with sequence GCCSDPRCAWRC, has 12 amino acids and contains a 4/3 m to n loop spacing pattern. α-CTx ImI was isolated from the crude venom of the worm-hunting *Conus imperialis* and was shown to inhibit heterologously expressed rat neuronal α7 and α9 homopentametic nAChRs with IC_{50} values of 220 nM and 1.8 μM, respectively.[75, 96] Low affinity activity toward the mouse muscle type nAChR receptor α1β1γδ was also observed, with an IC_{50} of 51 μM. Subsequent pharmacological characterization reported an IC_{50} of 595 nM toward heterologously expressed hα7 nAChR, and 40.8 nM toward hα3β2 nAChRs.[76] Activity towards hα3β2 nAChRs was surprising, because no effect was observed towards rα3β2 nAChRs at 5 μM.[96] Various mutagenesis experiments to probe the structure-activity relationship between ImI potency and selectivity toward particular nAChR subtypes have been performed.[77, 97-99] The Asp5, Pro6, and Arg7 present in the m-loop, as well as Trp10 in the n-loop were demonstrated to be critical for binding to a human α7/5HT3 chimera expressed in HEK293 cells.[76] Replacement of the DPR motif in the m-loop resulted in a two to three order of magnitude decrease in activity. The ImI [W10T] mutant demonstrated a 30-fold loss of activity, whereas maintenance of the aromatic side chain in the [W10F] mutant resulted in a modest

three-fold decrease of affinity. α-CTx ImI [R7L] and [D5N] mutations resulted in two orders of magnitude diminished activity towards hα7 expressed in *Xenopus* oocytes.[97] Further investigation into the role of the aromatic side chain in position 10 demonstrated that the analogue [W10Y] maintained activity toward rat α7 expressed in *Xenopus* oocytes, indicating that substitution of Trp10 for other aromatic residues does not strongly influence the activity of ImI.[98] To probe the interaction between Pro6 and a hydrophobic binding pocket observed in co-crystallization structures of α-CTxs in complex with AChBP, analogues of α-CTx ImI containing non-natural Pro6 derivatives were synthesized and pharmacologically characterized.[99] Activity was evaluated in tsA-201 cells transiently expressing α7/5-HT3 chimera using a [^{3}H]-methyllycaconitine completion binding assay, HEK293 cells stably expressing rα4β2, rα3β4, or rα4β4 nAChRs using a [^{3}H]-epibatidine competition binding assay, and GH3 cells stably expressing hα7 nAChR using the Fluo-4/Ca^{2+} assay. Addition of polar and charged groups on Pro6, such as 4-amino, 4-guanidino, and 4-betainamidyl, resulted in no significant binding or antagonistic activity toward hα7 nAChRs. Most aromatic and hydrophobic substituents to Pro6, such as 3-phenyl, 4-phenyl, 4-benzyl, and 4-naphthylmethyl resulted in varying degrees of diminished binding to hα7 nAChRs. The loss of activity depended upon both the position and stereochemistry of the substitution. For example, the 4-(R)-phenyl analogue resulted in an ~six-fold reduction in binding, while the 4-(S)-phenyl showed no significant binding at 100 μM. However, the 5-(R)-phenyl substitution resulted in significantly enhanced binding and antagonistic activity toward hα7 nAChR compared to the native conotoxin, with an observed 10-fold increased affinity compared to the wild type. None of the analogues demonstrated significant binding to hα4β2 or hα4β4 nAChR subtypes at 100 μM.

Computational chemistry was used to elucidate the mechanism behind the enhanced affinity of α-CTx ImI [P6/5-(R)-phenyl] substituent toward hα7 nAChR. A homology model of the hα7 nAChR ligand binding domain (LBD) was generated using Modeller 9 version 3,[100] based on the crystal structures of mouse LBD of α1 nAChR (PDB: 2QC1)[49] subunit and *Ac*-AChBP in complex with α-CTx ImI as templates (PDB: 2BYP).[46] Docking of α-CTx ImI [P6/5-(R)-phenyl] to the hα7 nAChR LBD model was performed using Schrödinger Glide.[101] Results of computational modeling and docking experiments suggest that the observed enhanced affinity may be due to π-stacking interactions between the P6/5-(R)-phenyl and Tyr93 in the receptor. This study was inspired by crystallographic data of α-CTxs in complex with AChBPs and demonstrates the utility of rational mutagenesis of α-CTxs to enhance binding affinity. Results of this rational design method demonstrate the utility of computational chemistry to broaden molecular insights of structure-activity relationships for the interaction of mutated CTxs with target receptors.

In contrast to the rational design approach focused on chemical modification of a single amino acid described in the previous study, α-CTx ImI has also been used as a template in an expansive PS-SCL experiment.[102] This experiment acquired information about three amino acids mutated in the n-loop of the α-CTx ImI framework, with the goal of generating α-CTx ImI analogues with improved activity and selectivity for the hα7 nAChR.[103] Using this approach, the amino acids Ala9, Try10, and Arg11 were mutated to any of 22 natural and non-natural amino acids using the “tea bag” synthetic strategy. The PS-SCL resulted in a total of 10,648 combinations, which were screened for activity in GH3 cells stably expressing hα7 nAChR using the Fluo-4/ Ca^{2+} assay. In the initial screening process, 66 PS-SCL mixtures, each containing 484 unique compounds, were

evaluated to determine the amino acid at a given position that resulted in the greatest potency for that mixture and were selected as promising candidates for more potent analogs. From this initial screen, the most active amino acids at position 9 were determined to be norvaline (F), with Leu and Ile at this position resulting in mixtures with high antagonist potency. In position 10, Trp was determined to be most potent, with Phe and Tyr also resulting in potent mixtures. In position 11, substitution with His proved most impactful, with Trp and α-aminobutyric acid (Abu) also resulting in potent mixtures. Thirty-six individual analogs were synthesized with position 9 occupied by Phe, Leu, or Ala (native), position 10 occupied by Trp, Phe, or Tyr (native), and position 11 occupied with Abu, His, Trp, or Arg (native). Sixty additional individual analogs were synthesized resulting in a subsequent screening of 96 compounds. The result of this study was creation of a α-CTx ImI mutant with 14-fold greater potency than native peptide; the mutant peptide contained Leu9, 4-aminophenylalanine (Aph) in position 10, and Abu11. The consensus sequence of the most potent mixtures from the initial screen –Nva9, Trp10, His11– had nearly a nine-fold enhanced potency and was one of the most effective analogs tested for inhibition of hα7 nAChR. A key observation from this study is that no single substitution resulted in increased antagonist potency, but rather, multiple substitutions acted synergistically to achieve significant increases in antagonist potency. This implies that although native toxins are well optimized for their interactions with the receptors, antagonist activity can be significantly enhanced by substitution with combinations of two or three residues.

α-CTx BuIA

α-CTx BuIA, with sequence GCCSTPPCAVLYC, was originally discovered by reverse transcription of RNA isolated from the venom duct of *Conus ballatus*. This peptide has a 4/4 m/n loop framework and can block multiple rat nAChR isoforms with nanomolar potency.[78] Chemical synthesis of the mature toxin allowed for pharmacological characterization through electrophysiology experiments in *Xenopus* oocytes expressing multiple rat nAChRs. Inhibition of several different nAChR subtypes was demonstrated, with the greatest potency shown for α6/α3β2 (IC_{50} 0.258 nM), α6/α3β4 (IC_{50} 1.54 nM), α3β2 (IC_{50} 5.72 nM), and finally α3β4 (IC_{50} 27.7 nM). Notably, it was discovered through kinetic studies that α-CTx BuIA can differentiate between rβ2 versus rβ4 containing nAChRs. It was shown that blockage of rβ2-containing nAChRs is quickly reversible (<10 min), while blockage of rβ4 containing nAChRs is slowly reversible (>25 min). With this knowledge of kinetic data, researchers designed mutant analogs of α-CTx BuIA to determine if selectivity with respect to potency, not just k_{off}, could be achieved. This led to the creation of the α-CTx BuIA [T5A, P6O] double mutant, which is ~200 fold more selective for the rα6/α3β4 nAChR (IC_{50} 58.1 nM) as compared to rα6/α3β2β3 nAChR, (IC_{50} >10,000 nM).[79] Figure 1.3 shows the differences in electrostatic surface between α-CTx MII [S4A, E11A, L15A], an analog of α-CTx MII that is highly selective for α6/α3β2β3-nAChR isoform discussed below,[91] and α-CTx BuIA [T5A, P6O] that exhibits different selectivity for the rα6/α3β2β3-nAChR isoform.

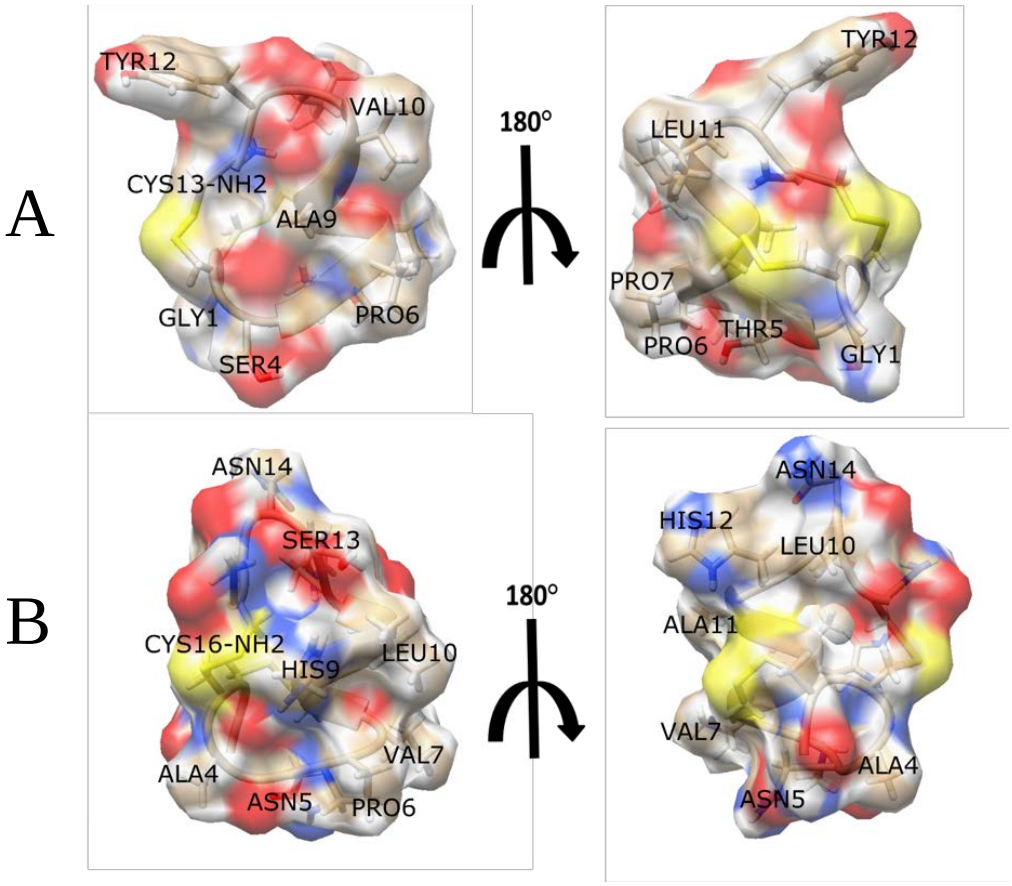

Figure 1.3. Differences in electrostatic topography for two conotoxins A) α-CTx BuIA and B) α-CTx MII [S4A, E11A, L15A] that exhibit different selectivity for nAChR subtypes. The increased positive charge, contributed by Asn14, His12 and His9, on α-CTx MII [S4A, E11A, L15A] as compared to α-CTx BuIA is thought to contribute to the different selectivity profile of these peptides (see Table 1.1). The negatively charged surface surrounding Tyr12, Thr5 and Ser4 of α-CTx BuIA is thought to contribute to binding affinity for α6α3β4-nAChR.

To understand how α-CTx BuIA differentiates between nAChR isoforms, another study mutated the rα4 subunit receptor residues 185-205 corresponding residues in the rα6 subunit.[104] Specifically, mutation of three rα4 residues—Y185, T187, R188—to the corresponding rα6 residues (K185, T187, and I188) showed ~2000-fold increase in α-CTx BuIA potency.

To explain the increase in peptide binding affinity, molecular modeling was used to build a model of BuIA bound to rα4-α6(185-188)-α4β2 extracellular domain from the

structure of the *Torpedo marmorata* AChR (PDB: 2BG9) and BuIA/AChBP co-crystal structure (PDB: 4EZ1) as the templates. While the potency profile implicates these residues, the molecular modeling experiment showed α-CTx BuIA binding more than 10 Å away from K185, D187, and I188. It was hypothesized that these critical three residues of the α6 subunit do not interact with BuIA directly, but instead potentially alter the structure and flexibility of the C-loop, which in turn may account for heightened potency. Figure 1.3 shows the sequence alignment of human α3, α4 and α6 subunits with conserved residues highlighted.

In order to enhance selectivity and potency toward inhibition of α3β4 nAChRs, α-CTx BuIA has been used as the framework for a PS-SCL experiment by Chang et al.[80] α3β4 nAChRs have been implicated in nicotine addiction and drug abuse, and potent and selective antagonists of these receptors may help elucidate the role of the receptors in these conditions.[105, 106] Chang et al. replaced six residues in the primary sequence of α-CTx BuIA with 22 natural and non-natural amino acids, while conserving the four cysteine residues, Gly1, Ser4, and Pro6. In total, 113,379,904 sequences were generated using the "tea bag" method with solid phase peptide synthesis (SPPS).[102] The initial screening was performed on 132 PS-SCL mixtures, each containing 5,153,632 compounds using the fluorescent membrane potential assay in HEK293 cells stably expressing either rat α3β4, α3β2, or α7 nAChRs.

A second generation of analogues was chosen based upon the two amino acid residues identified in each position that exhibited the greatest inhibition of α3β4 nAChR subtypes. The second-generation library consisted of 64 sequences, and screening was again conducted using the fluorescent membrane potential assay in α3β4 nAChRs

expressing HEK293 cells. Eleven sequences exhibited greater than 80% inhibition compared to 10 μM mecamylamine, which was the control treatment defined as 100% inhibition. Four compounds were further analyzed by competitive inhibition of [^{3}H]-epibatidine with α3β4 nAChR and α4β2 nAChR expressing HEK293 cells, with no significant binding to α4β2 nAChR observed. Ultimately, this experiment resulted in the discovery of the novel mutant peptide, named TP-2212-59, with the sequence α-CTx BuIA [T5H, P7B, A9F, V10B, L11Z], where B is 2-aminobutyric acid and Z is norvaline. Functional characterization of TP-2212-59 was undertaken using electrophysiology in *Xenopus* oocytes heterologously expressing α3β4, α3β2, or α7 nAChRs. The approach taken by researchers to mutate this non-selective conotoxin to selectively bind the target receptor, resulted in ~10-fold improvement in IC_{50} from 27.7 nM to 2.3 nM in α3β4 nAChRs. No inhibition was observed for α3β2 and α7 nAChRs at 10 μM, meaning a >1,000-fold selectivity for the α3β4 nAChR subtype had been established.

<u>α-CTx Lt1.3</u>

Recently, Chen, et al. identified and synthesized α-CTx Lt1.3, GCCSHPACSGNNPYFC.[81] They characterized the peptide with rα3β2 nAChR and found it to have an IC_{50} of 44.8 nM. As previously stated, smaller hydrophobic residues at position 10 in α-CTxs have been found to increase selectivity for rα3β2 nAChRs. It follows that Lt1.3 has Gly in position 10, and consequently selectively targets the rα3β2 nAChR isoform. The α-CTx Lt1.3 [S9A] mutant exhibits slightly enhanced potency, while [Y14A] has decreased potency by nearly five-fold. Given this level of nAChR activity adjustment, with minor primary sequence alteration, future characterization of this peptide is anticipated.

α-CTx TxIB

Native α-CTx TxIB, with sequence GCCSDPPCRNKHPDLC, is selective for rα6/α3β2β3 nAChRs (IC_{50} 28 nM).[82] This peptide demonstrated little or no inhibition of other tested nAChR subtypes at concentrations up to 10 μM. The [K11A] mutant of α-CTx TxIB exhibits selectivity for rα7 nAChRs with an IC_{50} of 200 nM.[83] While most α-CTxs have a hydrophobic patch in loop 1, the hydrophobic patch in TxIB, composed of only the four amino acids SDPP, is comparatively smaller. TxIB has two patches of positive charge character on either side of its hydrophobic patch. When rβ4 rather than rβ2 was co-expressed with α6/α3, inhibition by TxIB dropped by 400-fold, indicating that slight residue differences between homologous β2 and β4 subunits significantly influence binding.[83] Similarly, when α3 rather than α6/α3 was co-expressed with β2, antagonism by TxIB was 400-fold lower, indicating that slight residue differences between homologous α6 and α3 nAChR subunits also significantly influence binding.

Yu et al. studied TxIB binding with hα7 and rα7.[83] The ligand binding domain sequence of rα7 differs from the ligand binding domain sequence of hα7 by only 10 residues. The α-CTx TxIB [K11A] mutation (in loop 2) improved the potency towards rα7, but not hα7. Computer models of toxins complexed with a hα7-AChBP chimera indicate the importance of Arg185 to this result: receptor mutation R185K drastically decreased the activity of α-CTx TxIB [K11A] to inhibit rα7, whereas the inverse R185K mutation in hα7 essentially conferred onto hα7 the affinity level of rα7. The importance of R185 has also been implicated in modeling studies of PnIA [A10L, D14K] and ImI with hα7.

α-CTx GIC

α-CTx GIC, GCCSHPACAGNNQHIC, has a nearly identical sequence to Lt1.3 [S9A], differing by only the last four C-terminal residues.[84] α-CTx GIC inhibits hα3β2, hα4β2 and hα3β4 nAChRs, with IC_{50} values of 1.1 nM, 309 nM, and 755 nM, respectively. As with TxIB, the hydrophobic patch in GIC is comparatively smaller than most α-CTxs, suggesting GIC may have high selectivity for hα3β2. Indeed, GIC has remarkably high potency for hα3β2 nAChR isoforms (IC_{50} ~1 nM), compared to its next closest rival α-CTx MII, which has been the model antagonist for this receptor with an IC_{50} of 0.5 nM.[93] GIC and MII share identical m-loops but differ in seven out of eight residues in the n-loop, such that GIC is significantly more hydrophilic than MII.

Lin et al. built a model of the rα3β2 nAChR with bound GIC, based on the crystal structure of GIC bound to *Ac*-AChBP as a template (PDB: 5CO5), and proposed the key binding interactions between ligand and receptor.[85] Compared with TxIA [A10L] and ImI, GIC does not contain the same Arg5 or Trp10 residues conferring rα3β2 nAChR selectivity, but rather His5 (on the principal side of the receptor binding interface) and Gln13 (on the complementary side) in the homologous positions. According to this model, the residues in GIC that are most likely to interact with rα3β2 are His5, Ala7, Asn11, Asn12, and Gln13. An alanine scan was performed on various residues (H5A, A7G, A7L, N11A, N12A, and Q13A) that concluded all mutations except Q13A decreased activity with rα3β2. The model showed Gln13 of GIC surrounded by Glu61, Val111, Ser113, Ser117 and Phe119 of the rβ2 subunit. The corresponding residues in rβ4 are Glu62, Ile113, Arg115, Ser119 and Leu121; these are all the same or similar residues as those found in rβ2 except for Arg115. It is suspected that the long side chain of Arg115 may decrease the

activity with GIC in the rα3β4 nAChR subtype due to steric hindrance with Gln13 in GIC. Other interactions identified by the authors were between Asn11 of GIC and Asp152 in the rα3 subunit, and between His5 of GIC and three tyrosine residues (Tyr93, Tyr190 and Tyr197) in the rα3 subunit. Indeed, α-CTx GIC [H5A] showed decreased activity with rα3β2, likely from an absence of the tyrosine interactions.

α-CTx TxID

α-CTx TxID with sequence GCCSPHVCSAMSPIC, is a α-4/6-CTx identified from the genomic DNA of *Conus textile* that inhibits rα3β4, rα6/α3β4 and rα2β4 with IC_{50} values of 12.5 nM, 94 nM and 4.5 μM, respectively.[86] A series of activity assessment experiments for TxID were performed, similar to those described for TxIB.[81] By replacing rβ2 for rβ4 during co-expression with rα3, it was found that TxID potency was >800-fold lower, indicating that slight residue differences between highly homologous β2 and β4 subunits significantly influence binding, although the specific receptor residues involved in binding remain to be elucidated. Similarly, when α4 rather than α3 was co-expressed with β4, potency was >1000-fold lower, again indicating that amino acid residue differences between homologous α3 and α4 (for example, residues 148 and 196) significantly influence binding. TxID has a three amino-acid sequence of SHP in loop 1, which is present in several other α-CTxs with differing nAChR selectivity. Conversely, loop 2 of TxID contains the five amino-acid sequence SAMSP, which is not found in other pharmacologically tested α-CTxs and may be important for the unique selectivity and potency for rα3β4 nAChR exhibited by TxID.

Wu et al. performed an alanine screen to evaluate analog selectivity for rα3β4 and rα6/α3β4 and found that α-CTx TxID [S9A] had the greatest selectivity for rα3β4 as

compared to rα6/α3β4.[59] They found that S9A did not inhibit a range of other nAChR subtypes at a threshold of 10 μM, including α7, α9α10, α1β1δε, α2β2, α2β4, α3β2, α4β2, and α4β4. α-CTx TxID [S9A] appears to have a more tightly coiled α-helical between P6 and A10 as compared to native TxID. By contrast to Ser9, the hydroxyl group of Ser4 is not involved in any perceived interaction with the rα3β4 binding site, and S4A mutation was predicted to have no impact, which was consistent with experimental IC_{50} measurement of 10.8 nM compared to 3.6 nM for native TxID. Another mutation, α-CTx TxID [M11I], achieved preferential binding for rα6/α3β4 over rα3β4. According to the model produced by Wu et al of TxID in the binding pocket of the rα3β4 and rα6β4 nAChR interfaces (a homology model based on the crystal structure of AChBP bound to a TxIA variant, and the crystal structure of hα9 [PDB: 2UZ6]), Met11 contacts Cys218 of the α3 C-loop and [M11A] would be expected to result in a change of binding mode, due to the steric hindrance induced by the larger Met11 side chain is relieved. By contrast, M11I would not be expected to create a significant steric clash with α6 in the rα6β4 model, suggesting that this mutation would not be detrimental to rα6β4 binding. Indeed, α-CTx TxID [M11I] resulted in 20-fold decreased potency with rα3β4 but did not reduce inhibition of rα6/α3β4.

Yu, et al took previous α-CTx TxID studies further by mutating Ser9 with a series of 14 different amino acids.[60] The α-CTx TxID [S9K] mutant exhibited the greatest selectivity for rα3β4 over rα6/α3β4 of all the variations tested. The ligand binding domains of rα3β4 and rα6β4 with native TxID differ by only α subunit positions 148 and 196, where 196 is a bulkier Gln in α3 and a less bulky Thr in α6. The bulkier Gln196 interacts with the β8 strand of the α3 subunit, “pushing” the C-loop and TxID further toward the bottom of

the orthosteric binding site than in the TxID−rα6β4 model, resulting in a shift of the location of Ser9 in TxID to be within the binding site. In the TxID−rα3β4 model, the Ser9 side chain does not contact the β-strands of the β4 subunit, and the binding cavity is partly solvated, suggesting Ser9 substitution with an Ala or a long side chain amino acid, such as Lys or Arg, should be well accepted. The mutation data obtained by Yu et al. indeed show that Ser9 substitutions with Ala, Lys, or Arg are innocuous to rα3β4 binding. The Ser9 side chain of TxID in the TxID−rα6β4 model faces a positively charged Lys81 in β4 and is also in close proximity to a negatively charged Glu58 in β4. Substitution of Ser9 with a charged residue is expected to result in charge repulsion with either Glu58 or Lys81 of the β4-subunit. Additionally, in the TxID−rα6β4 nAChR complex, the Ser9 side chain of TxID establishes a hydrogen bond with the β4 Lys81 side chain. Indeed, Ser9 mutation to a charged residue such as Asp, Lys, or Glu shows a >300-fold decrease in rα6β4 activity in all three cases.

α-CTx GID

Native α-CTx GID, IRDγCCSPNACRVNNOHVC, was originally isolated by assay-directed fractionation from the crude venom *Conus geographus*.[87] The primary sequence is notable for the four-residue extended N-terminus, the post-translationally modified residues γ-carboxyglutamate (γ) and hydroxyproline (O), and because GID does not contain the amidated C-terminus typical of most α-CTxs. α-CTx GID was shown to inhibit rat α3β2, α7, and α4β2 with IC_{50} values of 3.1 nM, 4.5 nM and 152 nM, respectively. Deletion of the extended N-terminus decreased activity at α4β2 (IC_{50} 670 nM) but did not significantly decrease activity at α3β2 (IC_{50} 4.6 nM) or α7 (IC_{50} 5.5 nM). To determine the residues that are important for α-CTx GID inhibition of rat α3β2, α4β2, and α7 nAChRs,

alanine-scanning mutagenesis was employed.[107] Asp3, Arg12, and Asn14 were determined to be critical for inhibition of α7, while Pro9 was essential for α3β2 nAChR inhibition. More recently, Banerjee et al. measured α-CTx GID antagonist activity of rα3β2 and rα4β2 nAChRs, with IC_{50} values of 36 and 4800 nM, respectively using fluorescent membrane potential assays in HEK293 cells expressing rat nAChRs.[55] With the goal of obtaining further insights into α-CTx GID/nAChR interactions that could lead to the design of GID analogues with improved affinity for α4β2 nAChRs, a homology model of GID bound to hα4β2 was constructed. The model was created using an X-ray co-crystal structure of a PnIA variant bound to *Ac*-AChBP as a template (PDB: 2BR8). The models created by Banerjee et al. show that Asp3, Arg12, and Asn14 in α-CTx GID are required for binding the hα4β2 nAChR. Close proximity between the side chains of Arg2 and E189, the side chain of Asp3 and the backbone NH atom of Y188, and the side chains of Glu4 and R186 and K143 were observed. Banerjee et al. synthesized mutants of these key charged GID residues to either a smaller, less bulky, side chain or a neutral side chain, both to abolish the respective receptor-peptide interaction. Each mutation resulted in loss of activity for hα4β2 and/or hα3β2, indicating the importance of these interactions in receptor binding. The negatively charged carboxylate side chain of GID Glu4 is suspected to form salt bridges with the positively charged side chains of R186 and K143 residues in the α4 binding pocket. The α-CTx GID [E4Q] mutation introduced electrostatic repulsion between the amide hydrogen atoms of the Gln4 side chain and the positively charged R186 and K143 side chains. Additionally, Ser7 is in proximity for formation of a hydrogen bond between its side chain hydroxyl group and both the S36 hydroxyl and D169 carboxyl

groups of the β2-subunit, explaining the decreased potency of α-CTx GID [S7A] with hα4β2.

Steric hindrance frequently overwhelmed many of the hypotheses made by Banerjee, et al.[55] For example, the model produced by Banerjee et al. with hα4β2 also shows Val13 of GID in proximity to a cluster of aromatic residues consisting of F104 in the β2-subunit and W118 and W147 in α4-subunit, but mutation to aromatic residues decreased activity with hα4β2, presumably due to unfavorable steric interactions. Additionally, the Ala10 side chain of GID is oriented toward a polar pocket in the hα4β2 in such a way that mutation of Ala10 to serine or threonine may establish an interaction with the backbone carbonyl of S146 in α4, but the α-CTx GID [A10T] mutation resulted in loss of activity for both hα4β2 and hα3β2, which is attributed to steric hindrance of the β-methyl group of Thr10. Conversely, the α-CTx GID [A10S] mutation had comparable potency with hα4β2 and a 10-fold decrease in potency with hα3β2, indicating position 10 may still play an important role in determining the selectivity of GID between hα4β2 and hα3β2. Banerjee reported other important interactions including a polar contact between Asn15 and Y195 in α4, and a salt bridge between Arg12 and E59 in β2, suggesting α-CTx GID [R12A] would eliminate a key binding interaction. Indeed, this is observed experimentally, resulting in a more than three-fold increase in the IC_{50} for rα3β2, an almost 10-fold increase in the IC_{50} for rα7, and a loss of activity with rα4β2.[107]

The α-CTx GID [V18N] mutation exhibited comparable activity with rα4β2 (IC_{50} 1.85 μM) to the native peptide (IC_{50} 4.8 μM), while the [V18Q] mutation eliminated inhibitory activity for both rα4β2 and rα3β2. Banerjee et al. explains this result by suggesting the longer glutamine side chain experiences greater steric hindrance upon

binding as compared to the shorter side chain of asparagine. Important to note is that the GID [V18N] mutation exhibited no activity with rα3β2, indicating position 18 is essential for determining selectivity between rα4β2 and rα3β2. α-CTx GID [V18N] is the most selective α-CTx for rα4β2 over rα3β2 identified to date, with an IC_{50} of 1.85 μM and >100 μM, respectively. The hα4β2 model created by Banerjee et al. rationalizes the observed selectivity for rα4β2, showing a potential hydrogen bond interaction between the Asn18 amide in GID [V18N] and the hydroxyl group of Y195 of the α4 subunit, which is not present in hα3β2. This interaction seems to shift the position of the C-loop in the binding site of hα4β2 compared to hα3β2.

α-CTx GID inhibition of α4β2 nAChR was recently used for the development and validation of a docking algorithm integrated into ToxDock.[88] ToxDock uses ensemble-docking and conformational sampling to dock α-CTxs to nAChR homology models. The objectives of this study were to determine if an algorithm could perform two functions: (1) accurately dock α-CTx GID to the α4β2 nAChR by accounting for the conformational flexibility of these complexes, and (2) discover new α-CTx GID derivatives with functionally enhanced affinity or selectivity for α4β2 nAChRs. Three bioactive GID mutants (A10V, V13I, and V13Y), predicted by virtual screening using ToxDock, were experimentally validated. ToxDock employs two existing protocols in the Rosetta macromolecular suite,[108] Rosetta FastRelax and Rosetta FlexPepDock,[109, 110] to provide extensive conformational sampling of both the nAChR homology model and the conotoxin to refine models of these complexes. The α4β2 nAChR extracellular domain dimer was generated using Modeller version 9.11 based upon the X-ray structures of AChBP from *A. californica* in complex with the α-CTxs PnIA [A10L, D14K] (PDB: 2BR8), ImI (PDBs:

2C9T, 2BYP), BuIA (PDB: 4EZ1), and TxIA [A10L] (PDB: 2UZ6).[47, 48, 111-113] Docking and virtual screening of α-CTx GID and its analogs were based upon the NMR structure of α-CTx GID (PDB: 1MTQ).[107] To generate α-CTx GID analogs, non-conserved, hydrophobic, and buried GID residues were identified as candidates for mutation. The authors identified two residues, Ala10 and Val13 of α-CTx GID as promising candidates for point mutations. Based upon these two candidate residues, a library of 256 GID point mutants was prepared in silico using PyRosetta.[114] ToxDock was used to refine the α-CTx/α4β2 nAChR complexes. Twenty-five percent of the GID mutants were predicted to be active at the α4β2 nAChR, and the four mutants, [A10V], [A10Q], [V13I] and [V13Y] were selected for synthesis and experimental characterization. The α-CTx GID [A10Q] mutant was predicted to be inactive, while the other mutants were predicted to be active at the α4β2 nAChR subtypes. Pharmacological characterization was performed using the fluorescent membrane potential assays in HEK cells stably expressing human α7, α3β2, α3β4 or α4β2 nAChR subtypes. Electrophysiology was also conducted in *Xenopus* oocytes expressing human α4β2 nAChR subtypes. Two of the three α-CTx GID analogs identified by the virtual screening, GID [A10V] and GID [V13Y], had reduced activity at the human α7 nAChR without diminished activity at the α4β2 nAChR. The IC_{50} of α-CTx GID [A10V] and α-CTx GID [V13Y] were measured at 30 μM and 3 μM, respectively, for the α4β2 nAChR subtypes, while the wild type IC_{50} was demonstrated to be 3 μM. However, the IC_{50} for the α7 nAChR were observed to be diminished, with GID [A10V] measured at >10 μM, and α-CTx GID [V13Y] measured at 4 μM, compared to wild type IC_{50} of 0.1 μM. Activity was maintained in the α-CTx GID [V13I] mutant at both receptor subtypes, with IC_{50} values of 8 μM and 0.2 μM, for the α4β2 and α7 nAChR subtypes, respectively.

Potency was maintained at the α3β2 nAChR subtype for all three active mutants, with IC_{50} ranging from 1-3 nM, which is slightly more potent than the wild type, measured at 10 nM. This study demonstrated the feasibility of a predictive computational screening and experimental validation for the identification of novel α-CTx mutants with enhanced selectivity for a nAChR subtype. Further application of this approach could be used for additional peptide toxins and their ion channel targets.

α-CTx PnIA

α-CTx PnIA is a 16 amino-acid peptide originally isolated from the venom of *Conus pennaceus*.[115] Pharmacological characterization of α-CTx PnIA in *Xenopus* oocytes expressing rα3β2 and rα7 nAChRs demonstrated IC_{50} of 9.56 and 252 nM, respectively. The single mutation α-CTx PnIA [A10L] resulted in an altered receptor affinity with IC_{50} values of 12.6 nM for rα7 and 99.3 nM for rα3β2.[89] The finding that the subtle change in the hydrophobic side chain at position 10, from Ala to Leu, significantly altered receptor affinity was corroborated by additional studies.[116, 117] Modification to the structural characteristics at the Ala10 position through the incorporation of natural and non-natural amino acids, focusing on linear and branched aliphatic or aromatic residues provided detailed insights to the distinctions between the binding pockets of α3β2 and α7 nAChRs.[90] These receptor differences were further explored using electrophysiology measurements in *Xenopus* oocytes expressing either rat or human α3β2 and α7 nAChRs, and by evaluating affinity for α7 nAChRs using rat brain homogenate and measuring displacement of ^{125}I-α-bungarotoxin, which is known to bind selectively to the α7 nAChR subtype.[118] Polar and aromatic substitutions at Ala10 residue were found to result in a large reduction in affinity for both receptor subtypes. Molecular docking using the program AutoDock indicated

hydrophobic interactions with several α7 and α3β2 receptor residues via a hydrophobic funnel that is capable of accommodating linear and branched side chains, but not aromatic chains. Extending the Ala10 to norleucine (Nle) resulted in an increased binding affinity at both α7 and α3β2 receptor subtypes, with observed IC_{50} values of 4.3 nM and 0.7 nM, respectively. The α-CTx PnIA [A10Nle] mutation reverted selectivity back to the α3β2 nAChR. The binding affinity of the A10Nle was determined to be 44 nM as determined by ^{125}I-α-bungarotoxin radioligand competition studies of rat brain homogenate. Further lengthening the Ala10 side chain beyond the Nle mutant through the incorporation of amino heptanoic acid (Aha) or amino octanoic acid, extensions of one or two carbon-carbon bond lengths, respectively, resulted in decreased affinity for the α7 nAChR isoform of 136 nM and 756 nM, respectively. This study demonstrated that a single mutation to α-CTx PnIA [A10L] flips its selectivity profile from the α3β2 nAChR to the α7 nAChR, and showed the placement of a single methyl group can drastically alter binding affinity of the toxin. The impact of this finding is valuable detailed structure information about the α7 nAChR binding pocket, which may inform the development of more selective ligands in the future. This study also demonstrated the utility of computational experiments in understanding the molecular basis for ligand selectivity between α7 and α3β2 nAChRs, where the residue located at the equivalent position to R208 in α7 (equivalent to I186 in α3) is one of the key determinants for ligand selectivity.

α-CTx PnIA was recently used as a starting point to design mutants with enhanced affinity for α7 nAChR using protein surface topography (PST).[119] PST is a computational method used to understand ligand/receptor interactions that addresses bioactive peptides and their targets as interacting surfaces.[120] Ligand surfaces are simplified and transformed

into a machine-tractable format of 2D projection maps, which enable group analysis and produce a pattern that defines activity/selectivity for a group of molecules. The PST approach was initially used to study neurotoxic peptides from scorpion venom.[121] The extension of PST to α-CTxs inhibiting the α7 nAChR benefits from the considerable number of 4/7 α-CTxs identified and structurally characterized that are available to be used for structure-function analyses aimed at mapping ligand pharmacophores. The PST computational strategy began by establishing a database of 39 α-CTxs known to block α7 nAChRs and dividing this database into three groups based upon inhibition activity: "good" (IC_{50} < 16 nM), "average" (IC_{50} 39-390 nM), and "bad" (IC_{50} > 390 nM). A structural database was generated for the 39 α-CTxs either obtained from the PDB or built using homology modeling, and 2D spherical maps were generated of hydrophobic and electrostatic properties distributed over the peptide surface using PST.[119] Correlation of the relationship between the activity and properties of each α-CTx that was visualized in the 2D spherical maps resulted in group-averaged maps for the "good" and "bad" groups were generated. Differential maps were constructed to emphasize the prominent differences between "good" and "bad" groups, and these results were used to inform the design of α-CTx PnIA variants. Three α-CTx PnIA analogs were synthesized: PnIA [A9R], PnIA [A9R, A10L], and PnIA [L5R, A9R, A10L, D14R]. The L5R, A9R, and D14R mutations were chosen because of the observation that "good" 2D spherical maps contained more positive electrostatic potential compared to "bad" maps, and the A10L mutation was chosen due to literature precedent for increased α7 nAChR affinity.[89, 116, 117] The three PnIA analogs were synthesized and pharmacologically characterized using radioligand analysis and electrophysiology. The competitive radioligand assay with [^{125}I]-labeled α-Bgt and

[^{125}I]-labeled PnIA analogs were conducted in GH4C1 cells transfected with human α7 nAChR, and electrophysiology was conducted using two-electrode voltage clamp in *Xenopus* oocytes following rat α7 nAChR cDNA injection. The IC_{50} values for the three mutants were ~20 nM each, demonstrating high affinity binding to the α7 nAChR isoform. However, native α-CTx PnIA was not evaluated in this study, so a direct effect of these mutations on the potency of PnIA cannot be concluded. This study demonstrated that the PST approach can be applied to α-CTxs and may provide another computational strategy to design highly active and selective compounds for other nAChR subtypes.

α-CTx MII

α-CTx MII, originally isolated from the venom of *Conus magus,* is a 16 amino-acid peptide with the sequence GCCSNPVCHLEHSNLC.[93] α-CTx MII has a reported IC_{50} for the rα3β2 nAChR isoform of 0.5 nM as determined by electrophysiology voltage clamp experiments in *Xenopus* oocytes expressing rat α3β2 nAChRs. Alanine-screening of α-CTx MII identified three residues, Asn5, Pro6, and His12, as key to the potency of α-CTx MII, with diminished activity of >2,700-fold, 700-fold, and >2,700-fold, respectively for the single site mutants.[95] Shortly after the high affinity of α-CTx MII for the rα3β2 nAChR subtype was reported, the single site mutant, α-CTx MII [E11A] was shown to exhibit preferential binding for α6/α3β2β3 nAChR isoforms compared to α3β2 nAChR isoforms, with IC_{50}s of 0.160 nM and 8.72 nM, respectively, with an observed preference for α6/α3β2β3 of >50-fold.[35, 36, 122] The double mutant α-CTx MII [H9A, L15A], was found to be even more selective for α6/α3β2β3 versus α3β2, with IC_{50} values of 2.40 nM and 4850 nM, respectively, a 2020-fold preference for α6/α3β2β3 nAChRs. α-CTx MII [E11A, L15A] also demonstrated ~100-fold preference for the α6/α3β2β3 versus α6/α3β4

nAChRs, with an observed IC_{50} for the later of 269 nM. Through mutagenesis experiments of both the α-CTx MII ligand and the α3β2 nAChR isoform, the residues that play a critical role in CTx ligand binding to the α6 containing nAChRs were speculated to be E152, D184, K185, I188, and T195.[91] The α-CTx MII triple mutant, α-CTx MII [S4A, E11A, L15A] has been shown to block a chimeric receptor α6/α3β2β3 nAChR (IC_{50} = 1.2 nM) with threefold less potency than native α-CTx MII (IC_{50} = 0.39 nM), but also blocked the α3β2 nAChR isoform with >600-fold lower affinity (IC_{50} = 1400 nM) than native α-CTx MII (IC_{50} = 2.18 nM). These combined alanine substitutions resulted in mutant with >1000-fold preference for α6/α3β2β3 vs the α3β2 nAChR isoform. The potency of α-CTx MII to intact pentameric transmembrane spanning α3β2 nAChRs has been determined to require interaction with K185 and I188 residues on the α3 subunit of the receptor.[123] These two residues are present in both α6 and α3 subunit proteins, necessitating additional investigation into root determinants of α-CTx differentiation between the α3 and α6-containing nAChR isoforms. Figure 1.4 shows the sequence alignment of α3, α4, and α6 subunits with conserved residues highlighted in green for human nAChR proteins. Through mutating site-specific residues of the α3 subunit into the counterpart residues of the α6, it has been shown that E152, D184, and T195 play a critical role in ligand differentiation between α3β2 and α6β2 nAChR isoforms.[79] The triple mutant, α-CTx MII [S4A, E11A, L15A], showed ~150-fold increase in affinity to the α3 [K152E, E184D, Q195T] triple mutant as compared to the native α3 receptor (IC_{50}s of 9.7 nM and 1400 nM, respectively). The three order of magnitude preference for α6/α3β2β3 vs the α3β2 displayed by α-CTx MII [S4A, E11A, L15A] resulted in a CTx that can clearly differentiate between these closely related nAChR subtypes.

A subsequent study aimed to alter α-CTx MII to achieved higher affinity and specificity for α6β2 containing nAChR subtypes by identifying amino acid residues in the primary sequence of α-CTx PIA (RDPCCSNPVCTVHNPQIC) that could alter the binding profile of MII.[124] α-CTx PIA was cloned from DNA isolated from the hepatopancreas of *Conus purpurascens* using PCR primers for the 3′ end of the intron preceding the toxin region of the toxin prepropeptides and the 3′ untranslated region sequence of the α-prepropeptides.[125] α-CTx PIA was the first CTx found to discriminate between α6-containing and α3-containing nAChRs, with IC_{50} values for rα6/α3β2β3, hα6/α3β2β3, rα6/α3β2 and rα3β2 of 0.95 nM, 1.72 nM, 0.69 nM, and 74.2 nM, respectively, as determined by electrophysiology in *Xenopus* oocytes heterologously expressing nAChRs. α-CTx PIA has an N-terminal RDP sequence, and to determine if this extended N-terminus is important in α6β2 selectivity, the hybrid peptide RDP-MII was synthesized. Additionally, docking studies suggested the importance of Glu11 in MII that may determine α6β2-containing vs α3β2-containing nAChR selectivity. Both the α-CTx MII [E11R] and RDP-MII [E11R] were synthesized, and their binding affinity was evaluated in native rα6β2-containing nAChRs isolated from rat brain striatum, and in native rα3β2-containing nAChRs isolated from rat brain superior colliculus, and measured by displacement of [^{125}I]-epibatidine. K_i for native α-CTx MII was determined to be 5.6 nM and 62 nM for α6β2-containing and α3β2-containing nAChRs, respectively. The RDP-MII hybrid peptide demonstrated a 13-fold increased affinity for α6β2-containing nAChRs (K_i 0.43 nM), but similar affinity for α3β2-containing nAChRs (K_i 50 nM). The α-CTx MII [E11R] mutation did not alter affinity for α6β2-containing nAChRs (K_i 50 nM), but drastically reduced binding affinity for α3β2-containing nAChRs (K_i 4230 nM). The RDP-

MII [E11R] resulted in enhanced binding to α6β2-containing nAChRs, with a K_i of 0.9 nM, and drastically reduced affinity α3β2-containing nAChRs, with a K_i of 4410 nM. The results of this study were discovery of the novel RDP-MII [E11R] and MII [E11R] analogs selective for α6β2-containing nAChRs, and demonstration of the utility of CTx mutagenesis based on the detailed examination of the primary sequence of other CTxs.

Figure 1.4. α-Subunit sequence alignment for human nAChRs; α4 and α6 have 60.00% sequence homology, α4 and α3 have 61.43% sequence homology, and the α6 and α3 have 66.67% sequence homology. Homologous residues are highlighted in green. Stars are placed above residues that were mutated to assess the influence of residues of the α4 versus α6 responsible for the selectivity of α-CTx BuIA.

Our collaborator, Dr. Tim Andersen, and his students have developed an algorithm to search exceptionally large mutant libraries for sequences with optimal binding affinities for ion channel receptors.[126] The Genetic Algorithm Managed Peptide Mutant Screening (GAMPMS) program was used to search an α-CTx MII mutant library composed of approximately 41 billion possible peptide sequences for those peptides exhibiting the

greatest binding affinity for the α3β2 nAChR subtype. GAMPMS is a genetic algorithm designed for comprehensive structure-based high throughput virtual screening of very large mutant libraries.[10] Genetic algorithms have found utility in computational and combinatorial chemistry applications.[127-130] GAMPMS uses the popular AutoDock 4.0 molecular docking software to provide fitness scores and uses the results of previous docking jobs to make an informed decision as to which mutations increase or decrease peptide binding affinity.[131, 132] The use of AutoDock 4.0 additionally provides the added advantage of making the molecular docking results reproducible by other researchers. GAMPMS and the additional ancillary programs have been integrated into the open source DockoMatic v 2.1 software package, making this methodology readily available to the research community.[133] The α-CTx MII sequence was used as the base sequence for mutation, with Cys2, Cys3, Pro6, Cys8, and Cys16 residues being conserved during these simulations because of their importance in maintaining the molecular scaffold of the native peptide. The remaining 11 residues in α-CTx MII were constrained to mutations that maintained the polar/nonpolar character at each residue. Therefore, Ser4, Asn5, His9, Glu11, His12, Ser13, and Asn14, were mutated into any polar or charged amino acid excluding cysteine, and nonpolar residues Gly1, Val7, Leu19 and Leu15 residues were mutated to any nonpolar amino acids excluding proline. The result of these mutations was a large library consisting of 40.96 billion possible peptide sequences. Three-dimensional peptide mutant structures were generated by copying the coordinates of the mutable residue and two adjacent residues into a new pdb file, removing the side chain atoms of the mutable residue from the generated tripeptide pdb file, adding the substituted side chain atoms, submitting the peptide analogue to TreePack, and grafting the modified peptide segment

back into the original ligand pdb file. TreePack determines the appropriate orientation of the new side chain to eliminate side-chain spatial overlaps.[134] The fitness of an individual sequence is determined by the AutoDock score produced when the ligand is docked against the target receptor. The receptor structure used in the docking calculations was a homology model of the α3β2-nAChR isoform constructed from the amino acid sequences of the α3 and β2 subunits of rat neuronal nAChR using the *Torpedo marmorata* nAChR X-ray structure (PDB: 2BG9) as a structural template.[44] The homology models were created using the DockoMatic v 2.1 and MODELLER packages.[100, 133] In the GAMPMS workflow, three genetic operators derived from the natural evolutionary processes of elitism, crossover, and mutation are used in determining peptide sequences with the highest "fitness," which is binding affinity in this context. In determination of binding affinity, forty pose evaluations were used in the AutoDock docking simulation for ligand/receptor binding. Because of uncertainty in values of predicted binding free energies from molecular docking scoring functions, the best indicator that a side-chain mutation resulted in a beneficial effect on the predicted binding affinity is not the docking score directly but rather the conservation of any particular mutation that is observed among a population exhibiting the best docking scores. The conservation of residues across the peptides with the highest binding affinities was used to determine the final top sequence. The residue occurring with the highest frequency in the top 50 peptides, with all residues having a conservation of at least 50%, was included in the consensus sequence: WCCSYPGCYWSSSKWC. This consensus sequence, given the trivial name KTM, was subjected to further investigation and validation using molecular dynamics (MD) simulations and compared to sequences with known binding affinities with the α3β2 nAChR isoform. MD simulations were performed

using the GROMACS 5.0.4 software package with the AMBER03 force-field parameter set.[135-140] The GAMPMS-derived molecular docking results were used as the input structures for the MD simulations. The calculated ΔGbind for KTM was −45.59 kcal/mol, which is more than double that of MII at a predicted ΔGbind of −20.42 kcal/mol. The binding free energies of the reference PnIA and TxIA peptides were -31.53 kcal/mol and -32.20 kcal/mol, respectively. Although the calculated binding free energies of PnIA and TxIA are difficult to correlate with that of MII in absolute terms since there is no direct translation between ΔGbind and experimentally obtained IC_{50} values, the relative ΔGbind is in agreement with experimental results showing the significant predicted enhancement in binding affinity of these peptides for the rα3β2 nAChR.[112] Figure 1.5 shows a comparison between the 3D structures of α-CTx MII and KTM.

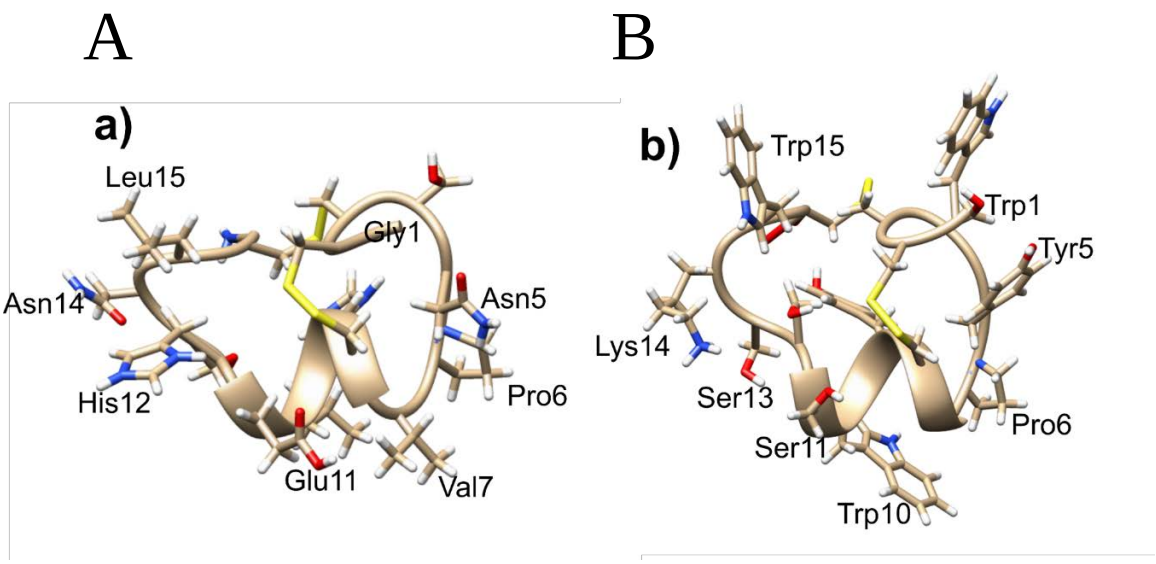

Figure 1.5. Structural comparison between A) α-CTx MII and B) the computationally predicted structure of KTM. Select amino acids are labeled. The backbone scaffold is predicted to be maintained by conserving the structurally important cysteine and proline residues. The cysteine pattern in both peptides is C1-C3 and C2-C4.

The GAMPMS protocol was used in this study to produce an α-CTx MII analogue with computationally predicted optimal binding to the rα3β2 nAChR by heuristically searching a vast set of amino acid residue combinations. The resulting consensus mutant peptide, KTM, was shown to have considerably higher binding affinity for the α3β2 nAChR than the precursor α-CTx MII peptide. However, the assumption that the allowed mutations would not alter the secondary structure of the α-CTx MII template is dubious, and the correlation between binding affinity and IC_{50} requires experimental validation to confirm channel pore influence. The KTM peptide was synthesized for structure and bioactivity evaluation.

Conclusions

The work described herein exemplifies the value of conotoxins as molecular probes to understand the delicate intricacies of nAChR isoform selectivity and inhibition of channel pore proteins required to develop treatments for neurological disorders. Despite the large number of α-CTxs that have been characterized, either through isolation from *Conus* venom, or synthesis based on sequences identified in *Conus* transcriptomes, designing potent and selective ligands for a particular nAChR subtype is still a challenge. The purpose of this chapter was to summarize strategies undertaken by researchers to alter the primary sequences of α-CTxs to enhance their affinity and selectivity for particular nAChR subtypes. Numerous examples of alanine scanning mutagenesis were illustrated. Mutagenesis inspired by detailed comparison of the primary sequence of several CTxs was illustrated in the examples of PeIA[42] and the MII.[124] Mutation of multiple amino acids through positional scanning synthetic combinatorial libraries was illustrated for ImI[103] and BuIA.[80] Particular attention was paid to novel computational strategies that hold promise

in limiting the cost and time required to develop more potent and selective α-CTx analogs, such as the novel ToxDock program used to introduce mutations to GID,[88] the Protein Surface Topography approach used for PnIA,[119] and the Genetic Algorithm Managed Peptide Mutant Screening utility in DockoMatic used for extensive mutation of MII.[126] Collectively, the work summarized in this chapter demonstrates the unique value provided by conotoxins to enhance our understanding of complex molecular systems.

CHAPTER TWO: QUALITATIVE ASSAY TO DETECT DOPAMINE RELEASE BY LIGAND ACTION ON NICOTINIC ACETYLCHOLINE RECEPTORS

Published in *Toxins* (Open access)

Leanna A. Marquart,[1] Matthew W. Turner,[2] and Owen M. McDougal[1]

[1] Department of Chemistry and Biochemistry, Boise State University

[2] Biomolecular Sciences Graduate Programs, Boise State University

A pheochromocytoma of the rat adrenal medulla derived (PC12) cell-based assay for dopamine measurement by luminescence detection was customized for the qualitative evaluation of agonists and antagonists of nicotinic acetylcholine receptors (nAChRs). The assay mechanism begins with ligand binding to transmembrane nAChRs, altering ion flow into the cell and inducing dopamine release from the cell. Following release, dopamine is oxidized by monoamine oxidase generating hydrogen peroxide that catalyzes a chemiluminescence reaction involving luminol and horseradish peroxidase, thus producing a detectable response. Results are presented for the action of nAChR agonists (acetylcholine, nicotine, and cytisine), and antagonists (α-conotoxins (α-CTxs) MII, ImI, LvIA, and PeIA) that demonstrate a luminescence response correlating to the increase or decrease of dopamine release.[141] A survey of cell growth and treatment conditions, including nerve growth factor, nicotine, ethanol, and temperature, led to optimal assay requirements to achieve maximal signal intensity and consistent response to ligand treatment. It was determined that PC12 cells treated with a combination of nerve growth

factor and nicotine, and incubated at 37°C, provided favorable results for reduction in luminescence signal upon treatment of cells with α-CTxs. The PC12 assay is intended for use as a fast, efficient, and economic qualitative method to assess the bioactivity of molecules that act on nAChRs, in which testing of ligand-nAChR binding hypotheses and computational predictions can be validated. As a screening method for nAChR bioactivity, lead compounds can be assessed for their likelihood of exhibiting desired bioactivity prior to being subjected to more complex quantitative methods such as electrophysiology, or live animal studies.

Keywords: PC12 cells; alpha-conotoxin; nicotinic acetylcholine receptor; dopamine; luminescence assay

Introduction

Nicotinic acetylcholine receptors (nAChRs) are pentameric transmembrane proteins present throughout the nervous system, brain, and muscle. Neuronal nAChRs are involved in critical brain functions, and have been implicated in a variety of neurological diseases and disorders.[34, 122, 142-144] Treatment options for neurological diseases including Parkinson's, Alzheimer's, schizophrenia, and nicotine addiction are limited by insufficient understanding of nAChR-mediated cell signaling in response to ligand binding.[145, 146] This gap in knowledge exists due to a multitude of factors, which include the lack of nAChR structure data due to difficulty in crystallizing these integral membrane proteins, the absence of robust heterologous non-recombinant expression systems,[147] and the complexity and accessibility of experimental methods to study ion flow through nAChRs

across cell membranes.[148, 149] Current methods of identifying ligand binding paradigms with nAChR subtypes include computational docking and molecular dynamics simulations,[57, 88, 94, 100, 101, 119, 120, 126, 133, 150-153] two-electrode voltage clamp electrophysiology with *Xenopus* oocytes that express the desired nAChR isoform,[154] patch clamping in cells over-expressing nAChRs such as HEK and neuroblastoma cells,[155] model studies using acetylcholine binding proteins (AChBPs),[46, 47, 49, 54] radiolabeling of nAChR antagonists, investigations using mouse brain slices,[156-158] and in vivo trials with animals[159] or humans.[160] Cell-based assays using fluorescent indicators, such as the FLIPR fluorescent membrane potential assay or the Flou-4AM calcium indicator assay are being used with increasing frequency to study nAChR activation.[161] Each of these strategies to study nAChR bioactivity are challenging to implement in their own unique ways. The use of computational docking and molecular dynamics simulation software programs to study the interaction of ligand binding to nAChRs has been significantly limited in the prediction of bioactivity, because binding affinity indirectly correlates with the physical dynamic changes associated with pore opening and closing of the membrane-bound channel.[1] Computational methods can be used to calculate the binding affinity for small molecule drugs by screening compound libraries, but correlating binding affinity to bioactivity is inherently inaccurate, and fails further in the assessment of a compound as an agonist or antagonist, necessitating wet-lab validation. Studies utilizing AChBPs allow assessment of ligand binding, but not the ion flow across a membrane required to trigger signaling mechanisms within a cell that result in dopamine release, because the AChBP lacks a transmembrane component. Electrophysiology experiments require extensive expertise, highly specialized equipment, and significant investment of time to obtain results. Using

electrophysiology to evaluate a wide range of compounds in order to test hypotheses about binding paradigms is impractical, either because the time and expense required to screen the compounds is so intensive, or because of the inaccessibility of high throughput and automated methods.[148, 149, 162, 163] Mouse brain studies involve probing slices of mammalian brain with fluorescently labeled conotoxin (CTx) to observe localized binding regions.[27, 158] However, the resources required to work with mammalian tissue or living animals, including animal centers and oversight boards, can present prohibitive challenges for researchers at many institutions. There is a need to establish methods that bridge the gap between computational results and extensive experimentation, such that predicted compounds can be proven to demonstrate desired bioactivity prior to exhaustive and expensive laboratory evaluation. An accessible, time and cost efficient, and reliable PC12 cell method to qualitatively assess ligand effect on nicotinic acetylcholine receptor-mediated control of dopamine release is presented.

The PC12 protocol reported in this study is an adaptation of a luminescence bioactivity assay that permitted measurement of dopamine release from rat PC12 cells, following activation by acetylcholine (ACh), bradykinin, muscarine, and ATP.[164, 165] Acetylcholine binds to both nicotinic and muscarinic acetylcholine receptors (mAChRs), bradykinin activates bradykinin receptors B1 and B2, muscarine activates mAChRs, and ATP activates P2X and P2Y purinoreceptors. Acetylcholine stimulates only n/mAChRs to release dopamine, while the other agonists (bradykinin, muscarine, and ATP) operate by alternative signaling pathways to release neurotransmitters that contribute to the signal measured by luminescence detection. The original work by Shinohara et al. demonstrated that real-time dopamine release by PC12 cells, upon stimulation by ACh, permitted

luminescence detection in a dose-dependent manner, and enhancement of dopamine release was achieved by augmentation of assay conditions to include nerve growth factor (NGF). Shinohara et al. presented their assay as a useful tool to assess drugs that affect the nervous system. Building upon the precedent set by Shinohara et al., our lab has adapted the PC12 assay for assessment of ligands that specifically target nAChRs, as opposed to muscarinic or ATP receptors that induce dopamine release through alternate pathways. In the presence of agonists including ACh, nicotine, or cytisine, nAChR channels will open to permit sodium ions into the cell. This influx of ions stimulates calcium ion influx resulting in vesicle expulsion of dopamine from PC12 cells. When dopamine is released from the cell, monoamine oxidase (MAO) oxidizes dopamine to generate hydrogen peroxide, which reacts with luminol in the presence of horseradish peroxidase (POD) to generate chemiluminescence, which can be measured by absorbance (Figure 2.1).

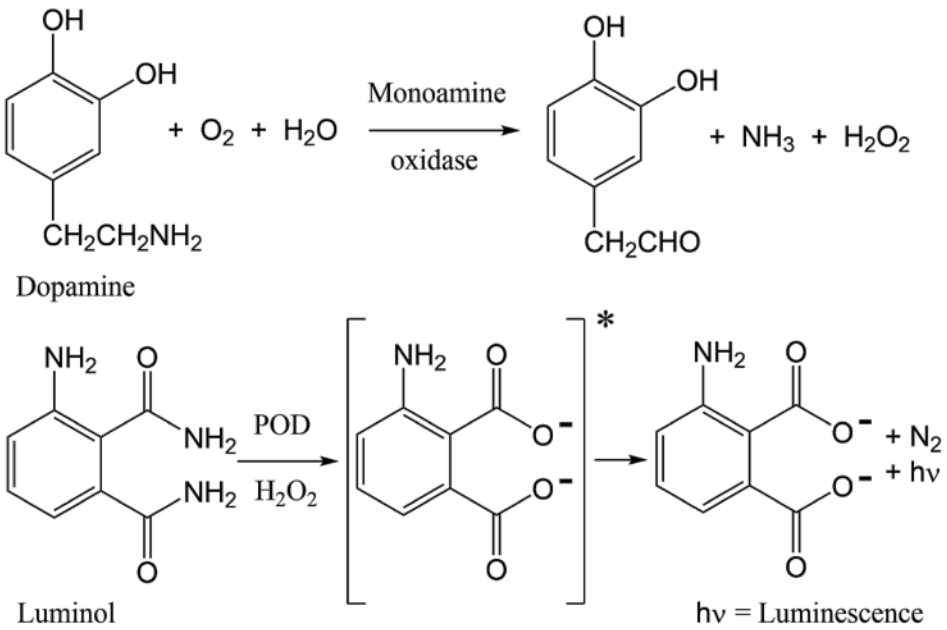

Figure 2.1. Chemical changes proposed to occur in the PC12 assay, from nAChR-induced dopamine release to luminescence detection. More dopamine release leads to a greater signal. Antagonists of nAChRs block dopamine release, diminishing signal.

In the present investigation, the PC12 assay protocol of Shinohara et al. was adapted for measurement of increased response following stimulation with ACh, nicotine, and cytisine.[164, 165] Acetylcholine is a neurotransmitter that acts as the principal biological agonist of nAChRs. Nicotine and cytisine are alkaloids widely used in addiction studies involving nAChRs, because they both act as nAChR agonists due to their similar structural and pharmacological attributes. ACh, nicotine, and cytisine are all nonspecific agonists of most nAChR isoforms. EC_{50} and E_{max} values for agonist-stimulated $^{86}Rb^{+}$ efflux in NGF-treated PC12 cells, as reported by Avila et al., are shown in Table 2.1.[166] While it is now recognized that some nAChRs can bind G-proteins and induce neurotransmitter release through a G-protein coupling mechanism as opposed to the more rapid ion translocation mechanism described above,[167] extracellular ligand effect on intracellular G-protein coupling of nAChRs remains unknown. However, numerous examples of associations between nAChRs with several types of G-proteins have been demonstrated, which may contribute to cross-talk between nAChRs and G-proteins.[168-170]

Table 2.1. EC_{50} and E_{max} values for agonist-stimulated $^{86}Rb^{+}$ efflux in NGF-treated PC12 cells for acetylcholine, nicotine, and cytisine. EC_{50} and E_{max} values are in units of µM.[166]

Agonist	EC_{50}	E_{max}
Acetylcholine	118±23	307±24
Nicotine	33±1.5	232±23
Cytisine	42±8.6	256±21

α-Conotoxins (α-CTxs) are known to be highly potent and selective for nAChR isoforms, and have been used extensively by scientists seeking to understand ligand binding paradigms for nAChR subtypes.[1] The reason α-CTxs were selected as antagonists of nAChRs is because PC12 cells express mRNA coding for α3, α5, α7, β2, and β4 subunits

but not α2, α4, α6, or β3.[171, 172] These subunits assemble into a variety of functional homo- and heteropentameric nAChRs, including predominantly α7, α3β4, and α3β2.[166, 171, 173] Nery et al. used a strategy of non-specific nAChR stimulation followed by specific inhibition of the α7 nAChR isoform by methyllycaconitine citrate to inform the extent of activity for which the α7 isoform was responsible.[171] They concluded that PC12 cells induced to neuronal differentiation are a good model for studying α7 expression and activity in which various nAChR isoforms are expressed. This present study aimed to use the same strategy of non-specific nAChR stimulation followed by specific inhibition of a targeted nAChR isoform to demonstrate the same conclusion regarding the rα3β2 nAChR isoform after optimizing PC12 cell growth conditions to favor its expression. Thus, to target ligand activity on rα3β2 nAChR subunits and demonstrate optimal assay conditions for its expression in PC12 cells, α-CTx ligands that selectively but differentially target the rα3β2 nAChR isoform were chosen. Suppression of rα3β2 nAChR-mediated cell signaling was evaluated using α-CTxs MII, ImI, LvIA, and PeIA (Figure 2.2). α-CTx MII is a 16-amino acid, 4/7 framework peptide, with primary sequence GCCSNPVCHLEHSNLC and disulfide bonds between C2-C8 and C3-C16, that selectively binds and inhibits rα3β2 nAChRs with an IC_{50} of 0.5 to 2.2 nM.[36, 93] α-CTx MII has a >200-fold selectivity for the α3β2 isoform over both the α3β4 and α7 isoforms.[93, 123] When used in the PC12 assay, suppression of luminescence response by α-CTx MII was broadly interpreted as a measure of relative rα3β2 nAChR expression in the cell system. Of the nAChR subtypes expressed in the PC12 system, α-CTxs ImI, LvIA, and PeIA were chosen for their high selectivity for the rα7 (IC_{50} = 220 nM),[75] rα3β2 (IC_{50} = 8.7 nM),[57] and rα3β2 (IC_{50} = 19.2 nM)[73] nAChR subtypes, respectively. The IC_{50} values for ImI, LvIA, and PeIA with rα3β2 nAChR are >5

μM,[75] 8.7 nM,[57] and 19.2 nM,[73] respectively. The IC_{50} values for ImI, LvIA, and PeIA with rα3β4 nAChR are >5 μM,[75] 148 nM,[57] and 480 nM,[73] respectively. This sampling of α-CTx antagonists was used to establish the reliability of achieving a qualitative luminescence response from ligand interaction with nAChRs that led to the excretion of dopamine. Each of these α-CTxs acts on nAChRs, but their effect can only be qualitatively assessed using this assay, due to their activity on multiple nAChR isoforms with varying affinity.

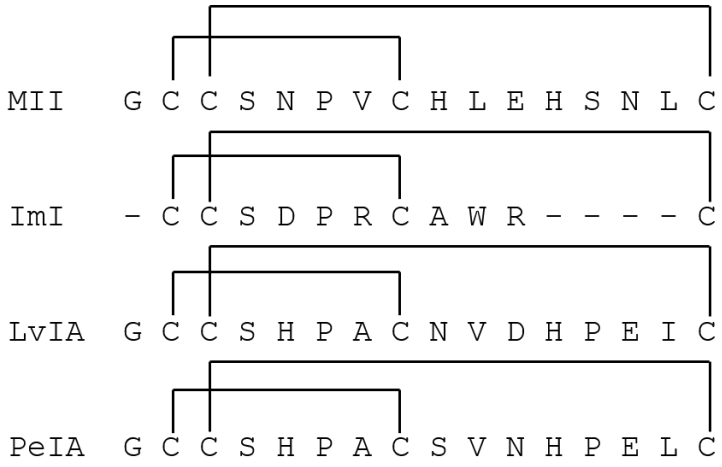

Figure 2.2. α-CTx peptide sequence and disulfide connectivity for rα3β2 nAChR antagonists evaluated in the PC12 assay.

PC12 cell growth and ligand treatment parameters were evaluated for enhanced response to the rα3β2 nAChR isoform selective antagonist α-CTx MII. PC12 assay results were assessed for influence by nerve growth factor, nicotine, ethanol, and temperature. Rogers et al. revealed that PC12 cells express the rα3β2 nAChR isoform among other receptor subtypes, and that NGF treatment provides growth conditions that favor expression of the β2 subunit.[174] In a complementary study, Shinohara et al. showed that NGF treatment enhanced luminescence response in the PC12 bioactivity assay, suggesting that NGF may increase nAChR expression.[165] Nerve growth factor treated cells were

evaluated in the presence of agonist and antagonist to determine whether NGF treatment would enhance the signal-to-noise ratio for the luminescence response. A separate investigation by Dohrman et al. demonstrated that addition of nicotine and ethanol to PC12 cells amplified nAChR expression.[175] Walsh et al. were able to enhance upregulation of rα3β2 nAChR expression, in HEK cells transfected with cDNA, upon long-term exposure to nicotine.[176] Cooper et al. observed that when TSA201 cells co-transfected with α4 and β2 cDNA were incubated at 30°C instead of 37°C, a 12-fold increase in α4β2 nAChR radioligand binding was observed with no changes in binding affinity, and a 5-fold increase in cell-surface receptors was achieved with no increase in total protein.[177] Avila et al. demonstrated through epibatidine binding and $^{86}Rb^{+}$ efflux studies that NGF treatment predominantly increases expression of an α3β4 receptor subtype in PC12 cells, while nicotine treatment predominantly increases expression of an α3β2 receptor subtype, and that these two treatments combined have a supplemental effect on increasing nAChR expression.[166] However, radioligand binding and $^{86}Rb^{+}$ efflux studies do not provide real-time observation of dopamine release through nAChR stimulation or suppression by ligands such as the study by Shinohara et al., which the current study aimed to achieve.

Given the wealth of data associated with nAChR expression in PC12 cells reported in literature, the PC12 cell assay conditions optimized in the present study were performed to achieve two objectives. The first objective was to obtain optimal response for nAChR agonist and antagonist activity by alteration of the PC12 assay experimental parameters including NGF, nicotine, ethanol, and temperature. The second objective was to establish optimal α-CTx suppression of dopamine release by inhibition of nAChRs in the context of the PC12 cell line expression system, as recorded by luminescence response.

Results

Figure 2.3 (A-C) shows the luminescence response following stimulation by ACh for PC12 cells under standard conditions (2.3A), treated with NGF (2.3B), and a combination of NGF and nicotine (2.3C). Treatment conditions were sustained for 3-4 days. Stimulated response by ACh is indicated by white diamonds and the suppression of response in the presence of α-CTx MII is indicated by black squares. ACh and α-CTx MII were used as a representative agonist/antagonist pair for non-specific nAChR stimulation and selective rα3β2 nAChR suppression in order to provide the clearest sensitivity of α-CTx effect on rα3β2 nAChR-induced dopamine release.

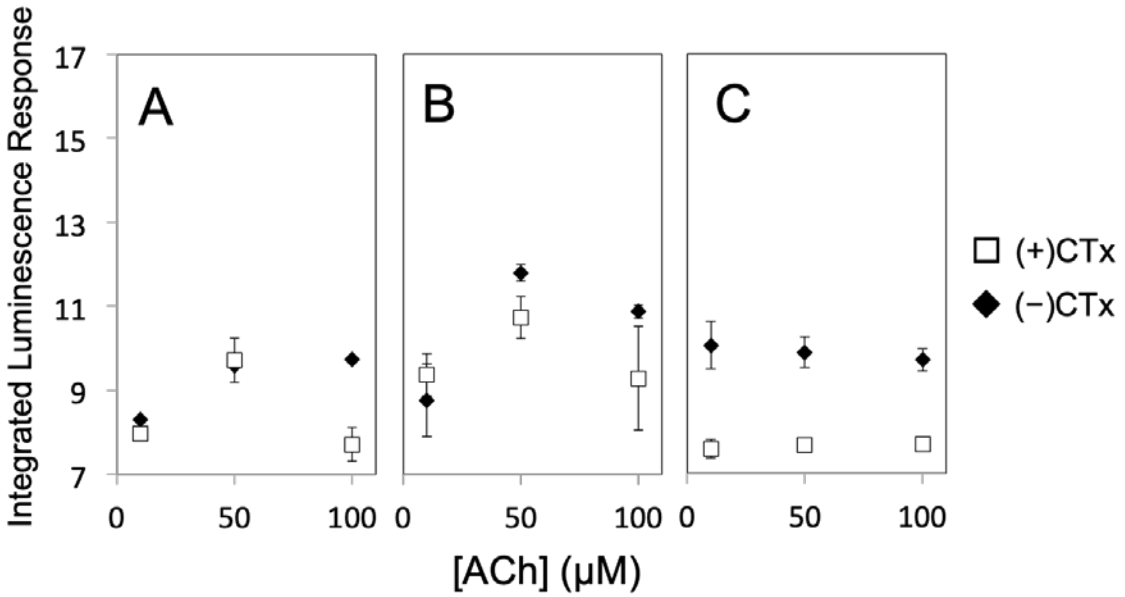

Figure 2.3. Integrated luminescence response versus ACh for (A) NGF(-), (B) NGF(+), and (C) NGF/nicotine. ACh response at 0 μM is not shown; the first point in each plot corresponds to the 10 μM ACh treatment to maximize visualization of data points and error bars.

Non-NGF-treated cells (Figure 2.3A) gave a lower luminescence response than NGF-treated cells (Figure 2.3B), and addition of α-CTx MII led to a decrease in luminescence response for both non-NGF and NGF-treated cells. Treatment with nicotine

relatively decreases luminescence, but increases sensitivity to α-CTx MII (Figure 2.3C). An additional PC12 assay was performed for combined treatment with NGF, nicotine, and ethanol, which increased the relative luminescence response, but decreased sensitivity to α-CTx MII. Unfortunately, the variability in the luminescence response under these treatment conditions did not lead to a reliable result and data are not shown here.

Effective NGF treatment was confirmed by cell morphology, in which NGF-treated cells contained neurite extensions indicative of neuron-like differentiation (Figure A.1). According to the treatment study in Figure 2.3, chemical treatment with NGF and nicotine provided the most apparent non-specific stimulation of nAChRs by ACh and most obvious suppression of nAChR-induced dopamine release by α-CTx MII (Figure 2.3C). The optimal PC12 assay conditions consisting of NGF and nicotine were further evaluated for temperature dependence at 37°C, 30°C, and 21°C for 1-2 hrs before detection of the luminescence response (Figure 2.4).

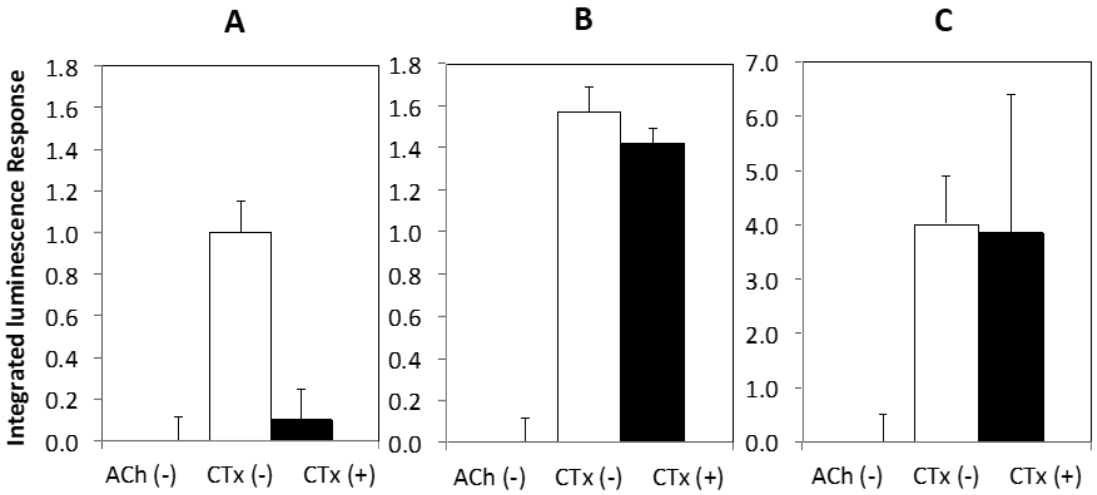

Figure 2.4. Luminescence response in the PC12 assay for normal cells incubated at 37°C (A), and cells incubated at 30°C for 1 hr (B) and room temperature (21°C) for 2 hrs (C) before detection. Incubating cells at a lower temperature before detection significantly increases response in a temperature-dependent manner, but decreases sensitivity to α-CTx MII.

Cells incubated at a lower temperature before luminescence recording showed a significantly increased response in a temperature-dependent manner, but sensitivity to α-CTx MII treatment was appreciably diminished. The luminescence response for cells incubated at 37°C was appreciably higher as compared to those incubated at lower temperatures.

Finally, Figure 2.5 shows the results of a compound screen with select nAChR agonists (ACh, nicotine, cytisine) and antagonists (α-CTxs MII, ImI, LvIA, PeIA) upon ACh stimulation, using the optimal conditions identified as a result of the investigations in Figures 2.3 and 2.4, which included chemical treatment with NGF and nicotine and incubation at 37°C.

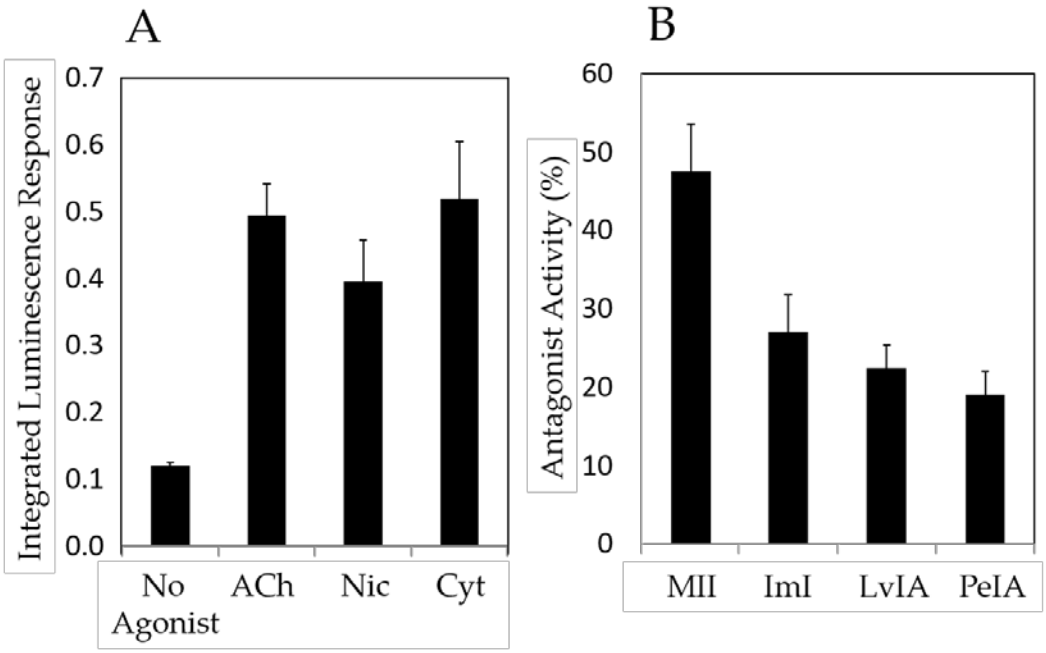

Figure 2.5. PC12 assay screen using (A) 50 µM nAChR agonists (acetylcholine, nicotine, cytisine), and (B) 10 µM nAChR antagonists (α-CTxs MII, ImI, LvIA, PeIA) upon stimulation with ACh, under the optimal growth conditions identified in Figures 2.3 and 2.4 (treatment with NGF and nicotine, and incubation at 37°C). The PC12 assay provided qualified bioactivity assessment for each agonist and antagonist.

Figure 2.5 shows that agonists amplified the luminescence response and antagonists suppressed the luminescence response, demonstrating that this PC12 assay may be used for qualitative assessment of ligands that bind nAChRs.

Discussion

Decreased luminescence response upon treatment with α-CTx MII indicates that α-CTx MII inhibition of rα3β2 nAChR-mediated release of dopamine in the PC12 cell assay can be observed and measured (Figure 2.3). Sensitivity to α-CTx MII antagonism was used as a measure of the relative expression of the rα3β2 nAChR isoform, because α-CTx MII is a highly selective and potent inhibitor of rα3β2 nAChR isoforms, while other nAChR isoforms expressed in PC12 cells are inhibited by α-CTx MII to a much lesser degree. Additionally, the increased luminescence response with NGF treatment (Figure 2.3B)

suggests that NGF increases the population of functional nAChRs on the surface of the PC12 cells. Increasing the concentration of nAChRs expressed is favorable for increasing the sensitivity of the PC12 assay. An increase in luminescence upon NGF treatment is consistent with the findings of Shinohara et al.[165]

Sensitivity to α-CTx MII treatment increased when both nicotine and NGF were used, suggesting that rα3β2 nAChR isoform expression is greater under this combined treatment condition (Figure 2.3C). This result is consistent with the findings of Walsh et al., who reported higher rα3β2 nAChR expression upon long-term exposure to nicotine in HEK cells transfected with cDNA.[176] Slightly decreased luminescence response upon 3-4 days of treatment with nicotine in combination with NGF can be interpreted as a decrease in the number of functional cell-surface nAChRs as a result of nicotine treatment, as compared to solely NGF-treated cells (Figure 2.3C). These results correlate well with the findings of Dohrman et al., who demonstrated that chronic nicotine induces overall upregulation of nAChRs in PC12 cells.[175] To detect the presence of nAChRs on the cell surface, Dohrman et al. used ^{125}I-labelled epibatidine, which binds more potently to α3β2, α3β4, and α4β2 nAChR subtypes than ACh. Additionally, epibatidine binding requires incubation at room temperature for 1 hour, which our results have shown drastically increases response (Figure 2.4), and suggests a subtype-nonspecific increase in nAChR cell-surface expression. It is possible the observation by Dohrman et al. of overall upregulation of nAChRs in PC12 cells does not specifically reflect physiological expression of functional cell-surface nAChRs at 37°C. An increase in cell-surface expression upon incubation at lower temperatures is consistent with the findings of Cooper et al., who observed that when TSA201 cells co-transfected with α4 and β2 cDNA were

incubated at 30°C instead of 37°C, there was a 5-fold increase in cell-surface receptors with no increase in total nAChR protein. Further support for this hypothesis is provided by Lukas et al., who found that chronic (3-72 hrs) nicotine treatment led to nearly a complete loss of functional nAChR response in PC12 cells by nicotine and the cholinergic agonist carbamylcholine.[178] It is possible with the combination of the PC12 cell line, treatment exposure time, and dosage used, that functional inactivation is seen instead of functional upregulation.

For normal cells treated with nicotine for 3-4 days and incubated at 37°C (Figure 2.4A), a >50% suppression of response to 50 μM ACh by α-CTx MII was observed. Cells incubated at lower temperatures (Figure 2.4B and 2.4C) before luminescence detection showed a significantly increased response compared to cells at 37°C. This is consistent with the findings of Cooper et al., who observed that when TSA201 cells co-transfected with α4 and β2 cDNA were incubated at 30°C instead of 37°C, there was a 5-fold increase in cell-surface receptors with no increase in total nAChR protein. While PC12 cells did not survive at 30°C for 24 hrs or more, incubating at 30°C and 21°C for only 1-2 hrs before detection showed a significant and temperature-dependent increase in luminescence response; however, sensitivity to α-CTx MII was essentially eliminated. Decreased sensitivity to α-CTx MII may suggest a subtype-nonspecific increase in nAChR cell-surface expression.

In summary, combined treatment with NGF and nicotine and incubation at 37°C provides the greatest level of sensitivity to α-CTx MII. Despite extensive repetition to obtain the results presented, it appears the PC12 assay may be limited to comparison of results within the same well plate. It is hypothesized that the rapid growth of PC12 cells

changes their condition too dynamically from subculture to subculture to permit comparison of luminescence intensity directly across well plates. Inconsistent expression from cell-to-cell, high background noise, and dynamic changes between subcultures can complicate results and cause absolute luminescence intensities and integrated luminescence response to differ widely across well plates, explaining the variability in absolute luminescence measurements in Figures 2.3-2.5. Regardless of these limitations, the PC12 assay conditions presented here can be applied to qualitative characterization of bioactivity of lead compounds with affinity for nAChRs.

The PC12 assay was examined for use as a qualitative bioactivity test for a range of known nAChR agonists (acetylcholine, nicotine, and cytisine) and antagonists (α-CTxs MII, ImI, LvIA, PeIA) (Figure 2.5). The PC12 assay accurately provided signal amplification in the presence of nAChR agonists (Figure 2.5A), and signal suppression upon treatment with nAChR antagonists (Figure 2.5B). These results further reflect relative potency between α-CTx MII and other less potent antagonists, with α-CTx MII showing the highest antagonistic activity. The responses obtained by this collection of α-CTx antagonists indicate that nAChR-mediated channel closing may be assessed qualitatively. α-CTx MII is known to potently and selectively suppress luminescence response generated by rα3β2 nAChR isoform, and was interpreted in this study as a measure of relative rα3β2 nAChR expression in the cell system. α-CTx MII achieved 50% suppression of luminescence response, suggesting a relatively high level of expression of functional rα3β2 nAChR subtypes in the cell system. The levels of suppression observed in Figure 2.5 by α-CTxs MII, ImI, LvIA, and PeIA reflect their relative specificities for rα3β2, rα7, rα3β2>rα3β4, and rα3β2>rα3β4, respectively, and suggest that rα3β2, rα3β4, and rα7

nAChRs are present to a high detectable degree in PC12 cells, consistent with previous literature.[166, 171, 173]

This study presents an accessible, time and cost efficient, and reliable luminescence-based method for detection of nAChR bioactivity, and demonstrates decreased response upon addition of α-CTx antagonist. As a result of the alterations made to the PC12 protocol (see Appendix A), this assay can be performed at any institution with a microplate reader that can detect luminescence. Simplifications to the protocol, such as reduction in the amount of required enzymes and eliminating the need for trypsinization, significantly reduce material costs. This study provides a simple method for measurement of nAChR bioactivity response that can be quickly and easily performed. Because PC12 cells grow quickly, the time from cryopreservation recovery to assay can be achieved within one week with 3-4 days of treatment. One response curve can be obtained within minutes, enabling evaluation of an entire 96-well plate within an hour. Optimal growth conditions for expression of rα3β2 nAChRs were measured by the degree of sensitivity to α-CTx MII suppression. According to the results of this study, combined treatment with NGF and nicotine and incubation at 37°C provides the greatest level of sensitivity to α-CTx MII. This adapted PC12 assay can be applied to qualitative characterization of bioactivity of lead compounds with nAChR, as demonstrated by the compound screen performed here under optimized growth conditions with non-specific agonists and selective antagonists of nAChRs.

Shinohara et al. permitted real-time detection of dopamine release upon stimulation of nAChR and bradykinin receptor agonists in PC12 cells without NGF treatment, as well as upon stimulation of mAChR, ATP receptor, and bradykinin receptor agonists in PC12

cells treated with NGF. The present investigation improves upon Shinhoara's original assay[164, 165] by exploring and identifying optimal growth conditions for nAChR expression, and the use of selective α-CTxs to assess nAChR isoforms responsible for assay response upon stimulation with ACh, demonstrating that nAChR expression can be easily manipulated by chemical treatment and growth conditions in order to qualitatively characterize the real-time ligand effect on nAChR-induced dopamine release. While we demonstrated that this assay provides accurate bioactivity validation, it is apparent that the assay's sensitivity is limited by a response resulting from the presence of non-rα3β2-nAChR subtypes. Additionally, inconsistent expression from cell-to-cell, and high background noise can complicate results. Possible reasons for such background noise in the response include inherent base-level activity of predominantly expressed nAChRs such as rα7, rα3β4, and rα3β2, as well as G-protein coupled activation of nAChRs as opposed to ion translocation.[167] While this mechanism of nAChR activation is now recognized in the literature, it is uncertain how the ligands evaluated here, which are responsible for affecting nAChR activity through ion translocation, might affect nAChR coupling to G-proteins. Thus, it is expected that the response obtained from G-coupled activation of nAChRs is corrected for with the negative controls used in this study. Future research directions include the adaptation of this assay coupled to overexpression of individual nAChR isoforms, or knockout or knockdown of particular nAChR subunits, resulting in an assay in which the pharmacology of a single nAChR subtype may be evaluated. This assay serves as a foundation for the design of engineered PC12 cell lines expressing specific human nAChR isoforms to enable the study of lead compounds for the treatment of neurological diseases in which non-rα3β2-nAChR isoforms are implicated (e.g.,

Parkinson's, schizophrenia, and Alzheimer's). The ease and simplicity with which PC12 cells can be cultured and manipulated is widely reported,[179] and makes PC12 cells an ideal cell line for the investigation of ligands that act on nAChRs.

Conclusions

A simple method for the measurement of ligand induced bioactivity on nAChRs that can be quickly and easily performed was presented. Because PC12 cells grow quickly, the time from cryopreservation recovery to assay can be achieved within one week with 3-4 days of treatment. Assay response curves can be obtained within minutes, enabling evaluation of an entire 96-well plate within an hour. Optimal growth conditions for expression of rα3β2 nAChRs were measured by the degree of sensitivity to α-CTx MII suppression. According to the results of this study, combined treatment with NGF and nicotine, and incubation at 37°C provides the greatest level of sensitivity to α-CTx MII. This adapted PC12 assay can be applied to qualitative characterization of the bioactivity of lead compounds with nAChRs, as demonstrated by the compound screen performed here under optimized growth conditions with non-specific agonists and antagonists of nAChRs.

Materials and Methods

The materials and methods for this PC12 assay represent an adaptation and modification of the foundational work originally reported by Shinohara et al.[164, 165] Key variations to their reported method are discussed in greater detail in Appendix A. Assays were performed using a Biotek Synergy H1 microplate reader (Winooski, VT, USA). All chemicals were purchased at the highest purity available (>95%) from Fisher Scientific, except for synthetic α-CTxs, which were purchased from CS Bio Inc. (Menlo, CA, USA).

ATCC® CRL1721™ PC12 cells were provided by the Biomolecular Research Center at Boise State University.

Cell Culture

PC12 cells were recovered from cryopreservation, seeded, and cultured into laminin-coated flasks according to Shinohara et al. with the exception that cells were not trypsinized to detach them from laminin.[164] Instead, cells were triturated from the bottom of the flask. Cells were initially grown in a T-75 flask until dense enough to plate onto either a laminin-coated flat-bottom 96-well plate at 10,000 cells per well, or 48-well plate at 30,000 cells per well, taking care to sufficiently disperse cell clumps when triturating. Plating at sufficiently low density and ensuring distribution of cells to evenly cover each well bottom was crucial to obtaining consistent assay response. After subculturing into a well plate, cells were allowed to equilibrate for 24 hrs before exchanging complete growth media for treated starvation media (30 ng/mL NGF 2.5S, 1 μM nicotine, 100 mM ethanol, in the desired combinations of treatment) and treating for 3-4 days before performing the assay, switching out fresh starvation media daily. Treatment concentrations of nicotine and ethanol were based on those used by Dohrman et al.[175] Well plates were sealed with Parafilm during treatment to prevent evaporation of ethanol from treatment media.

Cell Assay

Cells were washed with Locke's solution before introducing assay solution. An assessment of Modified Hank's Balanced Salt Solution was performed, but results were unfavorable (Figure A.2). Assay solution included 10 μM α-CTx MII, 0.8 ng/mL horseradish peroxidase (POD), 25 ng/mL monoamine oxidase (MAO), and 50 μM luminol to quench any dissolved oxygen in the cell environment and the assay solution. Cells were

allowed to sit for 5-10 min to allow equilibration, before adding 2 mM luminol and 50 µM agonist (acetylcholine, nicotine, or cytisine) immediately before detection, for a total well volume of 100 µL. Cells were allowed to sit for 5-10 min to allow equilibration, before adding 2 mM luminol and 50 µM agonist (acetylcholine, nicotine, or cytisine) immediately before detection, for a total well volume of 100 µL. (-)MAO and (-)cells were used as negative controls, replacing the volume with Locke's solution. Assays were performed at 37°C, detecting luminescence for 1-2 min per well or until response fully diminished to negative control levels in order to obtain a complete curve. Once luminescence response curves were obtained, curves with abnormal shapes indicating obvious faults in detection caused by anomalies such as air bubbles were excluded. Curves were then integrated and the area under the curve was used to build dosage curves for luminescence response versus concentration of agonist. To evaluate the influence of the temperature on assay results for a single well plate to avoid introducing unnecessary variation across well plates, cells were prepared as above, but after detecting the response for a portion of the wells at 37°C, the remaining wells were incubated at either 30°C or room temperature (21°C) for 1-2 hrs. The assay was then resumed after switching media with assay solution incubated at the corresponding lower temperature into the remaining wells for detection.

CHAPTER THREE: STRUCTURE AND BIOACTIVITY OF KTM, A COMPUTATIONALLY DESIGNED NICOTINIC ACETYLCHOLINE RECEPTOR ANTAGONIST INSPIRED BY A-CONOTOXIN MII

Published in *Marine Drugs* (Open access)

Leanna A. Marquart,[1] Matthew W. Turner,[2] Lisa R. Warner,[1] Matthew D. King,[1] James R. Groome,[3] and Owen M. McDougal[1]

[1] Department of Chemistry and Biochemistry, Boise State University

[2] Biomolecular Sciences Graduate Programs, Boise State University

[3] Department of Biological Sciences, Idaho State University

KTM is a 16 amino acid peptide with the sequence WCCSYPGCYWSSSKWC. Here, we present the nuclear magnetic resonance (NMR) structure and bioactivity of a rationally designed analog of α-conotoxin (α-CTx) MII that demonstrates potent inhibition of rat α3β2 nicotinic acetylcholine receptors (rα3β2-nAChRs).[180] Two bioassays were used to test the efficacy of KTM. First, a qualitative PC12 cell-based assay confirmed that KTM acts as a nAChR antagonist. Second, bioactivity evaluation by two-electrode voltage clamp electrophysiology was used to measure the inhibition of rα3β2-nAChRs by KTM (IC_{50} = 0.19±0.02 nM), and α-CTx MII (IC_{50} = 0.35±0.8 nM). The three-dimensional structure of KTM was determined by NMR spectroscopy, and the final set of 20 structures derived from 32 distance restraints, four dihedral angle constraints, and two disulfide bond constraints overlapped with a mean global backbone root-mean-square deviation (RMSD)

of 1.7 ± 0.5 Å. The structure of KTM did not adopt the disulfide fold of α-CTx MII for which it was designed, but instead adopted a flexible ribbon backbone and disulfide connectivity of C2-C16 and C3-C8 common to λ-CTxs, with an estimated 12.5% α-helical content. In contrast, α-CTx MII, which has a native fold of C2-C8 and C3-C16, has an estimated 38.1% α-helical secondary structure. KTM is the first reported instance of a Framework I (CC-C-C) α-CTx with ribbon connectivity to display sub-nanomolar inhibitory potency of rα3β2-nAChR subtypes.

Keywords: α-conotoxin; nicotinic acetylcholine receptor; NMR; two-electrode voltage clamp electrophysiology; PC12 cell; DockoMatic

Introduction

Conotoxins are 10-50 amino acid peptide toxins present in the venom of predatory marine snails of the genus *Conus*. With sequence hypervariability and disulfide bond constrained scaffolds, conotoxins have a complex classification system of 28 superfamilies, segregated in part by activity on ion channels present in excitable tissues such as nerve and muscle.[181] α-Conotoxins (α-CTxs) target ligand-gated nicotinic acetylcholine receptor (nAChR) ion channels and inhibit ion flow by causing a dynamic structural change upon binding that results in the closing of the channel. nAChRs are pentameric transmembrane channel proteins that form different combinations of homo and heteropentameric subtypes, leading to a range of functions and ligand specificity across the host nAChRs are found in many tissues including muscle and the central and peripheral nervous systems, and perform numerous physiological functions, such as the modulation

of neurotransmitter release in the central nervous system by post and presynaptic excitation.[182] In the modulation of neurotransmitter release, acetylcholine activation of presynaptic nAChRs causes sodium influx and subsequent cellular depolarization, resulting in activation of voltage-gated calcium channels and an influx of calcium ions that initiates a signaling cascade ending in release of dopamine-containing vesicles. Because of their involvement in neurotransmitter release, nAChRs play a central role in the pathology of Parkinson's disease (PD) and other neurological disorders. For example, PD patients experience degradation a of neurons expressing α6α4β2β3-nAChRs and consequently display symptoms reflecting loss of function dependent on dopamine release. Targeting specific nAChR isoforms is a promising strategy in the development of improved drug therapies for PD and other neurological diseases that have nAChRs implicated in their causation and/or symptoms, including Alzheimer's, Tourette's, and schizophrenia.[32, 34, 142-144] However, there still exists a gap in understanding of the mechanism of nAChR-ligand binding.

α-CTxs possess rigid scaffolds and are among the most potent inhibitors of nAChRs, making them insightful molecular probes for the elucidation of nAChR binding paradigms. α-CTx structure-activity relationships have been developed for α-CTxs and their analogs, leading to the discovery of disease-relevant nAChR subtypes and the identification of new ligand-nAChR binding sites.[1, 94, 122] Model systems used to study nAChR-ligand binding include pheochromocytoma (PC12) cell assay,[141] electrophysiology,[154] mouse brain studies,[156-158] and computational molecular dynamics simulations.[57, 88, 94, 100, 101, 119, 120, 126, 133, 150-153] Expression systems for studying nAChRs in vitro often prove costly and complex,[148, 149, 162, 163] highlighting the potential value of

computational studies. Emerging computational strategies can produce promising results for nAChR ligands, but potential small molecule drugs require evaluation by functional experimentation. Here, we present the validation results of a computational study that used the genetic algorithm managed peptide mutant screening (GAMPMS) program in DockoMatic v. 2.1 to predict the sequence for an α-CTx MII analog for optimal binding to the rat (r)α3β2 nAChR isoform; the outcome of the computational study was the designed peptide KTM.[126, 150, 151]

DockoMatic is an open source program with an intuitive user interface to run software applications for ligand and receptor structure file creation, perform high throughput virtual screening, and output docking results ranked in order from best to worst binding affinity.[133, 152, 153, 183-185] DockoMatic uses the highly innovative GAMPMS algorithm specifically designed for peptide library creation, and can correlate peptide structure to drug identity by way of the small-molecule peptide-influenced drug repurposing (SPIDR) utility that permits screening of molecular databases using a template structure derived from a peptide scaffold.[126, 150, 151] Previously, the GAMPMS algorithm was used to evaluate the binding affinity of over 41 billion combinations of α-CTx MII mutants for a homology model of the rα3β2 nAChR isoform.[126] α-CTx MII was selected as a template for this study because it has been well characterized as a very potent and selective inhibitor of the rα3β2 nAChR isoform. α-CTx MII is a 16 amino acid peptide with the primary sequence GCCSNPVCHLEHSNLC and disulfide bonds between C2-C8 and C3-C16. The globular structure of α-CTx MII is characterized by an α-helix initiated at P6 and ending at H12, providing the peptide with approximately 40% α-helical content. The GAMPMS program was used to change the primary sequence of α-CTx MII to create

a peptide library of nearly 41 billion unique α-CTxs.[126] All amino acids were varied in the primary sequence with the exception of the four cysteine residues required to form disulfide bonds and the conserved proline at position 6 required for initiation of the α-helix. Molecular docking in DockoMatic ranked the peptides by highest binding affinity for the rα3β2 nAChR isoform. The top fifty mutant peptides with highest affinity for the receptor were compared for amino acid identity at each site in the peptide primary sequence to generate a consensus peptide. Figure 3.1A-B shows the sequence and disulfide connectivity of KTM (A), and the sequence comparison of KTM to α-CTx MII (B). The consensus peptide, given the arbitrary name KTM (Figure 3.1A; dashed), represents a rationally designed peptide ligand that was computationally predicted to have enhanced binding affinity for the rα3β2 nAChR isoform.

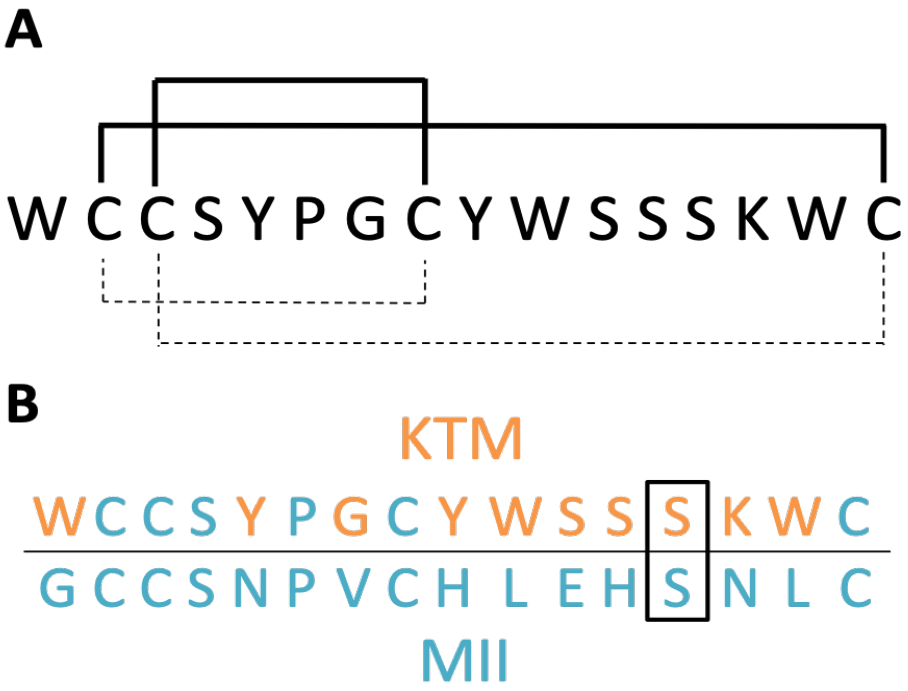

Figure 3.1. A) Sequence of KTM with disulfide bond connectivity consistent with the expected native folding (dashed line), and predominant cysteine pattern resulting from oxidative folding following solid phase peptide synthesis (solid line). B) Sequence comparison of KTM to α-CTx MII. Of the 10 residues in α-CTx MII that were allowed to vary in the GAMPMS algorithm (orange), all but one amino acid (S13, boxed) changed to give the sequence of KTM.

The sequences of α-CTx MII and KTM both contain 16 amino acids (Figure 3.1B). α-CTx MII has a Framework I cysteine pattern of CC-C-C, consisting of two disulfide bonds between C2-C8 and C3-C16, making it a globular connectivity pattern, and a 4/7 loop sequence common to many α-CTxs.[12] The design of KTM was inspired by the pharmacological features present in α-CTx MII and was anticipated to adopt the same globular disulfide connectivity. KTM activity on nAChRs was assessed qualitatively by an *in vitro* cell-based PC12 luminescence assay, and quantitatively for inhibition of rα3β2 nAChR isoforms using two electrode voltage clamp electrophysiology. KTM demonstrates remarkable sub-nanomolar inhibition of selective nAChR subtypes, commensurate with

that of α-CTx MII. In the present study, we show that synthetic KTM produced by undirected folding preferentially formed ribbon C2-C16 and C3-C8 disulfide linkages. In their review, Akondi, et al. suggest that correct folding of synthetic peptides is critical to the maintenance of biological activity,[12] but in the case of KTM, the globular disulfide pattern is not the same as that found in α-CTx MII, but rather resembles that of ribbon isomer AuIB.[186, 187] The net effect of the disulfide connectivity is that α-CTx MII adopts a globular scaffold, while KTM is consistent with a ribbon connectivity. Solution nuclear magnetic resonance (NMR) spectroscopy was used to determine the three dimensional structure of the synthesized KTM for comparison to α-CTx MII and the computationally predicted structure. Molecular dynamics simulations in Gromacs were used to assess peptide dynamics.

Results

Bioactivity

KTM was qualitatively evaluated for nAChR bioactivity using a PC12 cell assay and antagonist activity by KTM in the presence of acetylcholine (ACh) was confirmed (Figure 3.2), prompting quantitative evaluation of bioactivity by electrophysiology. In the preliminary screening qualitative assay, ACh is used to stimulate PC12 cells, opening nAChR channels and resulting in dopamine release.[164, 165] Following release, dopamine is oxidized by monoamine oxidase generating hydrogen peroxide that catalyzes a chemiluminescence reaction involving luminol and horseradish peroxidase, producing a detectable response. Incubation with α-CTxs prior to stimulation with ACh inhibits nAChRs, resulting in a diminished signal, as is observed for treatment with α-CTx MII (see

Figure 2). A decreased signal resulting from treatment with KTM indicates that nAChRs are inhibited by this compound.

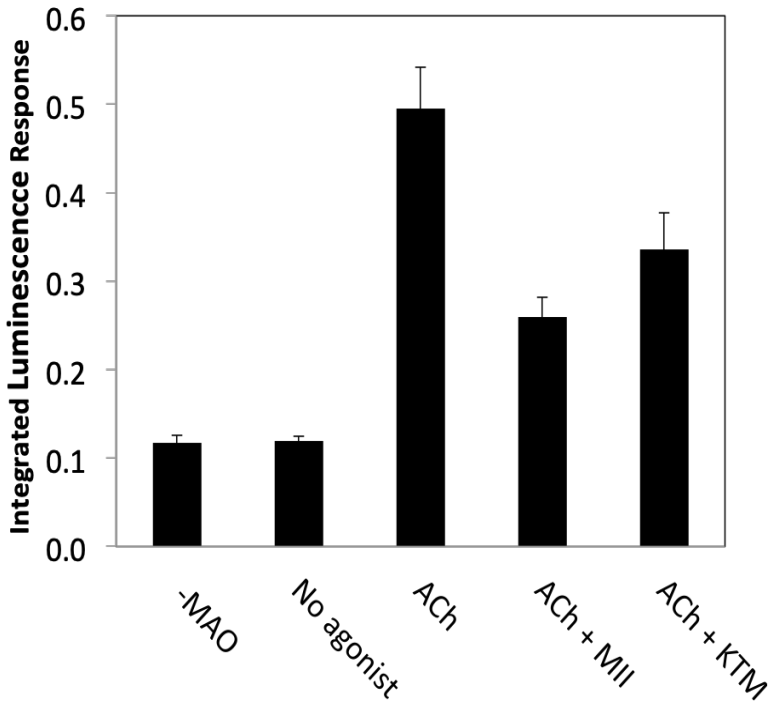

Figure 3.2. Qualitative PC12 assay luminescence responses upon stimulation of nAChRs with acetylcholine (ACh), with and without 10 µM toxin. Assays performed with the addition of α-CTx MII and KTM resulted in a diminished luminescence recording compared to an ACh control.

Two-electrode voltage clamp experiments were used to determine the IC_{50} for KTM on rα3β2 nAChRs expressed in *Xenopus laevis* oocytes. Figure 3.3 A-B shows the concentration-dependent dose curves for inhibition of rα3β2 nAChR by MII and KTM (A), and the Hill coefficients for concentration response that were used to calculate IC_{50} values for each peptide (B). KTM exhibited potent inhibition with an IC_{50} of 0.19±0.02 nM commensurate with α-CTx MII with an IC_{50} of 0.35±0.08 nM (Figure 3). α-CTx MII and KTM have Hill coefficients of 0.5 and 0.7, respectively.

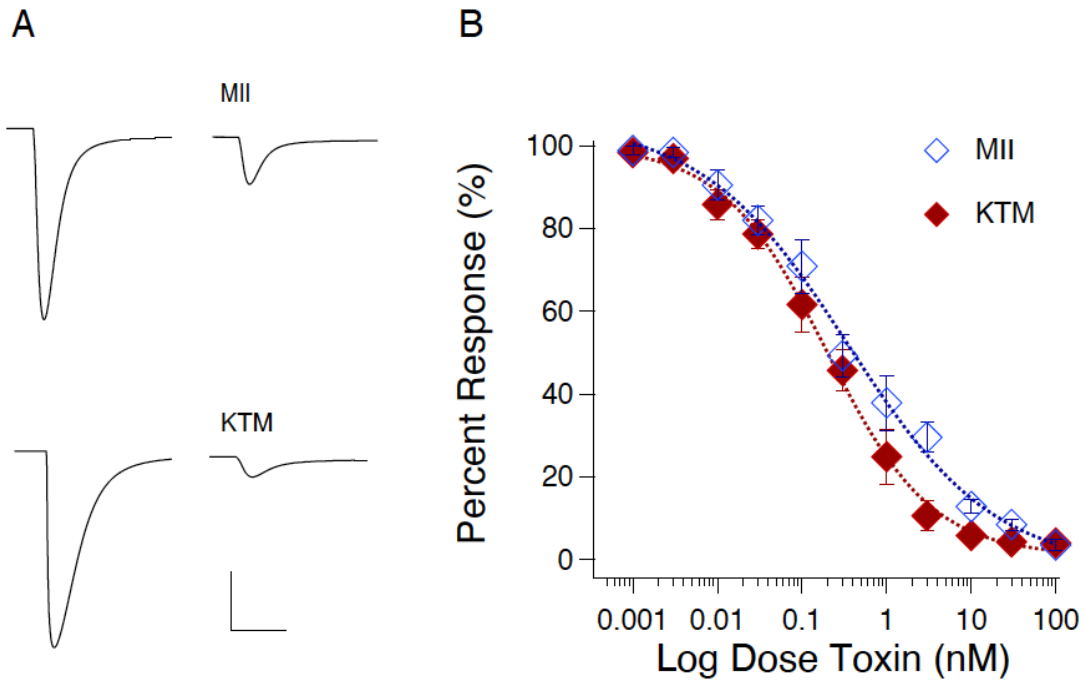

Figure 3.3. Responses to local application of ACh for 30 ms are shown for control and after 3 nM toxin application; calibration horizontal 3 sec, vertical 2.5 µA (A). Concentration-dependent response curves for blocking rα3β2 nAChR by α-CTx MII (red) and KTM (blue) (B). Hill coefficients for the concentration response curves of α-CTx MII and KTM are 0.5 and 0.7, respectively. IC_{50} values of KTM and α-CTx MII are 0.19±0.02 nM and 0.35±0.08 nM, respectively. Data are means ± SEM from 8 to 12 oocytes.

Structure Determination

Analysis of the circular dichroism (CD) spectrum for KTM (Figure 3.4, double lined grey) gave a predicted α-helical content of 12.5%, consistent with the ribbon-type isomer fold (C1-C4; C2-C3), and not the expected globular-type fold (C1-C3; C2-C4) characteristic of α-CTx MII, for which the α-helical content is 38.1% (Figure 3.4, solid black line). The large negative peak commonly observed for α-CTxs corresponds to the α-helical portion of the peptide, and is predominantly absent in the CD spectrum of KTM. The interpretation of CD spectra for flexible small peptides is representative of an ensemble of conformations, so it is difficult to draw definitive secondary structure conclusions based solely on CD data. The CD data in Figure 3.4 did identify variation in the secondary

structure between KTM and α-CTx MII that brought into question the disulfide connectivity in KTM, necessitating framework determination for KTM by partial reduction mass spectrometry.

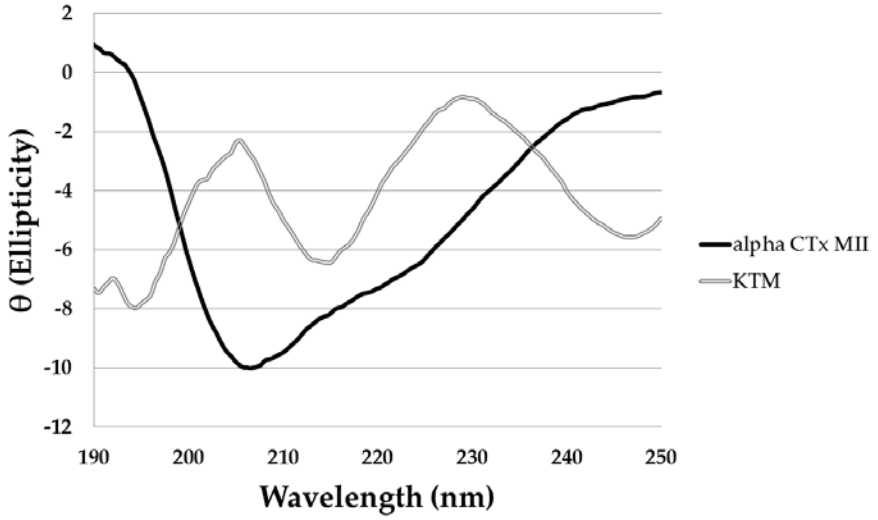

Figure 3.4. CD spectrum of α-CTx MII (solid black line) and KTM (double lined grey). Measurements for each peptide were taken in water at 50 μM each, and a pathlength of 1 mm. The α-helical content of α-CTx MII and KTM were estimated to be 38.1% and 12.5%, respectively, as calculated from the observed signal at 222 nm.

Partial reduction by TCEP of 100 pmol of synthetic KTM peptide gave expected product profiles in LC-MS chromatograms with mass increases corresponding to partial reduction (+2 m/z) and alkylation (NEM, +125 m/z; IAA, +59 m/z) (see Materials and Methods). Sequence analysis showed the disulfide bridging pattern was not consistent with the expected α-CTx C2-C8/C3-C16 globular linkage as found in α-CTx MII, but rather a C2-C16/C3-C8 ribbon linkage (Figure B.1), as observed in α-CTx AuIB.[186, 187]

NMR structure determination for KTM was performed to compare the computationally predicted C2-C8/C3-C16 globular structure to the synthesized C2-C16/C3-C8 ribbon structure. Assignment of ^{1}H resonances for KTM was achieved using standard methods.[188] A combination of COSY, TOCSY, and NOESY spectra in both 30%

ACN/70% water and 30% ACN/70% D_2O were used to reduce ambiguities in assignment. Fifteen amino acid spin systems were assigned in the fingerprint region (7.6 - 8.8 ppm), and the final amino acid, P6, was identified in the α-proton region (5.2-3.8 ppm). Table 3.1 shows the chemical shift assignments for each of the sixteen amino acids in KTM, and Figure 3.5 shows the calculated random coil chemical shift difference. Table 3.2 shows the 32 nuclear Overhauser effect (NOE) distance restraints, four dihedral angles, and two disulfide bond constraints that were input into CYANA for structure calculation. NMR structure determination using CYANA[189] confirms the peptide backbone exists as a ribbon, lacking a defined α-helix. Despite a reasonably rigid scaffold constrained by two disulfide bonds, the backbone structure of KTM reflects the influence of side chain mobility particularly evident for the aromatic Tyr and Trp residues. Figure 3.6 A-B shows a comparison of the NMR-derived structures (A) and an overlay of the median NMR-derived structure (cyan) to the computationally predicted structure (magenta) for KTM (B). The root-mean-squared deviation (RMSD) for backbone atoms to a mean structure was calculated to be 1.7 ± 0.4 Å (Figure 3.6A). The RMSD between the NMR solution structure of KTM and the computationally predicted KTM structure was 3.5 Å, which is expected considering the computationally predicted structure maintained the globular disulfide connectivity consistent with α-CTx MII (Figure 3.6B).

Table 3.1. Proton chemical shift assignments for amino acids in KTM.

Residue	NH	αH	βH	Other
W1	8.31	4.62	3.61,3.44	2H 7.37, N1H 10.23
C2	8.57	5.33	3.71,2.92	
C3	8.63	5.14	2.96,3.67	
S4	8.53	4.23	3.79	
Y5	7.91	4.84	3.39,3.23	
P6	--	4.07	1.99,2.20	δH 3.70,3.58
G7	7.96	4.08	--	
C8	8.40	4.53	3.62,3.11	
Y9	7.78	4.57	3.32,3.60	
W10	8.09	4.84	3.21	2H 7.74, N1H 10.52, 7H 7.88
S11	8.62	4.33	3.83	
S12	8.38	4.25	3.88	
S13	8.74	4.40	4.01	
K14	8.19	4.66	1.72,1.56	δH 1.39, γH 1.29, εH 2.91, N2H 8.00
W15	7.64	5.12	3.13,3.31	2H 7.48, N1H 10.33
C16	8.47	5.08	3.57,3.04	

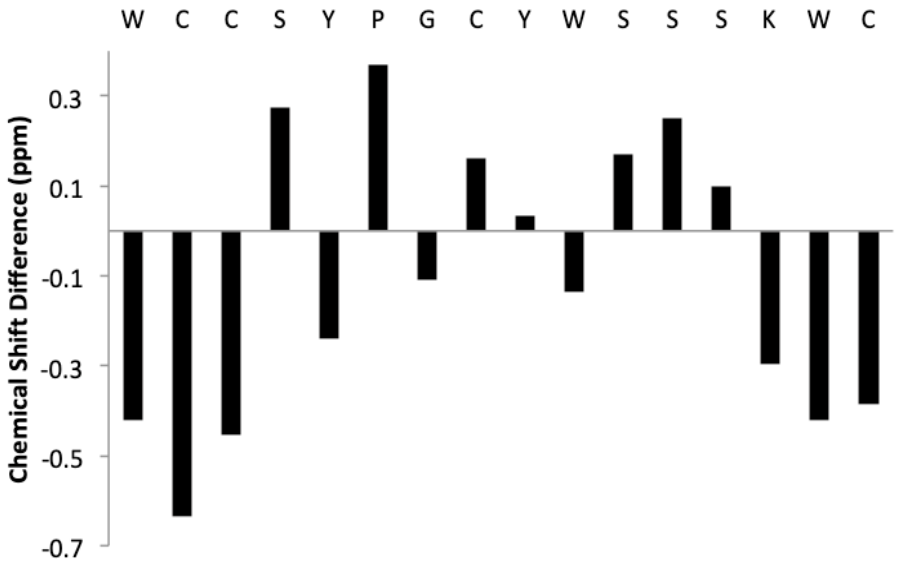

Figure 3.5. Chemical shift difference between α-protons of amino acids in KTM and predicted random coil chemical shifts for the same amino acids.

Table 3.2. NMR restraints used in CYANA and the resulting structure statistics for KTM.

Experimental Data	
Distance restraints	
Total NOE	32
Intra-residue	12
Inter-residue	20
Sequential	18
Short-range	30
Medium-range	2
Long-range	0
ϕ Dihedral angle restraints	4
Disulfide restraints	2
Total NOE violations exceeding 0.3 Å	0
Total NOE violations exceeding 2 Å	0
Structure statistics	
Average pairwise RMSD (Å)	
Backbone atoms (residues 1-16)	1.7±0.5
Heavy atoms (residues 1-16)	3.0±0.7
Ramachandran statistics	
% Favored and allowed regions	100
% Disallowed regions	0

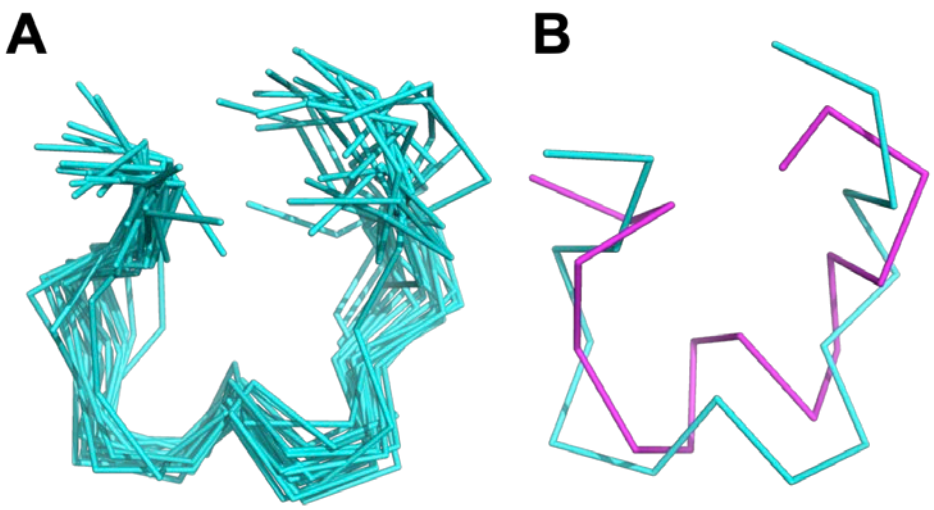

Figure 3.6. NMR solution structure of KTM, where (A) is a ribbon representation of an ensemble of the 20 lowest energy structures, with an average RMSD to the mean structure of 1.7 ± 0.4 Å, and (B) represents an overlay of the mean calculated structure from NMR (cyan) and the computationally predicted structure (magenta) that have an average RMSD of 3.5 Å.

Structure Determination

Figure 3.7 shows the root-mean-square fluctuations (RMSFs) for each residue after a 50 ns molecular dynamics simulation in Gromacs. According to these results, the side chains of KTM are expected to have a high degree of fluctuation. Residues W1, S4–G7, and K14, particularly, show the highest degrees of fluctuation.

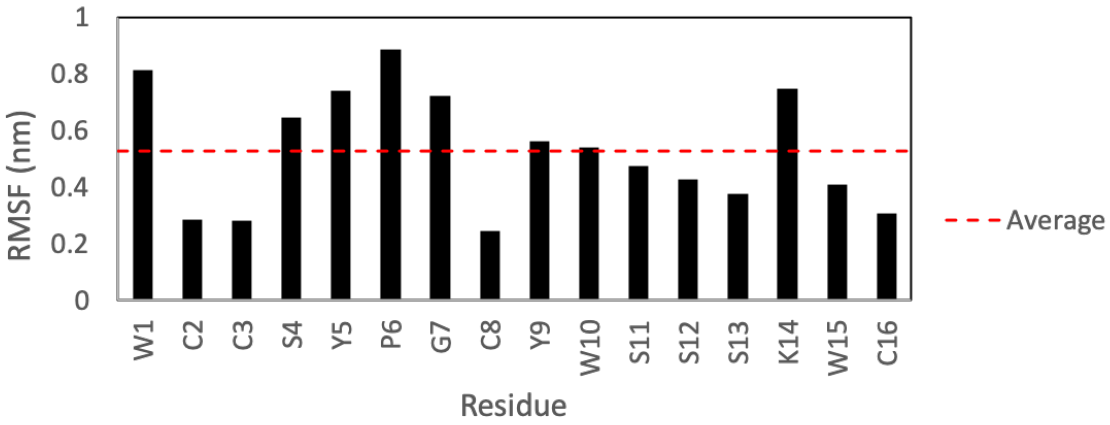

Figure 3.7. Root mean square fluctuations for each of the 16 residues of KTM over a 50 ns MD simulation. Residues W1, S4–G7, and K14 were observed to exhibit the greatest root-mean-square fluctuations (RMSFs).

Discussion

Qualitative evaluation of KTM bioactivity with the PC12 assay confirmed that KTM reduced the amount of dopamine released from the cells, presumably by blocking nAChRs (Figure 3.2).[141] To assess whether KTM acted on rα3β2-nAChRs, as it was designed to do, quantitative evaluation of its bioactivity was performed by two electrode voltage clamp electrophysiology using *Xenopus* oocytes expressing rα3β2-nAChRs. KTM caused blockage of rα3β2-nAChRs with an IC_{50} of 0.19±0.02 nM as compared to 0.35±0.08 nM for α-CTx MII (Figure 3.3). The similar efficacy of KTM compared to that of α-CTx MII supports the premise that the synthetic peptide is an effective antagonist of rα3β2-nAChR.

KTM exhibited potent inhibition of rα3β2-nAChRs commensurate with α-CTx MII, necessitating validation of synthetic peptide structure for comparison to the computationally predicted structure. The primary sequence of KTM differs from α-CTx MII with regard to nine of the sixteen amino acids. First, the NMR structure of KTM was

determined using the method established by Wüthrich.[188] Sequence, distance, dihedral angle, and disulfide bond restraints were entered into CYANA for structure calculation. It was anticipated that the disulfide bonds in synthesized KTM, which were formed by undirected folding, and those of α-CTx MII, would be consistent. Despite extensive analysis of NMR data and restraint assignment, CYANA failed to provide an ensemble of KTM backbone structures that converged better than a RMSD of 2.5 Å. An evaluation of the CD spectrum and partial reduction mass spectrometry data provided definitive evidence that the disulfide pattern for KTM synthesized by undirected folding was not the same as the globular fold of α-CTx MII (C1-C3, C2-C4), but rather was consistent with the ribbon fold observed for an isomer of α-CTx AuIB[186, 187] (C1-C4, C2-C3) (see Figure B.1). An ordered secondary structure commensurate with the common α-CTx 4/7 loop peptide α-helix of MII was not expected due to the α-helical content for KTM interpreted as 12.5% based on the CD spectrum, which is much lower than the α-helical content for α-CTx MII of 38.1% (Figure 3.4). Upon changing the disulfide bond connectivity restraints in CYANA, a final set of 20 KTM structures with an RMSD among backbone atoms of 1.7 ± 0.5 Å was obtained with no distance restraint or conformation violations detected (Figure 3.6). The RMSD between the NMR solution structure of KTM and the computationally predicted structure of KTM was 3.5 Å. The rough similarity in backbone shape between the computationally predicted and NMR solution structure generated for KTM, despite differing disulfide linkages, is suspected to be the reason for the observed nAChR bioactivity. Preliminary analysis of NMR data for chemical shift deviation from random coil was used as an indication of expected KTM peptide rigidity (Figure 3.5). Random coil peptides generally show amide proton chemical shifts between 8.09 and 8.45 ppm,[190] while

those in KTM were between 7.64 and 8.74, indicating regions of structure rigidity. Similarly, random coil peptides generally show α-proton chemical shifts between 4.4 and 4.8 ppm, while those in KTM were between 4.07 and 5.33 ppm. Thus, the chemical shift variation observed for amide and α-protons in KTM (Figure 3.5) were consistent with data expected for a peptide of reasonably rigid scaffold.

The relatively low number of distance and angle constraints for KTM was due to challenges associated with a 1942 Da peptide and the high redundancy of amino acids (4C, 4S, 3W, 2Y), resulting in many proton chemical shifts in similar or identical electronic environments. The interpretation of NMR spectra for KTM was severely complicated due to peak overlap, ring-flipping of aromatic side chains, and spectral shift between H_2O and D_2O spectra. Figure 3.7 shows an overlay of the fingerprint region for COSY and TOCSY spectra used to assign the spin systems in KTM from which the chemical shift assignments as summarized in Table 3.1 were generated. The proton chemical shifts for aromatic amino acids are largely missing from Table 3.1 due to assignment ambiguity originating from the three tryptophan and two tyrosine residues with overlapping chemical shifts further exacerbated by ring flipping. Additional structure challenges arose from the molecular weight of KTM correlating to the NOE detection minimum limiting the number of medium- and long-range NOEs that could be assigned as restraints. Conotoxin structure determination by NMR is inherently difficult due to weak NOE signals, limited distance for protons to provide an assignable NOE, and side chain mobility that provides conformations where protons enter in and out of detectable proximity to one another.[191] Additionally, the high number of heavy aromatic side chains in KTM is suspected to contribute to inherent flexibility.

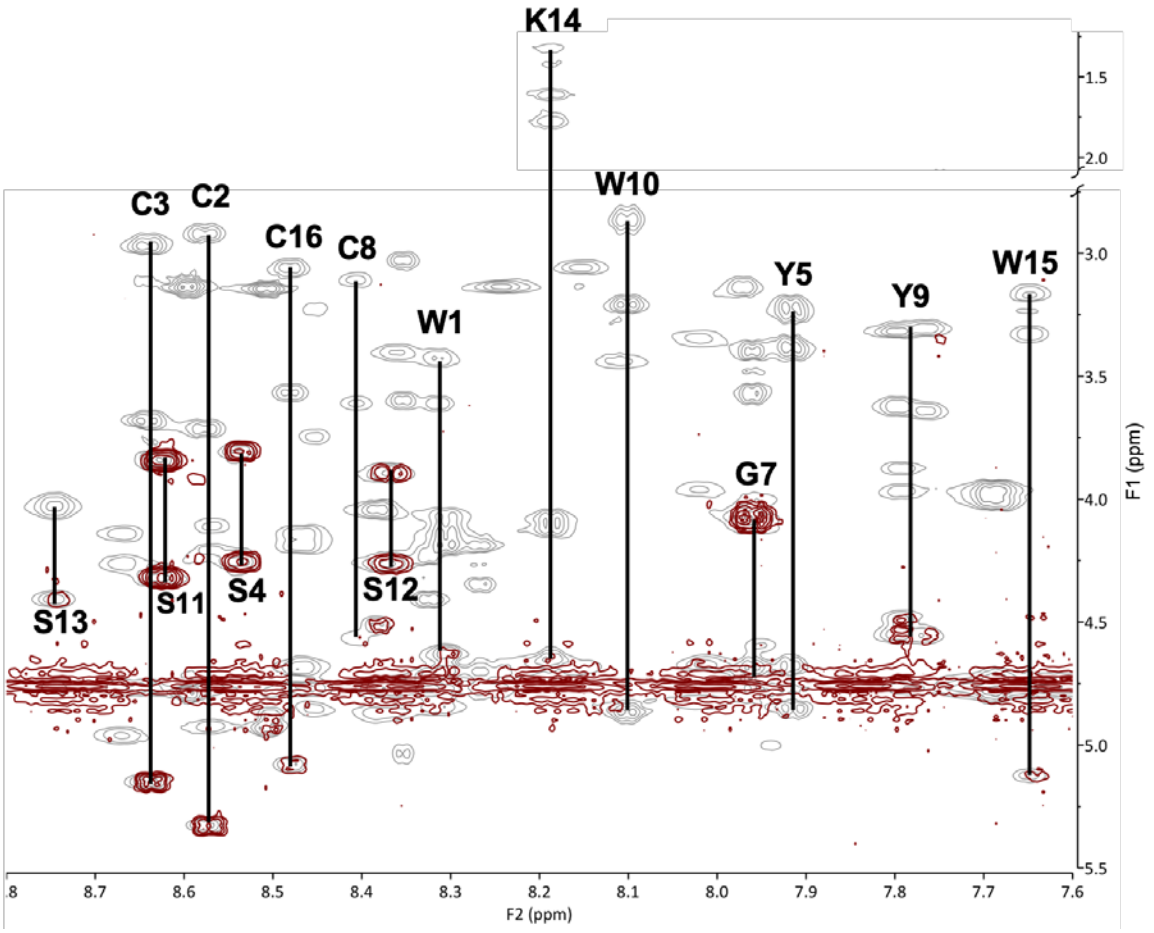

Figure 3.8. Fingerprint region of COSY (red) and TOCSY (grey) spectra overlaid for residues 1-5 and 7-16, acquired at 600 MHz for KTM at 298 K in 30% ACN/70% H2O. Residue assignments are indicated by their one-letter amino acid code.

Perhaps the most striking finding of this study was that KTM, which was predicted to act on rα3β2-nAChRs, did indeed do so, and with very high potency, despite having a ribbon-type α-CTx disulfide connectivity. There is precedent for ribbon isomers of Framework I α-CTxs with high dynamic flexibility and binding affinity for rα3β2-nAChRs. Dutton, et al. (2002) characterized a non-native ribbon disulfide bond isomer of recombinant α-CTx AuIB that, while more flexible than the native globular isomer, exhibited 10 times more potent activity with nAChRs in rat parasympathetic neurons than the native globular isomer.[187] They presumed that the flexibility of the non-native ribbon isomer allowed the peptide to adopt a complementary conformation with the receptor

binding site. KTM is the first example of a Framework I α-CTx with ribbon fold to demonstrate sub-nanomolar inhibition of rα3β2-nAChRs. To briefly explore why KTM exhibits functionality consistent with α-CTx MII, a comparison of the electrostatic maps of α-CTx MII and KTM was performed using the ABPS Electrostatics plugin in PyMOL[192] after performing a 50 ns molecular dynamics simulation in Gromacs. The simulation shows that the side chains for W1, S4–G7, and K14 have a high degree of fluctuation (Figure 3.7), and that loop 2 is especially dynamic (Figure 3.9), indicating that a single model may not well represent the peptide. To illustrate the dynamic flexibility of KTM and its potential for induced fit into the binding site of rα3β2 nAChR, the electrostatic surfaces of KTM at 0 ns (Figure 3.10A) and at 50 ns (Figure 3.10C) are shown in comparison to α-CTx MII (Figure 3.10B). KTM can adopt both a structure with a surface volume much larger than α-CTx MII with multiple points of protrusion from aromatic side chains and a hollow core (Figure 3.10A), as well as a more compact structure that more closely resembles that of α-CTx MII as loop 2 appears to flex inward (Figure 3.10C). The molecular depictions in Figure 3.10 permit visualization leading to a possible explanation for how KTM may have an induced fit in the binding site of rα3β2-nAChRs to exhibit the potent bioactivity observed (Figure 3.3).

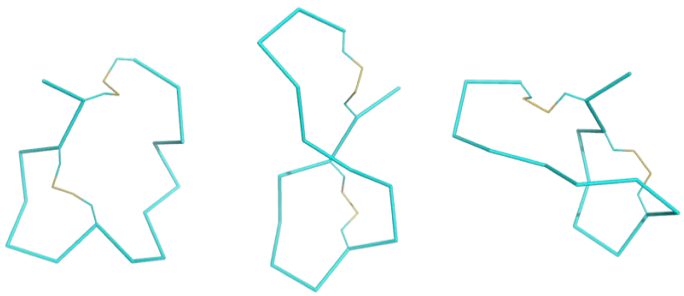

Figure 3.9. Ribbon structures of KTM at 0 ns (left), 25 ns (middle), and 50 ns (right) in the molecular dynamics simulation. Loop 2 appears to swing across the peptide over the course of the simulation.

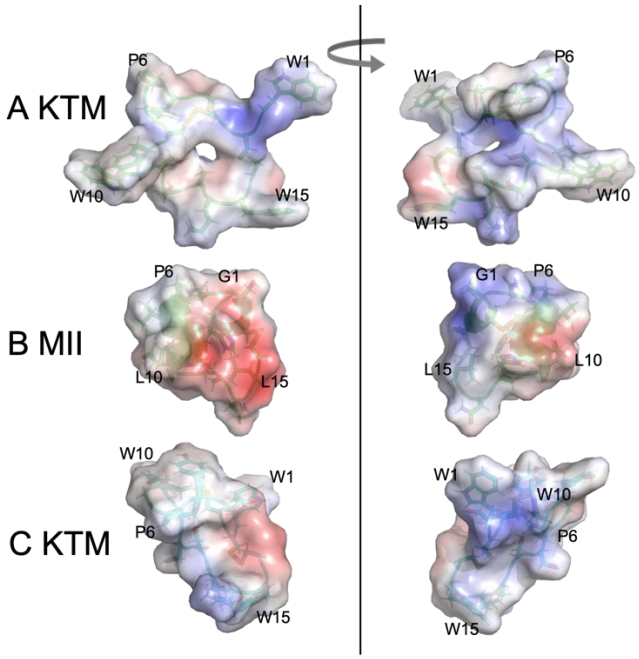

Figure 3.10. Electrostatic maps of KTM at 0 ns of the molecular dynamics simulation (A), α-CTx MII (B), and KTM at 50 ns of the molecular dynamics simulation (C). Images on the left and right are rotated by 180 degrees.

Materials and Methods

Synthesis

KTM was synthesized by and purchased from CS Bio (Menlo Park, CA) in folded form as a white powder. Following solid phase peptide synthesis, disulfide linkages were allowed to form into the most thermodynamically stable conformation under reducing conditions. The major isomer was collected by HPLC at ca. 98.36% purity. The peptide was collected at 10.71 min using a 20-50% gradient of Buffer B (0.1% TFA in ACN) over a 20 min run time, where Buffer A was 0.1% TFA in H_2O. The column was a Phenomenex Luna C_{18} with specifications of 5 µM, 100 Å, 4.6 x 250 mm. The flow rate was 1 mL/min and the injection volume was 20 µL. Peptide identity was confirmed by mass spectrometry

where the expected molecular weight was 1942.21 Da and the found molecular weight was 1941.52 Da.

Disulfide Bond Analysis

Analysis was performed using an UltiMate 3000 HPLC (Thermo Scientific, Waltham, MA, USA) equipped with a Corona Veo RS charged aerosol detector (CAD), an UltiMate 3000 Diode Array Detector (DAD), and MSQ Plus mass spectrometer (MS). HPLC separation of peptide species was achieved using an Acclaim 120 C_{18} column (2.1 × 150 mm, 3 µm) (Thermo Fisher), and mobile phases consisting of 0.1% formic acid (v/v) in water (Buffer A) and 0.1 % formic acid (v/v) in acetonitrile (Buffer B) with a flow rate of 0.3 mL/min. A linear gradient method beginning at 85% Buffer A and 15% Buffer B, up to 60% Buffer B over a 25 min run time achieved desired separation from a 10 µL sample injection volume. Data were analyzed with the Chromeleon 7.2 Chromatography Data System (Thermo Fisher). The partial reduction strategy of Gray[193] was used to sequentially reduce and alkylate disulfide bonds. Synthetic KTM peptide (0.1 nmol) from CS Bio was dissolved in 1 M equivalent of tris 2-carboxyethyl phosphine (TCEP) in 25 mM ammonium formate, at pH 4.5, and incubated at 37°C for 10 min. Following incubation, the reaction mixture was separated by HPLC, and the peptide reduction was monitored by mass spectrometry through observation of a mass increase of +2 m/z, corresponding to the peptide with one disulfide bond reduced. Two molar equivalents of N-ethylmaleimide (NEM) were added and the reaction mixture and alkylation was monitored by LC-MS for observation of a mass increase of +125 m/z. The increase in m/z of +125 in the doubly charged ion equates to a mass shift of +250 Da in KTM corresponding to the coupling of one thiol to NEM. Peptide fractions, as identified by UV

absorbance at 280 nm, were collected manually into 1.5 mL polypropylene centrifuge tubes and lyophilized to dryness. The resultant di- and tetra-alkylated peptides appeared as dull white powders. Monocyclic intermediates were reconstituted in 1:1 (v/v) acetonitrile/25 mM ammonium formate, reduced with dithiothreitol (DTT) at a final concentration of 10 mM for 1 hr at 37°C, and alkylated with iodoacetamide (IAA) at a final concentration of 55 mM for 1 hr in the dark at room temperature. The reaction mixture was injected onto the LC-MS to monitor reduction and alkylation by observation of a mass increase of +59 m/z, corresponding to the addition of acetamide. Doubly alkylated peptides were submitted for sequence analysis to determine the locations of S-carboxamidomethyl-L-cysteine residues, and confirm the disulfide connectivity (see Appendix B). MS/MS fragmentation for sequence analysis was achieved using a Velos Pro Dual-Pressure Linear Ion Trap mass spectrometer (Thermo Scientific) coupled to a Nanoscale LC system at a flow rate of 300 nL/min. A fused silica emitter directly attached to the analytical column through a zero dead volume union was used spray peptides at a voltage of 2.2 kV. MS/MS data was collected in data-dependent acquisition mode, using collision-induced dissociation (CID) with a normalized collision energy of 35% to fragment the precursor ions. Collect MS/MS data for the 10 most abundant precursor ions was selected from the proceeding full MS scan over the m/z range of 300 – 2000. Proteome Discoverer 2.2 (Thermo Scientific) was used to analyze the data.

Circular Dichroism Spectropolarimetry

Circular dichroism (CD) spectra were recorded on a Jasco J-810 spectropolarimeter (Jasco, Inc., Easton, MD, USA) with a cell path length of 0.1 cm at room temperature in a nitrogen atmosphere in water. Scans were acquired from 190 to 250 nm. The bandwidth of

1 nm, a speed of 50 nm/min, and a resolution of 0.5 nm were used. A total of 5 scans per sample were averaged, baselines were subtracted, and the sample was run in triplicate. A final concentration of 50 µM of each sample was used. Analysis and data processing were carried out with the Jasco system software and Microsoft Excel. Mean residue ellipticity (θMRE, in deg × cm^2× $dmol^{-1}$) for each spectrum was calculated from the formula θMRE = θ/(10Cr × *l*), where θ is the measured ellipticity in millidegrees, Cr is the molar concentration, and *l* is the path length in centimeters. The α-helical content was estimated from the formula θMRE = −30300fH − 2340, where fH is the fraction of α-helical content (fH × 100, expressed as a percentage) calculated from the θMRE at 222 nm, which is a widely used proxy for helical secondary structure that is useful to assess disruption of the secondary structure, as was performed here.[95, 194, 195]

2D Nuclear Magnetic Resonance Spectroscopy

NMR samples were prepared at a concentration of approximately 3 mM in either 30% deuterated acetonitrile (d-ACN)/70% water or 30% d-ACN/70% deuterium oxide (D_2O). d-ACN was used due to the limited solubility of KTM in water. D_2O samples were prepared by dissolving lyophilized sample in 30% d-ACN/70% D2O solvent and immediately acquiring spectra. Two-dimensional ^1H NMR experiments and spectral interpretation were performed by established methods.[188-190, 196-202]

All NMR data were acquired on a 600 MHz Bruker Avance III NMR spectrometer at 298 K. COSY, TOCSY, and NOESY spectra were acquired using water suppression for aqueous samples. A series of NOESY spectra were acquired with mixing times of 150, 200, 250, 300, and 350 ms. TOCSY spectra were acquired with an 80 ms mixing time (30% ACN/60% H_2O /10% D_2O). Parameter set details are provided in Appendix 2 (Table B.1).

Spectra were processed in Topspin and analyzed in CCPNMR v2 and v3[203] to correct resonance shifts, manually pick peaks, and identify spin systems.

Restraint Set Generation: Three-bond $^{1}H^{N}$-$^{1}H^{\alpha}$ coupling constant values were determined by visual inspection of a high-resolution 1D ^{1}H spectrum in Topspin. Backbone dihedral phi angle restraints were set to -120 ± 40 for $^{3}J_{HH}$ $^{1}H^{N}$-$^{1}H^{\alpha}$ coupling constant values greater than 7.5 Hz and to -65 ± 25 for $^{3}J_{HH}$ $^{1}H^{N}$-$^{1}H^{\alpha}$ coupling constant values less than 5 Hz.[202] Inter- and intraproton distance ranges were calibrated within CYANA. Distance restraints were derived from NOESY spectra recorded at 298 K and mixing time of 350 ms.

Structure Calculation: Input files were formatted for the CYANA program (v 2.1). The autoassign script in CYANA was used for assignment of 69 hydrogen atom chemical shift values. A chemical shift tolerance of 0.075 was used for both axes. Disulfide bonds were used as distance restraints. CYANA produced an ensemble of 20 top structures based on 32 restraints. The final set of 20 structures gave a root-mean-square deviation among backbone atoms of 1.7 ± 0.4 Å. The structure most representative of the mean structure was determined with WHATIF.[204] Procheck[205] and Verify3D[206] online servers were used to assess structure quality. Molprobity scores are reported in Table B.2.[207]

PC12 Assay

Cell culture and bioactivity assessment were performed according to Marquart, et al.[141] The PC12 assay was performed using a Biotek Synergy H1 microplate reader (Winooski, VT). All chemicals were purchased at the highest purity available (>95%) from Fisher Scientific. ATCC® CRL1721™ PC12 cells were provided by the Biomolecular Research Center at Boise State University.

Cell culture: PC12 cells were cultured into laminin-coated flasks and triturated to detach. Cells were grown in a T-75 flask until dense enough to plate onto a laminin-coated flat-bottom well plate and treated with starvation media (30 ng/mL NGF 2.5S, 1 µM nicotine) for 3-4 days before performing the assay.

Assay: Cells were washed with Locke's solution before introducing the assay solution, which included 10 µM toxin, 0.8 ng/mL POD, 25 ng/mL MAO, and 50 µM luminol. The luminol was added to quench any dissolved oxygen in the cell environment and the assay solution. Cells were allowed to equilibrate for 5-10 min before the addition of 2 mM luminol and 50 µM ACh, for a total well volume of 100 µL. Upon equilibration, the luminescence signal was detected. (-)MAO and (-)cells were used as negative controls. Assays were performed at 37°C, detecting luminescence for 1-2 min per well. Luminescence response curves were then integrated as a measure of dopamine secretion inhibition resultant from peptide treatment for analysis.

Electrophysiology

rα3β2-nAChR expression in Xenopus laevis oocytes: cDNA preparation, oocyte harvest, expression of nAChR subunits, and culture were performed as described previously.[63] The rat isoforms of neuronal nAChR subunits α3 and β2 in vectors pSP64 and pSP65, respectively, were generously provided by Dr. Steven Heinemann (Salk Institute, San Diego, CA). All salts and antibiotics were obtained from Sigma or Fisher Scientific. Oocytes were extracted from adult *Xenopus* according to protocols approved by the Institutional Animal Use and Care Committee at ISU and according to AAALAC guidelines. Oocytes were isolated with 2 mg/L collagenase and cultured at 17.5 °C in sterile ND-96 saline containing 96 mM NaCl, 2 mM KCl, 1.8 mM $CaCl_2$, 1mM $MgCl_2$, and 5

mM 4-(2-hydroxyethyl)-1-piperazineethanesulfonic acid (HEPES), with 5 mM Na pyruvate, 2% horse serum, 100 mg/L gentamicin, 100 mg/L amikacin, 50 mg/L ciprofloxacin, 20 mg/L tetracycline, and 100 U/L streptomycin/penicillin, at pH 7.4. Messenger RNA was transcribed as detailed previously; α3 and β2 mRNA was coinjected at 41 nL into oocytes 3 to 5 days prior to recordings.

Two-electrode voltage clamp: To record the response to ACh, oocytes were impaled with glass electrodes containing 3 M KCl for two-electrode voltage clamp electrophysiology. Oocytes were placed in a 300 µL recording chamber and perfused at 1.0 mL/min with ND-96 saline containing atropine sulfate (1 mM), at room temperature. Voltage clamp was performed with an OC-725C amplifier (Warner Instruments, Hamden, CT) with data acquisition achieved through an ITC-18 interface and PatchMaster 2.35 software (HEKA Instruments, Bellmore, NY). Oocytes were held at -70 mV between trials, and at -80 mV during trials of ACh application. During perfusion, a 20 to 50 ms pulse of ACh chloride (0.01 M, Sigma, St. Louis, MO) in the bath solution was locally applied from a glass capillary tube positioned above the oocyte, with pressure ejection using a PicoSpritzer II valve controller (General Valve Corporation, Fairfield, NJ). Once a reliable response was obtained, the chamber was perfused with α-CTx MII or KTM for 15 min, and the ACh pulse was applied. Inward sodium current amplitudes for each toxin trial were normalized against the control response to ACh as percent block. Each data point of the dose response curve represents the average value of 8 to 12 measurements. Dose-dependent response curves were fit to Equation 1:

$$\% \text{ response} = 100/[1 + ([\text{toxin}]/IC_{50})^{n}], \quad (1)$$

where *n* is the Hill coefficient and IC_{50} is the inhibitory concentration at half-maximal block, by non-linear regression analysis using Igor Pro 6.37 (Wavemetrics, Lake Oswego, OR, USA).

Molecular Dynamics Simulations

Molecular dynamics simulations were performed with the AMBER03 force-field parameter set[140] using the Gromacs 2019 software package.[136] The median conformation for KTM from the top 20 NMR solution structures was selected as the input structure for MD simulation in Gromacs. Since the NMR spectra were acquired for a sample in 30% acetonitrile/70% water, the solvated box was obtained by filling a dodecahedral box with the appropriate number of acetonitrile molecules to achieve the desired mixed solvent proportions. A topology for acetonitrile was created for this purpose. The shortest distance of peptide atoms from the box boundary was 1.2 Å. Simulations were carried out at 300 K in a periodic box with a minimum-image convention. The integration step was 1 fs, and total duration of each run was 50 ns. Water, acetonitrile, and ions were temperature coupled. Energy minimizations and N, V, T and N, P, T equilibrations were performed before running the simulation. A 500 ps equilibration was conducted under the NVT ensemble using a velocity-rescale thermostat at 300 K with a coupling time constant of 0.1 ps. A subsequent 500 ps NPT equilibration was performed using the isotropic Berendsen barostat with a time constant of 0.1 ps. Simulations and models were visualized in Pymol.[192]

Conclusions

This investigation sought to validate the accuracy and usefulness to rationally design a selective antagonist of a specific nAChR isoform based on the well characterized marine drug α-CTx MII. Synthetic KTM peptide was confirmed to be a potent sub-nanomolar inhibitor of rα3β2 nAChRs. It was expected that KTM would fold into the same C1-C3 and C2-C4 disulfide pattern, consistent with α-CTx MII. Instead, the folding of KTM resulted in a C1-C4 and C2-C3 ribbon Framework I α-CTx, consistent with the recombinant isomer of α-CTx AuIB.[186, 187] It has been stated in the literature that correct folding of synthetic peptides is critical to the maintenance of biological activity, but in the instance of KTM, the globular disulfide pattern is not the same as that found in α-CTx MII, but rather resembles the ribbon-connectivity studied for α-CTx AuIB.[186, 187] KTM is the first example of sub-nanomolar nAChR antagonism by a Framework I α-CTx of ribbon-connectivity. A compelling next step for this work would be the directed folding of KTM to assess whether the potency of the globular-connectivity Framework I peptide may be further enhanced for nAChR inhibition. Validation of computationally predicted peptide binding and biological activity may lead to a better understanding of molecular probes for the treatment of neurological diseases like Parkinson's Disease. Drugs that selectively target human α6α4β2β3 nAChR isoforms could be used as new therapies with fewer side effects than existing treatments. The current study offers a workflow to begin the search for drug therapies inspired by marine natural products.

CHAPTER FOUR: CONCLUSION AND FUTURE DIRECTIONS

The work in this thesis demonstrates the value of conotoxins as molecular probes to gain the understanding of nAChR isoform selectivity needed to develop treatments for neurological disorders. To better understand the effect α-CTx binding to nAChRs has on cell signaling, we presented a case study of a rationally designed peptide using computational tools to predict binding affinity along with structure activity relationship results. It may be concluded that the computational method used in this case study has merit and requires experimental validation. To increase efficiency of investigations into nAChR binding and function, an optimized PC12 cell assay was developed to quickly and economically pre-screen ligands for qualitative nAChR bioactivity prior to resource-intensive quantitative experiments. The current study provides a workflow to begin the search for small molecule drug therapies inspired by conotoxins, and future studies will involve using computational programs and online molecular databases to identify pharmacophore features of model peptides required for binding in order to discover small molecule scaffolds for lead compounds. These small molecules can then be characterized for desired activity in the PC12 assay. A future goal is to identify a variety of chemical treatment protocols for enhanced expression of select nAChR subunits in addition to the rα3β2 isoform focused on in this case study, and to create cell lines heterologously expressing disease-relevant nAChR subtypes. Drugs that selectively target human α6α4β2β3 nAChR isoforms could be used as new therapies for Parkinson's disease with fewer side effects than existing treatments like Levodopa. A workflow for efficient

validation of computationally predicted peptide binding and biological activity with nAChRs may spur understanding of molecular probes and result in identification of lead compounds in treatment of neurological diseases like Parkinson's.

REFERENCES

1. Turner, M. W.; Marquart, L. A.; Phillips, P. D.; McDougal, O. M., Mutagenesis of alpha-Conotoxins for Enhancing Activity and Selectivity for Nicotinic Acetylcholine Receptors. *Toxins* **2019,** *11* (2), 29.

2. Muttenthaler, M.; Akondi, K. B.; Alewood, P. F., Structure-Activity Studies on Alpha-Conotoxins. *Current Pharmaceutical Design* **2011,** *17* (38), 4226-4241.

3. Gray, W. R.; Olivera, B. M.; Cruz, L. J., Peptide Toxins from Venomous Conus Snails. *Annual Review of Biochemistry* **1988,** *57*, 665-700.

4. McIntosh, J. M.; Jones, R. M., Cone venom - from accidental stings to deliberate injection. *Toxicon* **2001,** *39* (10), 1447-1451.

5. Livett, B. G.; Gayler, K. R.; Khalil, Z., Drugs from the sea: Conopeptides as potential therapeutics. *Current Medicinal Chemistry* **2004,** *11* (13), 1715-1723.

6. Davis, J.; Jones, A.; Lewis, R. J., Remarkable inter- and intra-species complexity of conotoxins revealed by LC/MS. *Peptides* **2009,** *30* (7), 1222-1227.

7. Olivera, B. M., Conus venom peptides: Reflections from the biology of clades and species. *Annual Review of Ecology and Systematics* **2002,** *33*, 25-47.

8. ConoServer. http://www.conoserver.org (accessed October 8th, 2019).

9. Terlau, H.; Olivera, B. M., Conus venoms: A rich source of novel ion channel-targeted peptides. *Physiological Reviews* **2004,** *84* (1), 41-68.

10. Olivera, B. M.; Teichert, R. W., Diversity of the neurotoxic Conus peptides: A model for concerted pharmacological discovery. *Molecular Interventions* **2007,** *7* (5), 251-260.

11. Sharman, J. L.; Benson, H. E.; Pawson, A. J.; Lukito, V.; Mpamhanga, C. P.; Bombail, V.; Davenport, A. P.; Peters, J. A.; Spedding, M.; Harmar, A. J.; Nc, I., IUPHAR-DB: updated database content and new features. *Nucleic Acids Research* **2013,** *41* (D1), D1083-D1088.

12. Akondi, K. B.; Muttenthaler, M.; Dutertre, S.; Kaas, Q.; Craik, D. J.; Lewis, R. J.; Alewood, P. F., Discovery, Synthesis, and Structure Activity Relationships of Conotoxins. *Chemical Reviews* **2014,** *114* (11), 5815-5847.

13. Armishaw, C. J.; Alewood, P. F., Conotoxins as research tools and drug leads. *Current Protein & Peptide Science* **2005,** *6* (3), 221-240.

14. Lewis, R. J.; Dutertre, S.; Vetter, I.; Christie, M. J., Conus Venom Peptide Pharmacology. *Pharmacological Reviews* **2012,** *64* (2), 259-298.

15. Miljanich, G. P., Ziconotide: Neuronal calcium channel blocker for treating severe chronic pain. *Current Medicinal Chemistry* **2004,** *11* (23), 3029-3040.

16. Molinski, T. F.; Dalisay, D. S.; Lievens, S. L.; Saludes, J. P., Drug development from marine natural products. *Nature Reviews Drug Discovery* **2009,** *8* (1), 69-85.

17. Zouridakis, M.; Zisimopoulou, P.; Poulas, K.; Tzartos, S. J., Recent Advances in Understanding the Structure of Nicotinic Acetylcholine Receptors. *Iubmb Life* **2009,** *61* (4), 407-423.

18. Jensen, A. A.; Frolund, B.; Lijefors, T.; Krogsgaard-Larsen, P., Neuronal nicotinic acetylcholine receptors: Structural revelations, target identifications, and therapeutic inspirations. *Journal of Medicinal Chemistry* **2005,** *48* (15), 4705-4745.

19. Liu, W. Y.; Li, M. D., Insights into Nicotinic Receptor Signaling in Nicotine Addiction: Implications for Prevention and Treatment. *Current Neuropharmacology* **2018,** *16* (4), 350-370.

20. Millar, N. S.; Gotti, C., Diversity of vertebrate nicotinic acetylcholine receptors. *Neuropharmacology* **2009,** *56* (1), 237-246.

21. Le Novere, N.; Corringer, P. J.; Changeux, J. P., The diversity of subunit composition in nAChRs: Evolutionary origins, physiologic and pharmacologic consequences. *Journal of Neurobiology* **2002,** *53* (4), 447-456.

22. Taly, A.; Corringer, P. J.; Guedin, D.; Lestage, P.; Changeux, J. P., Nicotinic receptors: allosteric transitions and therapeutic targets in the nervous system. *Nature Reviews Drug Discovery* **2009,** *8* (9), 733-750.

23. Colquhoun, L. M.; Patrick, J. W., Pharmacology of neuronal nicotinic acetylcholine receptor subtypes. *Advanced Pharmacology* **1997,** *39*, 191-220.

24. Chatzidaki, A.; Millar, N. S., Allosteric modulation of nicotinic acetylcholine receptors. *Biochemical Pharmacology* **2015,** *97* (4), 408-417.

25. Wilson, G. G.; Karlin, A., Acetylcholine receptor channel structure in the resting, open, and desensitized states probed with the substituted-cysteine-accessibility method. *Proceedings of the National Academy of Sciences of the United States of America* **2001,** *98* (3), 1241-1248.

26. Wonnacott, S., Presynaptic nicotinic ACh receptors. *Trends in Neurosciences* **1997,** *20* (2), 92-98.

27. Berry, J. N.; Engle, S. E.; McIntosh, J. M.; Drenan, R. M., Alpha 6-Containing Nicotinic Acetylcholine Receptors in Midbrain Dopamine Neurons Are Poised to Govern Dopamine-Mediated Behaviors and Synaptic Plasticity. *Neuroscience* **2015,** *304*, 161-175.

28. Champtiaux, N.; Han, Z. Y.; Bessis, A.; Rossi, F. M.; Zoli, M.; Marubio, L.; McIntosh, J. M.; Changeux, J. P., Distribution and pharmacology of alpha 6-containing nicotinic acetylcholine receptors analyzed with mutant mice. *Journal of Neuroscience* **2002,** *22* (4), 1208-1217.

29. Dineley, K. T.; Pandya, A. A.; Yakel, J. L., Nicotinic ACh receptors as therapeutic targets in CNS disorders. *Trends in Pharmacological Sciences* **2015,** *36* (2), 96-108.

30. Ortells, M. O.; Lunt, G. G., Evolutionary history of the ligand-gated ion-channel superfamily of receptors. *Trends in Neurosciences* **1995,** *18* (3), 121-127.

31. Gotti, C.; Clementi, F., Neuronal nicotinic receptors: from structure to pathology. *Progress in Neurobiology* **2004,** *74* (6), 363-396.

32. Quik, M.; Bordia, T.; O'Leary, K., Nicotinic receptors as CNS targets for Parkinson's disease. *Biochemical Pharmacology* **2007,** *74* (8), 1224-1234.

33. Drenan, R. M.; Grady, S. R.; Whiteaker, P.; McClure-Begley, T.; McKinney, S.; Miwa, J. M.; Bupp, S.; Heintz, N.; McIntosh, J. M.; Bencherif, M.; Marks, M. J.; Lester, H. A., In Vivo Activation of Midbrain Dopamine Neurons via

Sensitized, High-Affinity alpha 6*Nicotinic Acetylcholine Receptors. *Neuron* **2008,** *60* (1), 123-136.

34. Quik, M.; Wonnacott, S., alpha 6 beta 2*and alpha 4 beta 2*Nicotinic Acetylcholine Receptors As Drug Targets for Parkinson's Disease. *Pharmacological Reviews* **2011,** *63* (4), 938-966.

35. Turner, M.; Eidemiller, S.; Martin, B.; Narver, A.; Marshall, J.; Zemp, L.; Cornell, K. A.; McIntosh, J. M.; McDougal, O. M., Structural basis for alpha-conotoxin potency and selectivity. *Bioorganic & Medicinal Chemistry* **2009,** *17* (16), 5894-5899.

36. McIntosh, J. M.; Azam, L.; Staheli, S.; Dowell, C.; Lindstrom, J. M.; Kuryatov, A.; Garrett, J. E.; Marks, M. J.; Whiteaker, P., Analogs of alpha-conotoxin MII are selective for alpha 6-containing nicotinic acetylcholine receptors. *Molecular Pharmacology* **2004,** *65* (4), 944-952.

37. Dutertre, S.; Nicke, A.; Tsetlin, V. I., Nicotinic acetylcholine receptor inhibitors derived from snake and snail venoms. *Neuropharmacology* **2017,** *127*, 196-223.

38. Armishaw, C. J., Synthetic alpha-Conotoxin Mutants as Probes for Studying Nicotinic Acetylcholine Receptors and in the Development of Novel Drug Leads. *Toxins* **2010,** *2* (6), 1471-1499.

39. Wu, R. J.; Wang, L.; Xiang, H., The Structural Features of alpha-Conotoxin Specifically Target Different Isoforms of Nicotinic Acetylcholine Receptors. *Current Topics in Medicinal Chemistry* **2016,** *16* (2), 156-169.

40. Giribaldi, J.; Dutertre, S., alpha-Conotoxins to explore the molecular, physiological and pathophysiological functions of neuronal nicotinic acetylcholine receptors. *Neuroscience Letters* **2018,** *679*, 24-34.

41. Abraham, N.; Lewis, R. J., Neuronal Nicotinic Acetylcholine Receptor Modulators from Cone Snails. *Marine Drugs* **2018,** *16* (6), 23.

42. Hone, A. J.; Ruiz, M.; Scadden, M.; Christensen, S.; Gajewiak, J.; Azam, L.; McIntosh, J. M., Positional Scanning Mutagenesis of alpha-Conotoxin PeIA Identifies Critical Residues That Confer Potency and Selectivity for alpha 6/alpha 3 beta 2 beta 3 and alpha 3 beta 2 Nicotinic Acetylcholine Receptors. *Journal of Biological Chemistry* **2013,** *288* (35), 25428-25439.

43. Miyazawa, A.; Fujiyoshi, Y.; Unwin, N., Structure and gating mechanism of the acetylcholine receptor pore. *Nature* **2003,** *423* (6943), 949-955.

44. Unwin, N., Refined structure of the nicotinic acetylcholine receptor at 4 angstrom resolution. *Journal of Molecular Biology* **2005,** *346* (4), 967-989.

45. Brejc, K.; van Dijk, W. J.; Klaassen, R. V.; Schuurmans, M.; van der Oost, J.; Smit, A. B.; Sixma, T. K., Crystal structure of an ACh-binding protein reveals the ligand-binding domain of nicotinic receptors. *Nature* **2001,** *411* (6835), 269-276.

46. Celie, P. H. N.; Klaassen, R. V.; van Rossum-Fikkert, S. E.; van Elk, R.; van Nierop, P.; Smit, A. B.; Sixma, T. K., Crystal structure of acetylcholine-binding protein from Bulinus truncatus reveals the conserved structural scaffold and sites of variation in nicotinic acetylcholine receptors. *Journal of Biological Chemistry* **2005,** *280* (28), 26457-26466.

47. Hansen, S. B.; Sulzenbacher, G.; Huxford, T.; Marchot, P.; Taylor, P.; Bourne, Y., Structures of Aplysia AChBP complexes with nicotinic agonists and antagonists reveal distinctive binding interfaces and conformations. *Embo Journal* **2005,** *24* (20), 3635-3646.

48. Celie, P. H. N.; Kasheverov, I. E.; Mordvintsev, D. Y.; Hogg, R. C.; van Nierop, P.; van Elk, R.; van Rossum-Fikkert, S. E.; Zhmak, M. N.; Bertrand, D.; Tsetlin, V.; Sixma, T. K.; Smit, A. B., Crystal structure of nicotinic acetylcholine receptor homolog AChBP in complex with an alpha-conotoxin PnIA variant. *Nature Structural & Molecular Biology* **2005,** *12* (7), 582-588.

49. Bourne, Y.; Talley, T. T.; Hansen, S. B.; Taylor, P.; Marchot, P., Crystal structure of a Cbtx-AChBP complex reveals essential interactions between snake alpha-neurotoxins and nicotinic receptors. *Embo Journal* **2005,** *24* (8), 1512-1522.

50. Dellisanti, C. D.; Yao, Y.; Stroud, J. C.; Wang, Z. Z.; Chen, L., Crystal structure of the extracellular domain of nAChR alpha 1 bound to alpha-bungarotoxin at 1.94 A resolution. *Nature Neuroscience* **2007,** *10* (8), 953-962.

51. Li, S. X.; Huang, S.; Bren, N.; Noridomi, K.; Dellisanti, C. D.; Sine, S. M.; Chen, L., Ligand-binding domain of an alpha(7)-nicotinic receptor chimera and its complex with agonist. *Nature Neuroscience* **2011,** *14* (10), 1253-U173.

52. Zouridakis, M.; Giastas, P.; Zarkadas, E.; Chroni-Tzartou, D.; Bregestovski, P.; Tzartos, S. J., Crystal structures of free and antagonist-bound states of human alpha 9 nicotinic receptor extracellular domain. *Nature Structural & Molecular Biology* **2014,** *21* (11), 976-980.

53. Morales-Perez, C. L.; Noviello, C. M.; Hibbs, R. E., X-ray structure of the human alpha 4 beta 2 nicotinic receptor. *Nature* **2016,** *538* (7625), 411-+.

54. Kombo, D. C.; Mazurov, A. A.; Strachan, J. P.; Bencherif, M., Computational studies of novel carbonyl-containing diazabicyclic ligands interacting with alpha 4 beta 2 nicotinic acetylcholine receptor (nAChR) reveal alternative binding modes. *Bioorganic & Medicinal Chemistry Letters* **2013,** *23* (18), 5105-5113.

55. Banerjee, J.; Yongye, A. B.; Chang, Y. P.; Gyanda, R.; Medina-Franco, J. L.; Armishaw, C. J., Design and Synthesis of alpha-Conotoxin GID Analogues as Selective alpha 4 beta 2 Nicotinic Acetylcholine Receptor Antagonists. *Biopolymers* **2014,** *102* (1), 78-87.

56. Lee, C.; Lee, S. H.; Kim, D. H.; Han, K. H., Molecular docking study on the alpha 3 beta 2 neuronal nicotinic acetylcholine receptor complexed with alpha-Conotoxin GIC. *Bmb Reports* **2012,** *45* (5), 275-280.

57. Luo, S. L.; Zhangsun, D. T.; Schroeder, C. I.; Zhu, X. P.; Hu, Y. Y.; Wu, Y.; Weltzin, M. M.; Eberhard, S.; Kaas, Q.; Craik, D. J.; McIntosh, J. M.; Whiteaker, P., A novel alpha 4/7-conotoxin LvIA from Conus lividus that selectively blocks alpha 3 beta 2 vs. alpha 6/alpha 3 beta 2 beta 3 nicotinic acetylcholine receptors. *Faseb Journal* **2014,** *28* (4), 1842-1853.

58. Yu, R. L.; Tae, H. S.; Tabassum, N.; Shi, J.; Jiang, T.; Adams, D. J., Molecular Determinants Conferring the Stoichiometric-Dependent Activity of alpha-Conotoxins at the Human alpha 9 alpha 10 Nicotinic Acetylcholine Receptor Subtype. *Journal of Medicinal Chemistry* **2018,** *61* (10), 4628-4634.

59. Wu, Y.; Zhangsun, D. T.; Zhu, X. P.; Kaas, Q.; Zhangsun, M. Q.; Harvey, P. J.; Craik, D. J.; McIntosh, J. M.; Luo, S. L., alpha-Conotoxin S9A TxID Potently Discriminates between alpha 3 beta 4 and alpha 6/alpha 3 beta 4 Nicotinic Acetylcholine Receptors. *Journal of Medicinal Chemistry* **2017,** *60* (13), 5826-5833.

60. Yu, J. P.; Zhu, X. P.; Harvey, P. J.; Kaas, Q.; Zhangsun, D. T.; Craik, D. J.; Luo, S. L., Single Amino Acid Substitution in alpha-Conotoxin TxID Reveals a Specific alpha 3 beta 4 Nicotinic Acetylcholine Receptor Antagonist. *Journal of Medicinal Chemistry* **2018,** *61* (20), 9256-9265.

61. McDougal, O. M.; Granum, D. M.; Swartz, M.; Rohleder, C.; Maupin, C. M., pK(a) Determination of Histidine Residues in alpha-Conotoxin MII Peptides by H-1 NMR and Constant pH Molecular Dynamics Simulation. *Journal of Physical Chemistry B* **2013,** *117* (9), 2653-2661.

62. Luo, S. L.; Akondi, K. B.; Zhangsun, D. T.; Wu, Y.; Zhu, X. P.; Hu, Y. Y.; Christensen, S.; Dowell, C.; Daly, N. L.; Craik, D. J.; Wang, C. I. A.; Lewis, R. J.; Alewood, P. F.; McIntosh, J. M., Atypical alpha-Conotoxin LtIA from Conus litteratus Targets a Novel Microsite of the alpha 3 beta 2 Nicotinic Receptor. *Journal of Biological Chemistry* **2010,** *285* (16), 12355-12366.

63. Sambasivarao, S. V.; Roberts, J.; Bharadwaj, V. S.; Slingsby, J. G.; Rohleder, C.; Mallory, C.; Groome, J. R.; McDougal, O. M.; Maupin, C. M., Acetylcholine Promotes Binding of alpha-Conotoxin MII at alpha(3)beta(2) Nicotinic Acetylcholine Receptors. *Chembiochem* **2014,** *15* (3), 413-424.

64. Xu, M. Y.; Zhu, X. P.; Yu, J. F.; Yu, J. P.; Luo, S. L.; Wang, X. Q., The crystal structure of Ac-AChBP in complex with alpha-conotoxin LvIA reveals the

mechanism of its selectivity towards different nAChR subtypes. *Protein & Cell* **2017,** *8* (9), 675-685.

65. Pettersen, E. F.; Goddard, T. D.; Huang, C. C.; Couch, G. S.; Greenblatt, D. M.; Meng, E. C.; Ferrin, T. E., UCSF chimera - A visualization system for exploratory research and analysis. *Journal of Computational Chemistry* **2004,** *25* (13), 1605-1612.

66. Sandall, D. W.; Satkunanathan, N.; Keays, D. A.; Polidano, M. A.; Liping, X.; Pham, V.; Down, J. G.; Khalil, Z.; Livett, B. G.; Gayler, K. R., A novel alpha-conotoxin identified by gene sequencing is active in suppressing the vascular response to selective stimulation of sensory nerves in vivo. *Biochemistry* **2003,** *42* (22), 6904-6911.

67. Jakubowski, J. A.; Keays, D. A.; Kelley, W. P.; Sandall, D. W.; Bingham, J. P.; Livett, B. G.; Gayler, K. R.; Sweedler, J. V., Determining sequences and post-translational modifications of novel conotoxins in Conus victoriae using cDNA sequencing and mass spectrometry. *Journal of Mass Spectrometry* **2004,** *39* (5), 548-557.

68. Satkunanathan, N.; Livett, B.; Gayler, K.; Sandall, D.; Down, J.; Khalil, Z., Alpha-conotoxin Vc1.1 alleviates neuropathic pain and accelerates functional recovery of injured neurones. *Brain Research* **2005,** *1059* (2), 149-158.

69. Clark, R. J.; Fischer, H.; Nevin, S. T.; Adams, D. J.; Craik, D. J., The synthesis, structural characterization, and receptor specificity of the alpha-conotoxin Vc1.1. *Journal of Biological Chemistry* **2006,** *281* (32), 23254-23263.

70. Vincler, M.; Wittenauer, S.; Parker, R.; Ellison, M.; Olivera, B. M.; McIntosh, J. M., Molecular mechanism for analgesia involving specific antagonism of

alpha 9 alpha 10 nicotinic acetylcholine receptors. *Proceedings of the National Academy of Sciences of the United States of America* **2006,** *103* (47), 17880-17884.

71. Nevin, S. T.; Clark, R. J.; Klimis, H.; Christie, M. J.; Craik, D. J.; Adams, D. J., Are alpha 9 alpha 10 nicotinic acetylcholine receptors a pain target for alpha-conotoxins? *Molecular Pharmacology* **2007,** *72* (6), 1406-1410.

72. Halai, R.; Clark, R. J.; Nevin, S. T.; Jensen, J. E.; Adams, D. J.; Craik, D. J., Scanning Mutagenesis of alpha-Conotoxin Vc1.1 Reveals Residues Crucial for Activity at the alpha 9 alpha 10 Nicotinic Acetylcholine Receptor. *Journal of Biological Chemistry* **2009,** *284* (30), 20275-20284.

73. Hone, A. J.; Scadden, M.; Gajewiak, J.; Christensen, S.; Lindstrom, J.; McIntosh, J. M., alpha-Conotoxin PeIA S9H,V10A,E14N Potently and Selectively Blocks alpha 6 beta 2 beta 3 versus alpha 6 beta 4 Nicotinic Acetylcholine Receptors. *Molecular Pharmacology* **2012,** *82* (5), 972-982.

74. Whiteaker, P.; Christensen, S.; Yoshikami, D.; Dowell, C.; Watkins, M.; Gulyas, J.; Rivier, J.; Olivera, B. M.; McIntosh, J. M., Discovery, synthesis, and structure activity of a highly selective alpha 7 nicotinic acetylcholine receptor antagonist. *Biochemistry* **2007,** *46* (22), 6628-6638.

75. Johnson, D. S.; Martinez, J.; Elgoyhen, A. B.; Heinemann, S. F.; McIntosh, J. M., Alpha-Conotoxin Im(I) Exhibits Subtype-Specific Nicotinic Acetylcholine-Receptor Blockade - Preferential Inhibition of Homomeric Alpha-7 and Alpha-9 Receptors. *Molecular Pharmacology* **1995,** *48* (2), 194-199.

76. Ellison, M.; Gao, F.; Wang, H. L.; Sine, S. M.; McLntosh, J. M.; Olivera, B. M., alpha-conotoxins ImI and ImII target distinct regions of the human alpha

7 nicotinic acetylcholine receptor and distinguish human nicotinic receptor subtypes. *Biochemistry* **2004,** *43* (51), 16019-16026.

77. Armishaw, C.; Jensen, A. A.; Balle, T.; Clark, R. J.; Harpsoe, K.; Skonberg, C.; Liljefors, T.; Stromgaard, K., Rational Design of alpha-Conotoxin Analogues Targeting alpha 7 Nicotinic Acetylcholine Receptors: Improved antagonistic activity by incorporation of proline derivatives. *Journal of Biological Chemistry* **2009,** *284* (14), 9498-9512.

78. Azam, L.; Dowell, C.; Watkins, M.; Stitzel, J. A.; Olivera, B. M.; McIntosh, J. M., alpha-conotoxin BuIA, a novel peptide from Conus bullatus, distinguishes among neuronal nicotinic acetylcholine receptors. *Journal of Biological Chemistry* **2005,** *280* (1), 80-87.

79. Azam, L.; Maskos, U.; Changeux, J. P.; Dowell, C. D.; Christensen, S.; De Biasi, M.; McIntosh, J. M., alpha-Conotoxin BuIA T5A;P6O : a novel ligand that discriminates between alpha 6 beta 4 and alpha 6 beta 2 nicotinic acetylcholine receptors and blocks nicotine-stimulated norepinephrine release. *Faseb Journal* **2010,** *24* (12), 5113-5123.

80. Chang, Y. P.; Banerjee, J.; Dowell, C.; Wu, J. H.; Gyanda, R.; Houghten, R. A.; Toll, L.; McIntosh, J. M.; Armishaw, C. J., Discovery of a Potent and Selective alpha 3 beta 4 Nicotinic Acetylcholine Receptor Antagonist from an alpha-Conotoxin Synthetic Combinatorial Library. *Journal of Medicinal Chemistry* **2014,** *57* (8), 3511-3521.

81. Chen, J. Q.; Liang, L.; Ning, H. Y.; Cai, F. T.; Liu, Z. G.; Zhang, L. X.; Zhou, L. Y.; Dai, Q. Y., Cloning, Synthesis and Functional Characterization of a Novel alpha-Conotoxin Lt1.3. *Marine Drugs* **2018,** *16* (4), 12.

82. Luo, S. L.; Zhangsun, D. T.; Wu, Y.; Zhu, X. P.; Hu, Y. Y.; McIntyre, M.; Christensen, S.; Akcan, M.; Craik, D. J.; McIntosh, J. M., Characterization of a Novel alpha-Conotoxin from Conus textile That Selectively Targets alpha 6/alpha 3 beta 2 beta 3 Nicotinic Acetylcholine Receptors. *Journal of Biological Chemistry* **2013,** *288* (2), 894-902.

83. Yu, J. P.; Zhu, X. P.; Zhang, L.; Kudryavtsev, D.; Kasheverov, I.; Lei, Y. M.; Zhangsun, D. T.; Tsetlin, V.; Luo, S. L., Species specificity of rat and human alpha 7 nicotinic acetylcholine receptors towards different classes of peptide and protein antagonists. *Neuropharmacology* **2018,** *139*, 226-237.

84. McIntosh, J. M.; Dowell, C.; Watkins, M.; Garrett, J. E.; Yoshikami, D.; Olivera, B. M., alpha-Conotoxin GIC from Conus geographus, a novel peptide antagonist of nicotinic acetylcholine receptors. *Journal of Biological Chemistry* **2002,** *277* (37), 33610-33615.

85. Lin, B.; Xu, M. Y.; Zhu, X. P.; Wu, Y.; Liu, X.; Zhangsun, D. T.; Hu, Y. Y.; Xiang, S. H.; Kasheverov, I. E.; Tsetlin, V. I.; Wang, X. Q.; Luo, S. L., From crystal structure of alpha-conotoxin GIC in complex with Ac-AChBP to molecular determinants of its high selectivity for alpha 3 beta 2 nAChR. *Scientific Reports* **2016,** *6*, 10.

86. Luo, S. L.; Zhangsun, D. T.; Zhu, X. P.; Wu, Y.; Hu, Y. Y.; Christensen, S.; Harvey, P. J.; Akcan, M.; Craik, D. J.; McIntosh, J. M.,

Characterization of a Novel alpha-Conotoxin TxID from Conus textile That Potently Blocks Rat alpha 3 beta 4 Nicotinic Acetylcholine Receptors. *Journal of Medicinal Chemistry* **2013,** *56* (23), 9655-9663.

87. Nicke, A.; Loughnan, M. L.; Millard, E. L.; Alewood, P. F.; Adams, D. J.; Daly, N. L.; Craik, D. J.; Lewis, R. J., Isolation, structure, and activity of GID, a novel alpha 4/7-conotoxin with an extended N-terminal sequence. *Journal of Biological Chemistry* **2003,** *278* (5), 3137-3144.

88. Leffler, A. E.; Kuryatov, A.; Zebroski, H. A.; Powell, S. R.; Filipenko, P.; Hussein, A. K.; Gorson, J.; Heizmann, A.; Lyskov, S.; Tsien, R. W.; Poget, S. F.; Nicke, A.; Lindstrom, J.; Rudy, B.; Bonneau, R.; Holford, M., Discovery of peptide ligands through docking and virtual screening at nicotinic acetylcholine receptor homology models. *Proceedings of the National Academy of Sciences of the United States of America* **2017,** *114* (38), E8100-E8109.

89. Luo, S.; Nguyen, T. A.; Cartier, G. E.; Olivera, B. M.; Yoshikami, D.; McIntosh, J. M., Single-residue alteration in alpha-conotoxin PnIA switches its nAChR subtype selectivity. *Biochemistry* **1999,** *38* (44), 14542-14548.

90. Hopping, G.; Wang, C. I. A.; Hogg, R. C.; Nevin, S. T.; Lewis, R. J.; Adams, D. J.; Alewood, P. F., Hydrophobic residues at position 10 of alpha-conotoxin PnIA influence subtype selectivity between alpha 7 and alpha 3 beta 2 neuronal nicotinic acetylcholine receptors. *Biochemical Pharmacology* **2014,** *91* (4), 534-542.

91. Azam, L.; Yoshikami, D.; McIntosh, J. M., Amino acid residues that confer high selectivity of the alpha 6 nicotinic acetylcholine receptor subunit to alpha-

conotoxin MII S4A, E11A, L15A. *Journal of Biological Chemistry* **2008,** *283* (17), 11625-11632.

92. McIntosh, J. M.; Plazas, P. V.; Watkins, M.; Gomez-Casati, M. E.; Olivera, B. M.; Elgoyhen, A. B., A novel alpha-conotoxin, PeIA, cloned from Conus pergrandis, discriminates between rat alpha 9 alpha 10 and alpha 7 nicotinic cholinergic receptors. *Journal of Biological Chemistry* **2005,** *280* (34), 30107-30112.

93. Cartier, G. E.; Yoshikami, D. J.; Gray, W. R.; Luo, S. Q.; Olivera, B. M.; McIntosh, J. M., A new alpha-conotoxin which targets alpha 3 beta 2 nicotinic acetylcholine receptors. *Journal of Biological Chemistry* **1996,** *271* (13), 7522-7528.

94. Yu, R. L.; Kompella, S. N.; Adams, D. J.; Craik, D. J.; Kaas, Q., Determination of the alpha-Conotoxin Vc1.1 Binding Site on the alpha 9 alpha 10 Nicotinic Acetylcholine Receptor. *Journal of Medicinal Chemistry* **2013,** *56* (9), 3557-3567.

95. Everhart, D.; Cartier, G. E.; Malhotra, A.; Gomes, A. V.; McIntosh, J. M.; Luetje, C. W., Determinants of potency on alpha-conotoxin MII, a peptide antagonist of neuronal nicotinic receptors. *Biochemistry* **2004,** *43* (10), 2732-2737.

96. McIntosh, J. M.; Yoshikami, D.; Mahe, E.; Nielsen, D. B.; Rivier, J. E.; Gray, W. R.; Olivera, B. M., A nicotinic acetylcholine-receptor ligand of unique specificity, alpha-conotoxin ImI. *Journal of Biological Chemistry* **1994,** *269* (24), 16733-16739.

97. Quiram, P. A.; Sine, S. M., Structural elements in alpha-conotoxin ImI essential for binding to neuronal alpha(7) receptors. *Journal of Biological Chemistry* **1998,** *273* (18), 11007-11011.

98. Rogers, J. P.; Luginbuhl, P.; Pemberton, K.; Harty, P.; Wemmer, D. E.; Stevens, R. C., Structure-activity relationships in a peptidic alpha 7 nicotinic acetylcholine receptor antagonist. *Journal of Molecular Biology* **2000,** *304* (5), 911-926.

99. Utkin, Y. N.; Zhmak, M. N.; Methfessel, C.; Tsetlin, V. I., Aromatic substitutions in alpha-conotoxin ImI. Synthesis of iodinated photoactivatable derivative. *Toxicon* **1999,** *37* (12), 1683-1695.

100. Sali, A.; Blundell, T. L., Comparative Protein Modeling by Satisfaction of Spatial Restraints. *Journal of Molecular Biology* **1993,** *234* (3), 779-815.

101. Friesner, R. A.; Banks, J. L.; Murphy, R. B.; Halgren, T. A.; Klicic, J. J.; Mainz, D. T.; Repasky, M. P.; Knoll, E. H.; Shelley, M.; Perry, J. K.; Shaw, D. E.; Francis, P.; Shenkin, P. S., Glide: A new approach for rapid, accurate docking and scoring. 1. Method and assessment of docking accuracy. *Journal of Medicinal Chemistry* **2004,** *47* (7), 1739-1749.

102. Houghten, R. A., General-method for the rapid solid-phase synthesis of large numbers of peptides - specificity of antigen-antibody interaction at the level of individual amino-acids. *Proceedings of the National Academy of Sciences of the United States of America* **1985,** *82* (15), 5131-5135.

103. Armishaw, C. J.; Singh, N.; Medina-Franco, J. L.; Clark, R. J.; Scott, K. C. M.; Houghten, R. A.; Jensen, A. A., A Synthetic Combinatorial Strategy for Developing alpha-Conotoxin Analogs as Potent alpha(7) Nicotinic Acetylcholine Receptor Antagonists. *Journal of Biological Chemistry* **2010,** *285* (3), 1809-1821.

104. Kim, H. W.; McIntosh, J. M., alpha 6 nAChR subunit residues that confer alpha-conotoxin BuIA selectivity. *Faseb Journal* **2012,** *26* (10), 4102-4110.

105. Glick, S. D.; Maisonneuve, I. M.; Kitchen, B. A., Modulation of nicotine self-administration in rats by combination therapy with agents blocking alpha 3 beta 4 nicotinic receptors. *European Journal of Pharmacology* **2002,** *448* (2-3), 185-191.

106. Berrettine, W.; Yuan, X.; Tozzi, F.; Song, K.; Francks, C.; Chilcoat, H.; Waterworth, D.; Muglia, P.; Mooser, V., alpha-5/alpha-3 nicotinic receptor subunit alleles increase risk for heavy smoking. *Molecular Psychiatry* **2008,** *13* (4), 368-373.

107. Millard, E. L.; Nevin, S. T.; Loughnan, M. L.; Nicke, A.; Clark, R. J.; Alewood, P. F.; Lewis, R. J.; Adams, D. J.; Craik, D. J.; Daly, N. L., Inhibition of Neuronal Nicotinic Acetylcholine Receptor Subtypes by alpha-Conotoxin GID and Analogues. *Journal of Biological Chemistry* **2009,** *284* (8), 4944-4951.

108. Das, R.; Baker, D., Macromolecular modeling with Rosetta. In *Annual Review of Biochemistry*, Annual Reviews: Palo Alto, 2008; Vol. 77, pp 363-382.

109. Raveh, B.; London, N.; Schueler-Furman, O., Sub-angstrom modeling of complexes between flexible peptides and globular proteins. *Proteins-Structure Function and Bioinformatics* **2010,** *78* (9), 2029-2040.

110. Tyka, M. D.; Keedy, D. A.; Andre, I.; DiMaio, F.; Song, Y. F.; Richardson, D. C.; Richardson, J. S.; Baker, D., Alternate States of Proteins Revealed by Detailed Energy Landscape Mapping. *Journal of Molecular Biology* **2011,** *405* (2), 607-618.

111. Fiser, A.; Sali, A., MODELLER: Generation and refinement of homology-based protein structure models. *Macromolecular Crystallography, Pt D* **2003,** *374*, 461-491.

112. Dutertre, S.; Ulens, C.; Buttner, R.; Fish, A.; van Elk, R.; Kendel, Y.; Hopping, G.; Alewood, P. F.; Schroeder, C.; Nicke, A.; Smit, A. B.; Sixma, T. K.; Lewis, R. J., AChBP-targeted alpha-conotoxin correlates distinct binding orientations with nAChR subtype selectivity. *Embo Journal* **2007,** *26* (16), 3858-3867.

113. Ulens, C.; Hogg, R. C.; Celie, P. H.; Bertrand, D.; Tsetlin, V.; Smit, A. B.; Sixma, T. K., Structural determinants of selective alpha-conotoxin binding to a nicotinic acetylcholine receptor homolog AChBP. *Proceedings of the National Academy of Sciences of the United States of America* **2006,** *103* (10), 3615-3620.

114. Baugh, E. H.; Lyskov, S.; Weitzner, B. D.; Gray, J. J., Real-Time PyMOL Visualization for Rosetta and PyRosetta. *Plos One* **2011,** *6* (8), 5.

115. Fainzilber, M.; Hasson, A.; Oren, R.; Burlingame, A. L.; Gordon, D.; Spira, M. E.; Zlotkin, E., New mollusk-specific alpha-conotoxins block aplysia neuronal acetylcholine-receptors. *Biochemistry* **1994,** *33* (32), 9523-9529.

116. Hogg, R. C.; Miranda, L. P.; Craik, D. J.; Lewis, R. J.; Alewood, P. F.; Adams, D. J., Single amino acid substitutions in alpha-conotoxin PnIA shift selectivity for subtypes of the mammalian neuronal nicotinic acetylcholine receptor. *Journal of Biological Chemistry* **1999,** *274* (51), 36559-36564.

117. Hogg, R. C.; Hopping, G.; Alewood, P. F.; Adams, D. J.; Bertrand, D., alpha-conotoxins PnIA and A10L PnIA stabilize different states of the alpha 7-L247T nicotinic acetylcholine receptor. *Journal of Biological Chemistry* **2003,** *278* (29), 26908-26914.

118. Drisdel, R. C.; Green, W. N., Neuronal alpha-bungarotoxin receptors are alpha 7 subunit homomers. *Journal of Neuroscience* **2000,** *20* (1), 133-139.

119. Kasheverov, I. E.; Chugunov, A. O.; Kudryavtsev, D. S.; Ivanov, I. A.; Zhmak, M. N.; Shelukhina, I. V.; Spirova, E. N.; Tabakmakher, V. M.; Zelepuga, E. A.; Efremov, R. G.; Tsetlin, V. I., High-Affinity alpha-Conotoxin PnIA Analogs Designed on the Basis of the Protein Surface Topography Method. *Scientific Reports* **2016,** *6*, 11.

120. Koromyslova, A. D.; Chugunov, A. O.; Efremov, R. G., Deciphering Fine Molecular Details of Proteins' Structure and Function with a Protein Surface Topography (PST) Method. *Journal of Chemical Information and Modeling* **2014,** *54* (4), 1189-1199.

121. Chugunov, A. O.; Koromyslova, A. D.; Berkut, A. A.; Peigneur, S.; Tytgat, J.; Polyansky, A. A.; Pentkovsky, V. M.; Vassilevski, A. A.; Grishin, E. V.; Efremov, R. G., Modular Organization of alpha-Toxins from Scorpion Venom Mirrors Domain Structure of Their Targets, Sodium Channels. *Journal of Biological Chemistry* **2013,** *288* (26), 19014-19027.

122. Bordia, T.; Grady, S. R.; McIntosh, J. M.; Quik, M., Nigrostriatal damage preferentially decreases a subpopulation of alpha 6 beta 2*nAChRs in mouse, monkey, and Parkinson's disease striatum. *Molecular Pharmacology* **2007,** *72* (1), 52-61.

123. Harvey, S. C.; McIntosh, J. M.; Cartier, G. E.; Maddox, F. N.; Luetje, C. W., Determinants of specificity for alpha-conotoxin MII on alpha 3 beta 2 neuronal nicotinic receptors. *Molecular Pharmacology* **1997,** *51* (2), 336-342.

124. Pucci, L.; Grazioso, G.; Dallanoce, C.; Rizzi, L.; De Micheli, C.; Clementi, F.; Bertrand, S.; Bertrand, D.; Longhi, R.; De Amici, M.; Gotti, C., Engineering of alpha-conotoxin MII-derived peptides with increased selectivity for native

alpha 6 beta 2*nicotinic acetylcholine receptors. *Faseb Journal* **2011,** *25* (11), 3775-3789.

125. Dowell, C.; Olivera, B. M.; Garrett, J. E.; Staheli, S. T.; Watkins, M.; Kuryatov, A.; Yoshikami, D.; Lindstrom, J. M.; McIntosh, J. M., alpha-conotoxin PIA is selective for alpha 6 subunit-containing nicotinic acetylcholine receptors. *Journal of Neuroscience* **2003,** *23* (24), 8445-8452.

126. King, M. D.; Long, T.; Andersen, T.; McDougal, O. M., Genetic Algorithm Managed Peptide Mutant Screening: Optimizing Peptide Ligands for Targeted Receptor Binding. *Journal of Chemical Information and Modeling* **2016,** *56* (12), 2378-2387.

127. Sheridan, R. P.; Kearsley, S. K., Using a genetic algorithm to suggest combinatorial libraries. *Journal of Chemical Information and Computer Sciences* **1995,** *35* (2), 310-320.

128. Sheridan, R. P.; SanFeliciano, S. G.; Kearsley, S. K., Designing targeted libraries with genetic algorithms. *Journal of Molecular Graphics & Modelling* **2000,** *18* (4-5), 320-+.

129. Fonseca, C. M.; Fleming, P. J., An Overview of Evolutionary Algorithms in Multiobjective Optimization. *Evolutionary Computation* **1995,** *3* (1), 1-16.

130. Gillet, V. J.; Khatib, W.; Willett, P.; Fleming, P. J.; Green, D. V. S., Combinatorial library design using a multiobjective genetic algorithm. *Journal of Chemical Information and Computer Sciences* **2002,** *42* (2), 375-385.

131. Morris, G. M.; Goodsell, D. S.; Halliday, R. S.; Huey, R.; Hart, W. E.; Belew, R. K.; Olson, A. J., Automated docking using a Lamarckian genetic algorithm and

an empirical binding free energy function. *Journal of Computational Chemistry* **1998,** *19* (14), 1639-1662.

132. Huey, R.; Morris, G. M.; Olson, A. J.; Goodsell, D. S., A semiempirical free energy force field with charge-based desolvation. *Journal of Computational Chemistry* **2007,** *28* (6), 1145-1152.

133. Bullock, C.; Cornia, N.; Jacob, R.; Remm, A.; Peavey, T.; Weekes, K.; Mallory, C.; Oxford, J. T.; McDougal, O. M.; Andersen, T. L., DockoMatic 2.0: High Throughput Inverse Virtual Screening and Homology Modeling. *Journal of Chemical Information and Modeling* **2013,** *53* (8), 2161-2170.

134. Xu, J. B.; Berger, B., Fast and accurate algorithms for protein side-chain packing. *Journal of the Acm* **2006,** *53* (4), 533-557.

135. Hess, B.; Kutzner, C.; van der Spoel, D.; Lindahl, E., GROMACS 4: Algorithms for highly efficient, load-balanced, and scalable molecular simulation. *Journal of Chemical Theory and Computation* **2008,** *4* (3), 435-447.

136. Van der Spoel, D.; Lindahl, E.; Hess, B.; Groenhof, G.; Mark, A. E.; Berendsen, H. J. C., GROMACS: Fast, flexible, and free. *Journal of Computational Chemistry* **2005,** *26* (16), 1701-1718.

137. Berendsen, H. J. C.; Vanderspoel, D.; Vandrunen, R., GROMACS - A MESSAGE-PASSING PARALLEL MOLECULAR-DYNAMICS IMPLEMENTATION. *Computer Physics Communications* **1995,** *91* (1-3), 43-56.

138. Sorin, E. J.; Pande, V. S., Exploring the helix-coil transition via all-atom equilibrium ensemble simulations. *Biophysical Journal* **2005,** *88* (4), 2472-2493.

139. DePaul, A. J.; Thompson, E. J.; Patel, S. S.; Haldeman, K.; Sorin, E. J., Equilibrium conformational dynamics in an RNA tetraloop from massively parallel molecular dynamics. *Nucleic Acids Research* **2010,** *38* (14), 4856-4867.

140. Duan, Y.; Wu, C.; Chowdhury, S.; Lee, M. C.; Xiong, G. M.; Zhang, W.; Yang, R.; Cieplak, P.; Luo, R.; Lee, T.; Caldwell, J.; Wang, J. M.; Kollman, P., A point-charge force field for molecular mechanics simulations of proteins based on condensed-phase quantum mechanical calculations. *Journal of Computational Chemistry* **2003,** *24* (16), 1999-2012.

141. Marquart, L. A.; Turner, M. W.; McDougal, O. M., Qualitative assay to detect dopamine release by ligand action on nicotinic acetylcholine receptors. *Toxins* **2019,** *11* (12), 682.

142. Sharma, G.; Vijayaraghavan, S., Nicotinic receptors: role in addiction and other disorders of the brain. *Substance Abuse: Research and Treatment* **2008,** (1), 81-95.

143. Young, J. W.; Geyer, M. A., Evaluating the role of the alpha-7 nicotinic acetylcholine receptor in the pathophysiology and treatment of schizophrenia. *Biochemical Pharmacology* **2013,** *86* (8), 1122-1132.

144. Lombardo, S.; Maskos, U., Role of the nicotinic acetylcholine receptor in Alzheimer's disease pathology and treatment. *Neuropharmacology* **2015,** *96*, 255-262.

145. Bertrand, D.; Terry, A. V., The wonderland of neuronal nicotinic acetylcholine receptors. *Biochemical Pharmacology* **2018,** *151*, 214-225.

146. Terry, A. V.; Callahan, P. M., Nicotinic Acetylcholine Receptor Ligands, Cognitive Function, and Preclinical Approaches to Drug Discovery. *Nicotine & Tobacco Research* **2019,** *21* (3), 383-394.

147. Millar, N. S., A review of experimental techniques used for the heterologous expression of nicotinic acetylcholine receptors. *Biochemical Pharmacology* **2009,** *78* (7), 766-776.

148. Xu, J.; Wang, X. B.; Ensign, B.; Li, M.; Wu, L.; Guia, A.; Xu, J. Q., Ion-channel assay technologies: quo vadis? *Drug Discovery Today* **2001,** *6* (24), 1278-1287.

149. Accardi, M. V.; Pugsley, M. K.; Forster, R.; Troncy, E.; Huang, H.; Authier, S., The emerging role of in vitro electrophysiological methods in CNS safety pharmacology. *Journal of Pharmacological and Toxicological Methods* **2016,** *81*, 47-59.

150. King, M. D.; Long, T.; Pfalmer, D. L.; Andersen, T. L.; McDougaL, O. M., SPIDR: small-molecule peptide-influenced drug repurposing. *Bmc Bioinformatics* **2018,** *19*, 11.

151. Long, T.; McDougal, O. M.; Andersen, T., GAMPMS: Genetic algorithm managed peptide mutant screening. *Journal of Computational Chemistry* **2015,** *36* (17), 1304-1310.

152. Jacob, R. B.; Andersen, T.; McDougal, O. M., Accessible High-Throughput Virtual Screening Molecular Docking Software for Students and Educators. *Plos Computational Biology* **2012,** *8* (5), 5.

153. Jacob, R. B.; Bullock, C. W.; Andersen, T.; McDougal, O. M., DockoMatic: Automated Peptide Analog Creation for High Throughput Virtual Screening. *Journal of Computational Chemistry* **2011,** *32* (13), 2936-2941.

154. Kuryatov, A.; Lindstrom, J., Expression of Functional Human alpha 6 beta 2 beta 3*Acetylcholine Receptors in Xenopus laevis Oocytes Achieved through Subunit Chimeras and Concatamers. *Molecular Pharmacology* **2011,** *79* (1), 126-140.

155. Xiao, C.; Srinivasan, R.; Drenan, R. M.; Mackey, E. D. W.; McIntosh, J. M.; Lester, H. A., Characterizing functional alpha 6 beta 2 nicotinic acetylcholine receptors in vitro: Mutant beta 2 subunits improve membrane expression, and fluorescent proteins reveal responsive cells. *Biochemical Pharmacology* **2011,** *82* (8), 852-861.

156. Alkondon, M.; Albuquerque, E. X., Nicotinic receptor subtypes in rat hippocampal slices are differentially sensitive to desensitization and early in vivo functional up-regulation by nicotine and to block by bupropion. *Journal of Pharmacology and Experimental Therapeutics* **2005,** *313* (2), 740-750.

157. Arvin, M. C.; Wokosin, D. L.; Banala, S.; Lavis, L. D.; Drenan, R. M., Probing Nicotinic Acetylcholine Receptor Function in Mouse Brain Slices via Laser Flash Photolysis of Photoactivatable Nicotine. *Jove-Journal of Visualized Experiments* **2019,** (143), 10.

158. Engle, S. E.; Broderick, H. J.; Drenan, R. M., Local Application of Drugs to Study Nicotinic Acetylcholine Receptor Function in Mouse Brain Slices. *Jove-Journal of Visualized Experiments* **2012,** (68), 8.

159. Temburni, M. K.; Blitzblau, R. C.; Jacob, M. H., Receptor targeting and heterogeneity at interneuronal nicotinic cholinergic synapses in vivo. *Journal of Physiology-London* **2000,** *525* (1), 21-29.

160. Kimes, A. S.; Horti, A. G.; London, E. D.; Chefer, S. I.; Contoreggi, C.; Ernst, M.; Friello, P.; Koren, A. O.; Kurian, V.; Matochik, J. A.; Pavlova, O.; Vaupel,

D. B.; Mukhin, A. G., 2- F-18 F-A85380: PET imaging of brain nicotinic acetylcholine receptors and whole body distribution in humans. *Faseb Journal* **2003,** *17* (8), 1331-+.

161. Malysz, J.; Gronlien, J. H.; Anderson, D. J.; Hakerud, M.; Thorin-Hagene, K.; Ween, H.; Wetterstrand, C.; Briggs, C. A.; Faghih, R.; Bunnelle, W. H.; Gopalakrishnan, M., In Vitro Pharmacological Characterization of a Novel Allosteric Modulator of alpha 7 Neuronal Acetylcholine Receptor, 4-(5-(4-Chlorophenyl)-2-methyl-3-propionyl-1H-pyrrol-1-yl)benzenesulfona mide (A-867744), Exhibiting Unique Pharmacological Profile. *Journal of Pharmacology and Experimental Therapeutics* **2009,** *330* (1), 257-267.

162. Armstrong, L. C.; Kirsch, G. E.; Fedorov, N. B.; Wu, C. Y.; Kuryshev, Y. A.; Sewell, A. L.; Liu, Z. Q.; Motter, A. L.; Leggett, C. S.; Orr, M. S., High-Throughput Patch Clamp Screening in Human alpha 6-Containing Nicotinic Acetylcholine Receptors. *Slas Discovery* **2017,** *22* (6), 686-695.

163. Dunlop, J.; Bowlby, M.; Peri, R.; Vasilyev, D.; Arias, R., High-throughput electrophysiology: an emerging paradigm for ion-channel screening and physiology. *Nature Reviews Drug Discovery* **2008,** *7* (4), 358-368.

164. Shinohara, H.; Wang, F. F.; Hossain, S. M. Z., A convenient, high-throughput method for enzyme-luminescence detection of dopamine released from PC12 cells. *Nature Protocols* **2008,** *3* (10), 1639-1644.

165. Mir, T. A.; Shinohara, H.; Shimizu, Y., Enzyme-luminescence method: Tool for evaluation of neuronal differentiation based on real-time monitoring of dopamine release response from PC12 cells. *Analytical Methods* **2011,** *3* (4), 837-841.

166. Avila, A. M.; Davila-Garcia, M. I.; Ascarrunz, V. S.; Xiao, Y. X.; Kellar, K. J., Differential regulation of nicotinic acetylcholine receptors in PC12 cells by nicotine and nerve growth factor (Reprinted from Soc Neurosci Abstr, vol 26, pg 373, 2000). *Molecular Pharmacology* **2003,** *64* (4), 974-986.

167. Kabbani, N.; Nordman, J. C.; Corgiat, B. A.; Veltri, D. P.; Shehu, A.; Seymour, V. A.; Adams, D. J., Are nicotinic acetylcholine receptors coupled to G proteins? *Bioessays* **2013,** *35* (12), 1025-1034.

168. Nordman, J. C.; Kabbani, N., An interaction between alpha 7 nicotinic receptors and a G-protein pathway complex regulates neurite growth in neural cells. *Journal of Cell Science* **2012,** *125* (22), 5502-5513.

169. Quarta, D.; Ciruela, F.; Patkar, K.; Borycz, J.; Solinas, M.; Lluis, C.; Franco, R.; Wise, R. A.; Goldberg, S. R.; Hope, B. T.; Woods, A. S.; Ferre, S., Heteromeric nicotinic acetylcholine-dopamine autoreceptor complexes modulate striatal dopamine release. *Neuropsychopharmacology* **2007,** *32* (1), 35-42.

170. King, J. R.; Nordman, J. C.; Bridges, S. P.; Lin, M. K.; Kabbani, N., Identification and Characterization of a G Protein-binding Cluster in alpha 7 Nicotinic Acetylcholine Receptors. *Journal of Biological Chemistry* **2015,** *290* (33), 20060-20070.

171. Nery, A. A.; Resende, R. R.; Martins, A. H.; Trujillo, C. A.; Eterovic, V. A.; Ulrich, H., Alpha7 Nicotinic Acetylcholine Receptor Expression and Activity During Neuronal Differentiation of PC12 Pheochromocytoma Cells. *Journal of Molecular Neuroscience* **2010,** *41* (3), 329-339.

172. Henderson, L. P.; Gdovin, M. J.; Liu, C. L.; Gardner, P. D.; Maue, R. A., Nerve growth factor increases nicotinic ACh receptor gene expression and current

density in wild-type and protein kinase A-deficient PC12 cells. *Journal of Neuroscience* **1994,** *14* (3), 1153-1163.

173. Rezvani, K.; Teng, Y. F.; Pan, Y. P.; Dani, J. A.; Lindstrom, J.; Gras, E. A. G.; McIntosh, J. M.; De Biasi, M., UBXD4, a UBX-Containing Protein, Regulates the Cell Surface Number and Stability of alpha 3-Containing Nicotinic Acetylcholine Receptors. *Journal of Neuroscience* **2009,** *29* (21), 6883-6896.

174. Rogers, S. W.; Mandelzys, A.; Deneris, E. S.; Cooper, E.; Heinemann, S., The Expression of Nicotinic Acetylcholine-Receptors by PC12 Cells Treated with NGF. *Journal of Neuroscience* **1992,** *12* (12), 4611-4623.

175. Dohrman, D. P.; Reiter, C. K., Chronic ethanol reduces nicotine-induced dopamine release in PC12 cells. *Alcoholism-Clinical and Experimental Research* **2003,** *27* (11), 1846-1851.

176. Walsh, H.; Govind, A. P.; Mastro, R.; Hoda, J. C.; Bertrand, D.; Vallejo, Y.; Green, W. N., Up-regulation of nicotinic receptors by nicotine varies with receptor subtype. *Journal of Biological Chemistry* **2008,** *283* (10), 6022-6032.

177. Cooper, S. T.; Harkness, P. C.; Baker, E. R.; Millar, N. S., Up-regulation of cell-surface alpha 4 beta 2 neuronal nicotinic receptors by lower temperature and expression of chimeric subunits. *Journal of Biological Chemistry* **1999,** *274* (38), 27145-27152.

178. Lukas, R. J., Effects of Chronic Nicotinic Ligand Exposure on Functional-Activity of Nicotinic Acetylcholine-Receptors Expressed by Cells of the PC12 Rat Pheochromocytoma or the Te671/Rd Human Clonal Line. *Journal of Neurochemistry* **1991,** *56* (4), 1134-1145.

179. Westerink, R. H. S.; Ewing, A. G., The PC12 cell as model for neurosecretion. *Acta Physiologica* **2008,** *192* (2), 273-285.

180. Marquart , L. A.; Turner , M. W.; Warner , L. R.; King , M. D.; Groome, J. R.; McDougal, O. M., Ribbon α-Conotoxin KTM Exhibits Potent Inhibition of Nicotinic Acetylcholine Receptors. *Marine Drugs* **2019,** *17* (12), 669.

181. Kaas, Q.; Yu, R. L.; Jin, A. H.; Dutertre, S.; Craik, D. J., ConoServer: updated content, knowledge, and discovery tools in the conopeptide database. *Nucleic Acids Research* **2012,** *40* (D1), D325-D330.

182. Albuquerque, E. X.; Pereira, E. F. R.; Alkondon, M.; Rogers, S. W., Mammalian Nicotinic Acetylcholine Receptors: From Structure to Function. *Physiological Reviews* **2009,** *89* (1), 73-120.

183. Jacob, R. B.; Bullock, C., Automatic DockOmatic: Ligand and receptor screening made easy. *Abstracts of Papers of the American Chemical Society* **2010,** *240*, 1.

184. King, M. D.; Phillips, P.; Turner, M. W.; Katz, M.; Lew, S.; Bradburn, S.; Andersen, T.; McDougal, O. M., Computational Exploration of a Protein Receptor Binding Space with Student Proposed Peptide Ligands. *Biochemistry and Molecular Biology Education* **2016,** *44* (1), 63-67.

185. Bullock, C. W. J., R.B.McDougal, O.M.Hampikian, G.Andersen, T., DockoMatic – automated ligand creation and docking. *BMC Research Notes* . **2010,** *3*, 289-297.

186. Grishin, A. A.; Wang, C. I. A.; Muttenthaler, M.; Alewood, P. F.; Lewis, R. J.; Adams, D. J., alpha-Conotoxin AuIB Isomers Exhibit Distinct Inhibitory

Mechanisms and Differential Sensitivity to Stoichiometry of alpha 3 beta 4 Nicotinic Acetylcholine Receptors. *Journal of Biological Chemistry* **2010,** *285* (29), 22254-22263.

187. Dutton, J. L.; Bansal, P. S.; Hogg, R. C.; Adams, D. J.; Alewood, P. F.; Craik, D. J., A new level of conotoxin diversity, a non-native disulfide bond connectivity in alpha-conotoxin AuIB reduces structural definition but increases biological activity. *Journal of Biological Chemistry* **2002,** *277* (50), 48849-48857.

188. Wüthrich, K., *NMR of Proteins and Nucleic Acids*. Wiley: New York, 1986.

189. Güntert, P., Automated NMR Structure Calculation With CYANA. In *Protein NMR Techniques*, Downing, A. K., Ed. Humana Press: New York, 2004; Vol. 278, pp 353-378.

190. Wishart, D. S.; Sykes, B. D.; Richards, F. M., The Chemical-Shift Index - A Fast and Simple Method for the Assignment of Protein Secondary Structure through NMR-Spectroscopy. *Biochemistry* **1992,** *31* (6), 1647-1651.

191. Robinson, S. D.; Norton, R. S., Conotoxin Gene Superfamilies. *Marine Drugs* **2014,** *12* (12), 6058-6101.

192. *The PyMOL Molecular Graphics System*, 2.1.1; Schrödinger, LLC: New York, 2019.

193. Gray, W. R., Disulfide Structures of Highly Bridged Peptides - A New Strategy for Analysis. *Protein Science* **1993,** *2* (10), 1732-1748.

194. Chen, Y. H.; Yang, J. T., New Approach to Calculation of Secondary Structures of Globular Proteins by Optical Rotatory Dispersion and Circular Dichroism. *Biochemical and Biophysical Research Communications* **1971,** *44* (6), 1285-&.

195. Turner, M. W.; Cort, J. R.; McDougal, O. M., alpha-Conotoxin Decontamination Protocol Evaluation: What Works and What Doesn't. *Toxins* **2017,** *9* (9), 10.

196. Wishart, D. S.; Bigam, C. G.; Holm, A.; Hodges, R. S.; Sykes, B. D., H-1, C-13 and N-15 Random Coil NMR Chemical-Shifts of the Common Amino-Acids 1. Investigations of Nearest-Neighbor Effects. *Journal of Biomolecular Nmr* **1995,** *5* (3), 332-332.

197. Wishart, D. S.; Sykes, B. D.; Richards, F. M., Relationship between Nuclear Magnetic Resonance Chemical Shift and Protein Secondary Structure. *Journal of Molecular Biology* **1991,** *222* (2), 311-333.

198. Wishart, D. S.; Sykes, B. D.; Richards, F. M., Simple techniques for the quantification of protein secondary structure by H-1-NMR spectroscopy. *Febs Letters* **1991,** *293* (1-2), 72-80.

199. Bax, A., Two-dimensional NMR and protein structure. *Annual Review of Biochemistry* **1989,** *58*, 223-256.

200. Jeener, J.; Meier, B. H.; Bachmann, P.; Ernst, R. R., Investigation of exchange processes by 2-dimensional NMR-spectroscopy. *Journal of Chemical Physics* **1979,** *71* (11), 4546-4553.

201. Braunschweiler, L.; Ernst, R. R., Coherence transfer by isotropic mixing - application to proton correlation spectroscopy. *Journal of Magnetic Resonance* **1983,** *53* (3), 521-528.

202. McDougal, O. M.; Turner, M. W.; Ormond, A. J.; Poulter, C. D., Three-dimensional structure of conotoxin tx3a: An m-1 branch peptide of the M-superfamily. *Biochemistry* **2008,** *47* (9), 2826-2832.

203. Vranken, W. F.; Boucher, W.; Stevens, T. J.; Fogh, R. H.; Pajon, A.; Llinas, P.; Ulrich, E. L.; Markley, J. L.; Ionides, J.; Laue, E. D., The CCPN data model for NMR spectroscopy: Development of a software pipeline. *Proteins-Structure Function and Bioinformatics* **2005,** *59* (4), 687-696.

204. Vriend, G., WHAT IF - A molecular modeling and drug design program. *Journal of Molecular Graphics* **1990,** *8* (1), 52-&.

205. Laskowski, R. A.; Rullmann, J. A. C.; MacArthur, M. W.; Kaptein, R.; Thornton, J. M., AQUA and PROCHECK-NMR: Programs for checking the quality of protein structures solved by NMR. *Journal of Biomolecular Nmr* **1996,** *8* (4), 477-486.

206. Eisenberg, D.; Luthy, R.; Bowie, J. U., VERIFY3D: Assessment of protein models with three-dimensional profiles. *Macromolecular Crystallography, Pt B* **1997,** *277*, 396-404.

207. Chen, V. B.; Arendall, W. B.; Headd, J. J.; Keedy, D. A.; Immormino, R. M.; Kapral, G. J.; Murray, L. W.; Richardson, J. S.; Richardson, D. C., MolProbity: all-atom structure validation for macromolecular crystallography. *Acta Crystallographica Section D-Structural Biology* **2010,** *66*, 12-21.

APPENDIX A

Supplementary Materials to Chapter Two: Method Optimization and Troubleshooting

Effective NGF treatment was confirmed by cell morphology, in which NGF treated cells contain neurite extensions indicative of neuron-like differentiation (Figure A.1).

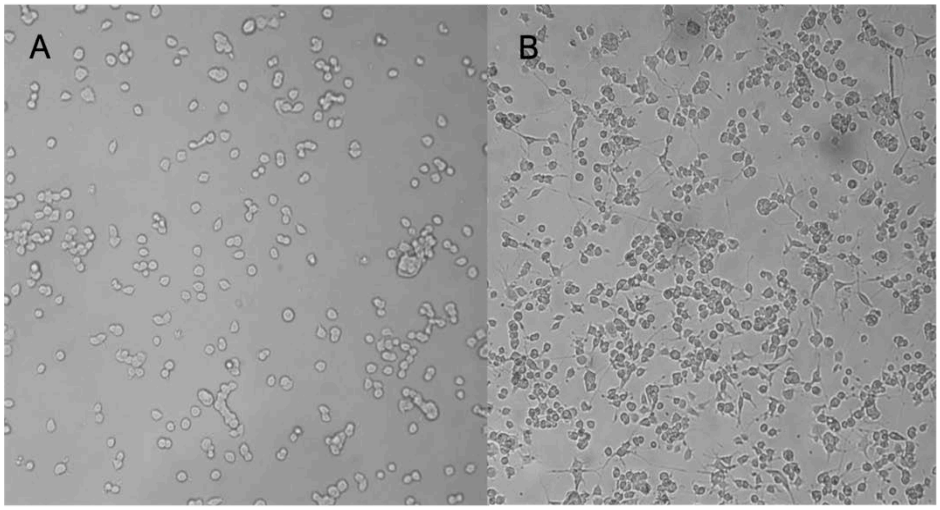

Figure A.1 Light microscopy images of PC12 cell morphology. Non-NGF-treated cells (A) remain round, while NGF-treated cells (B) show long, reaching dendrites at 3 days. No visual difference was observed in cell morphology for treatments including nicotine and/or ethanol in addition to NGF.

The trypsinization step used by Shinohara et al. was removed, not only to simplify growth procedures, but also because it has been shown that trypsinization is damaging to cell surface proteins [1]. In order to prolong the life of the PC12 cells and maximize assay response, cells were instead triturated from the bottom of the flask to detach them for subculturing. It was observed that without trypsinization, cells responded well to ACh over a longer period of time, 2-3 weeks from cryopreservation recovery. The results presented in this study are from cells that had been cultured for at least 2 weeks. Extensive optimization was necessary to adapt the Shinohara et al. method to the 96 well plate α-CTx MII-dependent rα3β2 nAChR isoform specific response system, which constituted the objective for the current study. Adaption of Shinohara's method was designed such that reliable results could be obtained for studies involving rα3β2 nAChR isoform specific

antagonists, as represented by α-CTx MII, as well as adapt the protocol for accessibility, and time and cost efficiency. Initial attempts to recreate the results of Shinohara et al. proved challenging due to lack of access to an autoinjector for instantaneous detection of ACh response. To overcome this deficiency, it was necessary to decrease [POD] and [MAO] in order to slow down the reaction and increase [luminol] so that the luminescence response could be delayed beyond the time required for pipette addition of ACh to beginning of detection by the microplate reader. Slowing the reaction resulted in a broader luminescence detection peak from 30-60 sec, rather than the rapid, sharp peak over 2-3 sec observed by Shinohara. Thus, it was not practical to measure the maximum luminescence intensity for each peak when interpreting data, as was reported by Shinohara. Instead, the area under the curve was measured for a more accurate, reliable interpretation of luminescence response.

It is important to note that one limitation to the PC12 assay is that results must be compared within the same well plate, since the rapid growth of PC12 cells changes their condition too dynamically from subculture to subculture to permit comparison of luminescence intensity directly across well plates. The goal for the treatment study in Figure 2.8 was to compare four different PC12 growth conditions for luminescent response upon treatment with and without α-CTx MII and optimize the concentration of ACh for maximum sensitivity. Thus, to be able to compare all four treatment conditions (NGF, nicotine, ethanol, and combined nicotine and ethanol) together over a range of ACh doses for both +/- α-CTx MII with multiple negative controls, an n=2 was allowed for a full 96-well plate. The occurrence of faulty wells (for example, caused by anomalies such as air bubbles or uneven conditions at the edges of the well plate) reduced some data points to

n=1. Considering a cellular-level response is being detected, further reducing the growth surface area by using a 192- or 384-well plate was expected to introduce problems with sensitivity given the current level of progress toward optimization of nAChR expression. For an experiment in which the goal of the assay was to qualitatively screen a range of compounds, a simpler scheme with one dose of 50 µM ACh would be sufficient, allowing for more statistically complete data. For example, a more statistically complete result is demonstrated in the temperature study shown in Figure 2.5, for which an n=4 was used.

It was found that a better zero response for 0 µM ACh was obtained when a small amount of luminol was added to the assay solution before detection, because luminol addition is expected to quench residual oxygen dissolved in the assay solution or cell environment capable of breaking down the luminol and cause a luminescence response irrelevant to dopamine release, enabling a more level base response across all wells. It was found that the cells consume this small amount of luminol (50 µM) very quickly over the 5-10 min equilibration time even without activation by ACh, necessitating addition of a larger dose of luminol along with the ACh before detection. In an attempt to maximize the sensitivity of the assay, the luminol concentration was arbitrarily spiked to 5 mM, for which a consistent assay response was not achieved. It was then considered that the 1 M NaOH necessarily used to dissolve the luminol stipulated a maximum luminol concentration allowable before exceeding Locke's buffer capacity. Thus, while maximum luminescence response was desired, the maximum allowable [luminol] was limited by the buffer capacity.

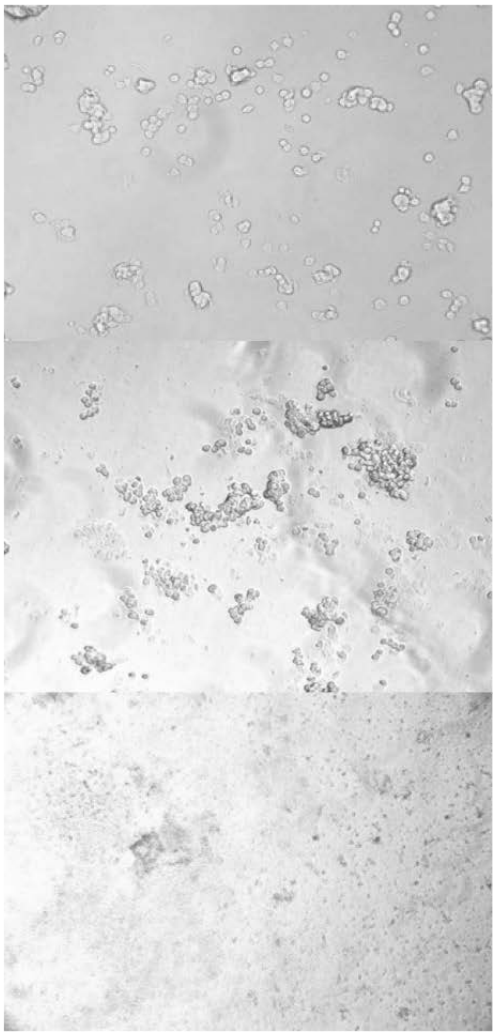

Figure A.2 Visual state of PC12 cells pre-assay (A) and post-assay after performing assay with both Locke's buffer (B) and HBSS (C). Cells post-assay using HBSS appeared severely lysed and damaged.

Subsequent to the release of Shinohara et al.'s initial study in 2008, Locke's buffer was replaced with Modified Hank's Balanced Salt Solution (HBSS) in their 2011 study [2,3]. In step with their decision, when simple HBSS was attempted in this study, interpretable results were drastically eliminated. Both buffers have a comparable osmolality of 270-305 mOsm/kg, and the greatest difference between Locke's buffer and simple HBSS is the absence of Mg2+ in Locke's buffer. After multiple unsuccessful attempts to recreate assay results with HBSS, it was discovered that the state of the cells

post-assay under a microscope appeared surprisingly damaged and most cells were lysed. Figure A.2 shows the state of the cells pre- and post-assay when using both Locke's buffer and HBSS. It is presumed that the Modified HBSS used in Shinohara et al.'s 2008 study was Mg-free HBSS [2]. This conclusion is consistent with literature precedent describing the depolarization of neuronal cells by Mg2+ [4].

1. Huang, H.L.; Hsing, H.W.; Lai, T.C.; Chen, Y.W.; Lee, T.R.; Chan, H.T.; Lyu, P.C.; Wu, C.L.; Lu, Y.C.; Lin, S.T., et al. Trypsin-induced proteome alteration during cell subculture in mammalian cells. Journal of Biomedical Science 2010, 17, 10, doi:10.1186/1423-0127-17-36.

2. Shinohara, H.; Wang, F.F.; Hossain, S.M.Z. A convenient, high-throughput method for enzyme-luminescence detection of dopamine released from PC12 cells. Nature Protocols 2008, 3, 1639-1644, doi:10.1038/nprot.2008.158.

3. Mir, T.A.; Shinohara, H.; Shimizu, Y. Enzyme-luminescence method: Tool for evaluation of neuronal differentiation based on real-time monitoring of dopamine release response from PC12 cells. Analytical Methods 2011, 3, 837-841, doi:10.1039/c0ay00769b.

4. Dribben, W.H.; Eisenman, L.N.; Mennerick, S. Magnesium induces neuronal apoptosis by suppressing excitability. Cell Death & Disease 2010, 1, 9, doi:10.1038/cddis.2010.39.

APPENDIX B

Supplementary Materials to Chapter Three

NMR Assignments

Table S1 provides parameter set details for all NMR experiments performed. Assignment of spin systems to the amino acid primary sequence was accomplished as follows: Spin systems were identified by confirming the presence of H-βH NOESY peaks and βH-βH NOESY peaks. All spin systems were confirmed on both sides of the diagonal.

The fingerprint region (Figure 8A) revealed an obvious lysine spin system pattern unique to any other residue in the peptide, clearly identifying K14. This assignment was used as a handle for other assignments. The W15 and C16 spin systems were then easily identified by two large NOESY peaks with the K14 NH resonance in the NH region. The W15 spin system was distinguished between the C16 system by a clear NOESY peak between the NH resonance and an N2H resonance in the downfield N2H region. S13 was identified based on a clear NOESY between the S13 NH resonance and the K14 NH resonance in the NH region. S12 was then identified by a clear NOESY between the S13 and S12 NH resonances in the NH region.

The alpha proton of P6 at 4.07 ppm was easily identified in the upfield a-B region by its spin system pattern unique to any other residue in the peptide. This assignment was also used as a handle for other assignments. G7 was also clearly identified by its unique spin system. The C8 spin system was confirmed by an NH-NH NOESY peak to G7, then Y9, W10, and S11 were identified in the same manner. The remaining unassigned serine spin system was then assigned as S4 by elimination. These assignments were fortified by corresponding aH-NH/βH-NH NOESY peaks between adjacent residues. C2 and C3 were predicted to have similar environments. As expected, the remaining two appropriate spin systems were identified at nearly overlapping chemical shifts, showing clear NH-NH and NH-aH NOESY peaks. The only remaining unassigned spin system for the peptide was then identified as W1 by elimination. C2 was distinguished from

C3 by an NH-NH NOESY peak to W1. Additional inter-residue NOESY peaks were then identified based on these assignments.

Table B.1 Parameter set details for NMR experiments.

Sample	Spectrum	pulse program	mix (ms)	Spectral width F1 (Hz)	Spectral width F2 (Hz)	scans	size of fid (F1)	size of fid (F2)
30% ACN/ 70% H_2O	noesy	noesyfgpphwg	50	8417.5	8417.5	64	256	2048
	noesy	noesyfgpphwg	150	8417.5	8417.5	64	256	2048
	noesy	noesyfgpphwg	250	8417.5	8417.5	64	256	2048
	noesy	noesyfgpphwg	350	8417.5	8417.5	64	256	2048
	tocsy	mlevgpphw5	80	6002.4	7194.24	64	300	6144
	cosy	cosygpprqf	n/a	7215	7211.5	32	600	8192
	hsqc	hsqcetgpsi	n/a	25000	7812.5	256	200	1024
30% ACN/ 70% D_2O	noesy	noesygpphpr	50	8417.5	8417.5	64	256	2048
	noesy	noesyfgpphwg	150	8417.5	8417.5	64	256	2048
	noesy	noesyfgpphwg	250	8417.5	8417.5	64	256	2048
	noesy	noesyfgpphwg	350	8417.5	8417.5	64	256	2048
	tocsy	mlevphpr	80	6002.4	7194.24	64	300	6144
	cosy	cosygpqf	n/a	7211.5	7211.5	32	600	8192
	hsqc	hsqcetgpsi	n/a	25000	7812.5	256	200	1024

Partial Reduction MS-MS

B and Y fragments were analyzed as the most accurate fragments for MS-MS fragmentation. Relevant fragments identified that distinguished a C2-C16/C3-C8 disulfide connectivity over a C2-C8/C3-C16 connectivity are shown in Figure S1.

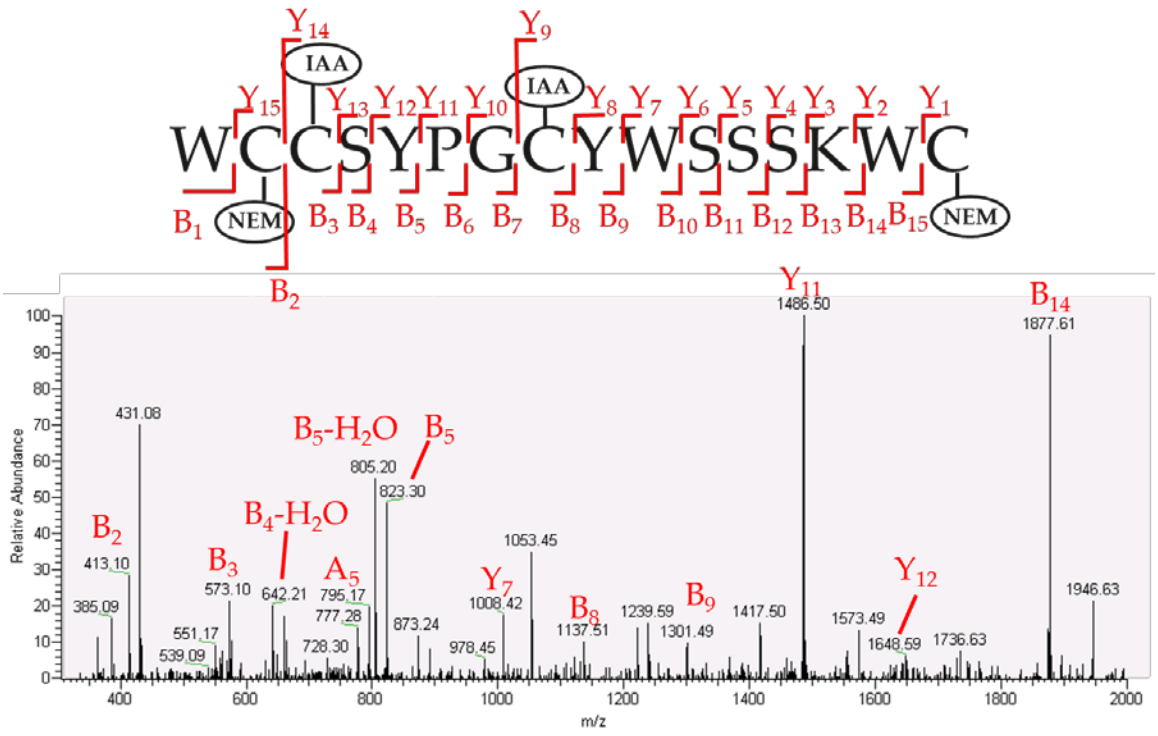

Figure B.1 Annotated MS-MS spectrum of relevant distinguishing B and Y fragments. Fragments are numbered along the KTM sequence, showing position of corresponding alkylations with N-ethylmaleimide (NEM) and iodoacetamide (IAA).

Molprobity Scores

Molprobity scores for all 20 models in the NMR ensemble are reported in Table S2. Clash scores and Ramachandran outliers were zero for all models, with no bad bonds or angles and no Cβ deviations >0.25Å.

Table B.2 Molprobity scores for the 20 NMR ensemble structures. The lowest percentile was 76th for model 10.

Model	Molprobity Score	Percentile
1	1.13	99
2	1.77	86
3	1.15	99
4	1.33	98
5	0.50	100
6	2.06	73
7	1.33	98
8	1.77	86
9	1.15	99
10	2.00	76
11	0.50	100
12	1.15	99
13	1.33	98
14	1.15	99
15	0.50	100
16	1.77	86
17	1.15	99
18	1.95	78
19	1.33	98
20	1.77	86